AD-A045 831 RCA LABS PRINCETON N J F/G 9/5
BASIC ADHESION MECHANISMS IN THICK AND THIN FILMS.(U)
JAN 77 K R BUBE, T T HITCH N00019-76-C-0256
UNCLASSIFIED PRRL-77-CR-2 NL

1 OF 2
ADA045831

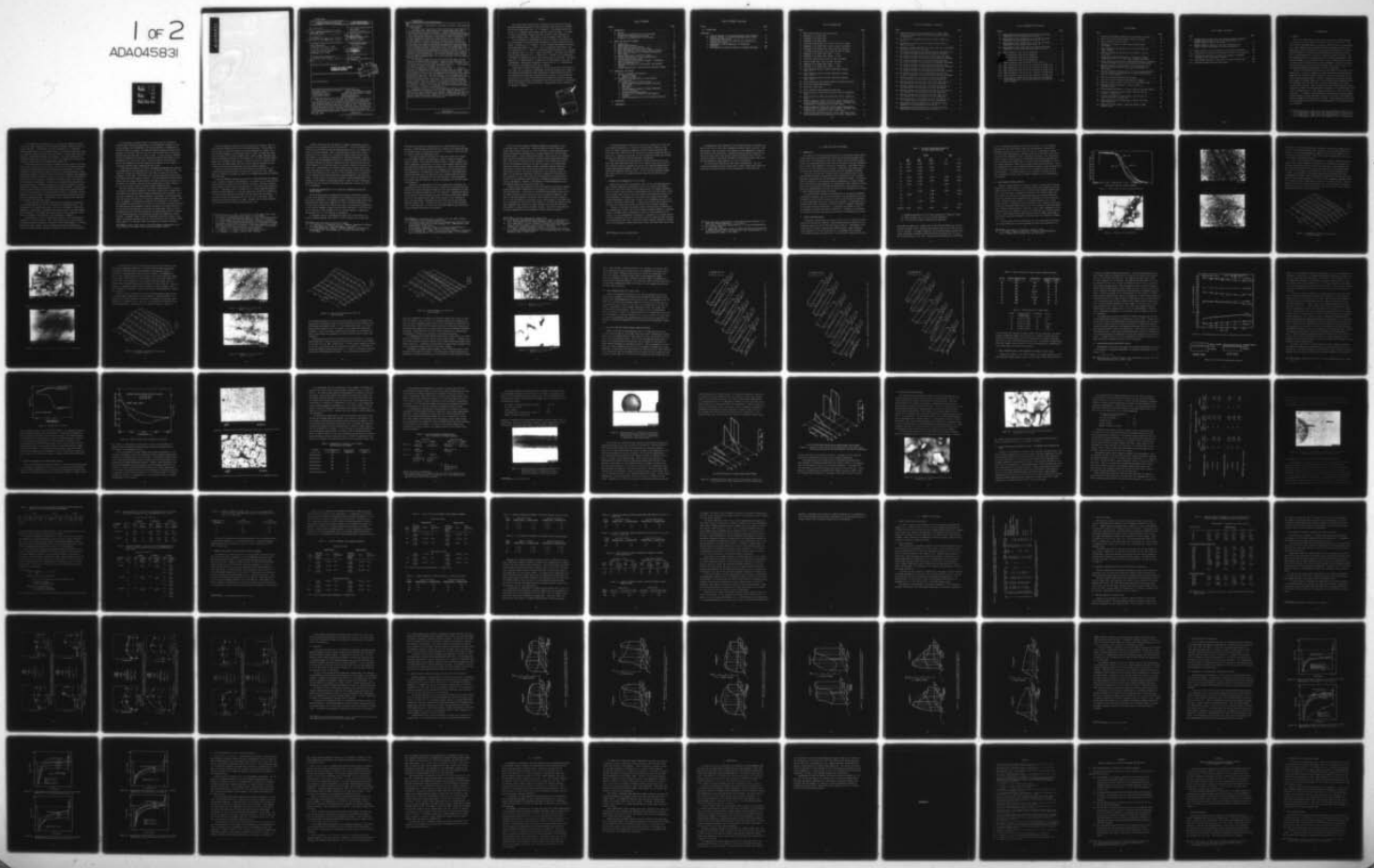

UNCLASSIFIED

SECURITY CLASSIFICATION OF THIS PAGE (When Data Entered)

REPORT DOCUMENTATION PAGE	READ INSTRUCTIONS BEFORE COMPLETING FORM
1. REPORT NUMBER	2. GOVT ACCESSION NO. / 3. RECIPIENT'S CATALOG NUMBER
4. TITLE (and Subtitle): BASIC ADHESION MECHANISMS IN THICK AND THIN FILMS	5. TYPE OF REPORT & PERIOD COVERED: Final Report (1-1-76 to 12-31-76)
	6. PERFORMING ORG. REPORT NUMBER: PRRL-77-CR-2
7. AUTHOR(s): Kenneth R. Bube [redacted] Thomas T. Hitch	8. CONTRACT OR GRANT NUMBER(s): N00019-76-C-0256
9. PERFORMING ORGANIZATION NAME AND ADDRESS: RCA Laboratories, Princeton, New Jersey 08540	10. PROGRAM ELEMENT, PROJECT, TASK AREA & WORK UNIT NUMBERS: 12 116 p.
11. CONTROLLING OFFICE NAME AND ADDRESS: Naval Air Systems Command, Washington, DC 20361	12. REPORT DATE: Jan [redacted] 1977
	13. NUMBER OF PAGES: 116
14. MONITORING AGENCY NAME & ADDRESS (if different from Controlling Office): 9 Final rept. 1 Jan-31 Dec 76	15. SECURITY CLASS. (of this report): Unclassified
	15a. DECLASSIFICATION/DOWNGRADING SCHEDULE: N/A

16. DISTRIBUTION STATEMENT (of this Report)

APPROVED FOR PUBLIC RELEASE: DISTRIBUTION UNLIMITED

17. DISTRIBUTION STATEMENT (of the abstract entered in Block 20, if different from Report)

18. SUPPLEMENTARY NOTES

19. KEY WORDS (Continue on reverse side if necessary and identify by block number)

Solderable thick-film metallization
Sintering kinetics
Glass-ceramic wetting
Glass-metal wetting
Solder wettability
Thermally aged adhesion strength
Thermally shocked adhesion strength
Au-Pt metallization
Au-Pt-Pd metallization

20. ABSTRACT (Continue on reverse side if necessary and identify by block number)

In this third year of the study, multicomponent systems (consisting of gold plus one or two platinum group metals) were examined in both model and commercial ink form, in order to understand the parameters which affect film adhesion and solderability. Solderable Au-Pt and Au-Pt-Pd metallizations are the second most widely used films in military hybrid circuits. Therefore, the factors which broadly influence metallization solderability, adhesion strength, and aged film

DD FORM 1 JAN 73 1473

UNCLASSIFIED

SECURITY CLASSIFICATION OF THIS PAGE (When Data Entered)

299 000

20.

adhesion strength, in the presence and absence of solders, were examined in some detail.

Two model inks, 75Au-25Pt and 75Au-12.5Pt-12.5Pd, were formulated for study after first characterizing the compositional purity and sintering behavior of each constituent. Because solderable metallizations require the formation of alloys resistant to dissolution by molten solder, two methods were used to determine the degree of alloying that occurred during the sintering of metal powders. X-ray diffraction studies indicated the shift from elemental mixtures to alloys by observing changes in lattice constants. Secondly, since alloying in metals adds to the temperature-independent contribution of electrical resistivity, the degree of alloying was monitored by observing changes in the resistivity ratio when measured at 298°K (room temperature) and 77°K (in liquid nitrogen). From these tests it was learned that complete alloying would be accomplished by firing the films at 900°C. Subsequently, solder-to-metallization contact angles were used to observe changes in film solderability. These studies resulted in the development of layered metallizations that could be soldered without burnishing, provided a modified glaze, i.e., E1527 glass plus 5 wt pct alumina (Al_2O_3), was used.

The adhesion strengths of the Au-Pt and Au-Pt-Pd model inks were found to be statistically comparable, suggesting that economical substitution of Pd for Pt was plausible. However, adhesion strength losses of the Pd-bearing films were more significant when aged in the presence and absence of solder (60Sn-40Pb) at 150°C for 500 h.

Of 21 commercially available Au-Pt and Au-Pt-Pd inks initially analyzed for composition, and adhesion strength (aged and unaged), five of these and a related ink were selected for more detailed study. Adhesion strength of the six inks was evaluated as a function of three print thicknesses, four peak firing temperatures, and two cooling rates from peak firing temperature. Data are presented for the inks fired on both 96 and 99.5 wt pct alumina substrates. Values for adhesion strength were also determined after aging, both with and without 62Sn-36Pb-2Ag solder present. With one exception, the adhesion strength of the inks was generally sensitive to peak firing temperature and less sensitive to thickness. Cooling rate changes did not affect solderability significantly in any of the six film materials.

Significant physical testing and compositional analytic techniques were developed in the course of the work and promise to provide the industry with more standardized test methods. Suggestions were made for the continued study of metal powder particle size distribution, the influence of pre-alloying the powders, and the determination of chemical species formed in the reactively bonded inks.

PREFACE

This final report described work performed in the Process and Applied Materials Research Laboratory of RCA Laboratories under Contract No. N00019-76-C-0256 and under RCA funds. Dr. P. Rappaport is the Laboratory Director and Dr. G. L. Schnable is the Project Supervisor and Group Head. Dr. Thomas T. Hitch is the Project Scientist and with Kenneth R. Bube comprises the principal research team. James Willis is the Government Project Monitor.

It is a pleasure to acknowledge the help of a number of individuals who have contributed to this work by the performance of several analytical techniques. Notable are H. H. Whitaker - optical emission spectrometry and atomic absorption spectrometry, R. J. Paff - x-ray fluorescence spectrometry, and x-ray diffraction, B. J. Seabury - scanning electron microscopy, B. L. Goydish - wet chemistry, and G. R. Auth - surface profilometry. We particularly acknowledge the able assistance of E. J. Conlon and A. Z. Miller in the preparation of samples for analysis and in the day-to-day pursuit of the study. The assistance of R. D. Vibronek and W. I. Rogers with certain phases of the study is acknowledged. Discussions throughout the study with Dr. G. L. Schnable and his reviews of the manuscript were most valuable.

Space does not permit mentioning all the persons who have contributed to this study, but we gratefully acknowledge helpful discussions with a number of the scientists studying thick-film technology at Sandia Laboratories and at Bell Laboratories, Allentown; representatives of several of the ink manufacturers; Dr. E. P. Bertin of RCA Laboratories; members of the Naval Research Laboratories team working in coordination with RCA (particularly Dr. Jim Murday and Dr. Paul Becher); the Project Monitor, James Willis; and his supervisor, Dr. Herbert J. Mueller.

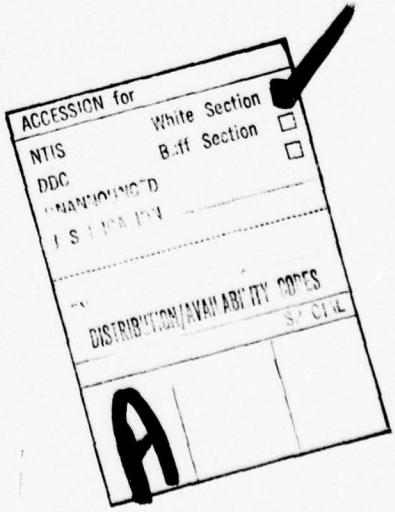

TABLE OF CONTENTS

TABLE OF CONTENTS (Continued)

LIST OF ILLUSTRATIONS

LIST OF ILLUSTRATIONS (Continued)

LIST OF ILLUSTRATIONS (Continued)

LIST OF TABLES

LIST OF TABLES (Continued)

I. INTRODUCTION

A. GENERAL

This is the Final Report of the third in a series of studies entitled *Identification of Basic Adhesion Mechanisms in Thick and Thin Films*. The first two were performed during the calendar years 1974 and 1975 under Naval Air Systems Command Contracts N00019-74-C-0270 and N00019-75-C-0145 [1,2], respectively, and were devoted to achieving better understanding of the way adhesion develops, to improving the reproducibility of hybrid structures, and to studying methods for testing the adhesion of hybrid materials. The 1976 program expands the overall objectives to include multicomponent metallization systems, i.e., Au-Pt and Au-Pt-Pd, since a large portion of hybrid circuitry relies on these films for device attachment. Prior to discussing the characteristics peculiar to multicomponent inks, a brief review of the work already performed on monometallic systems is desirable.

The 1974 work studied Au thick films on substrates of 96 and 99.5 wt pct alumina [1]. A survey of commercial Au inks and studies of RCA-formulated model inks and ink materials were combined to yield a broad picture of sintered Au metallization systems. Seventeen commercial Au inks were analyzed with respect to chemical composition, Au and binding agent morphology, adhesion strength via an RCA peel test, electrical conductivity, and screen-printed line resolution. Study of model inks and related glass-gold layered structures provided the first quantitative estimate of the contribution of sintered Au microstructure to total adhesion strength as it varies with firing conditions. In addition, basic measurements of glass-gold and glass-ceramic wetting behavior provided information necessary to a better understanding of device attachment and interconnection problems. These problems are related to the displacement of pure metal by the binding agent(s) at the bonding surface in Au inks [1].

---

1. T. T. Hitch and K. R. Bube, *Basic Adhesion Mechanisms in Thick and Thin Films*, Final Report, NASC Contract No. N00019-74-C-0270, 31 January 1975.
2. T. T. Hitch and K. R. Bube, *Basic Adhesion Mechanisms in Thick and Thin Films*, Final Report, NASC Contract No. N00019-75-C-0145, 31 January 1976.

In the commercial ink evaluations, it was found that adhesion strength varied with binder composition, screen-printed thickness, substrate type, and firing conditions. Three binder types were identified, i.e., reactively bonded, mixed-bonded, and frit-bonded systems. The highest strength was found in a reactively bonded ink when fired above 1000°C. At lower peak firing temperatures, mixed-bonded materials were superior. The chief constituent in reactively bonded inks is copper oxide, while both copper oxide and glass are present as binder agents in the mixed-bonded systems [1].

The 1975 study [2] was directed to broadening the basic study of Au thick films by the study of Ag and Cu films on 96 and 99.5 wt pct alumina substrates. The reasons for evaluating Ag and Cu metallization are numerous. By way of comparison, Au thick films are highly conductive, corrosion-resistant, thermocompression bondable, virtually free from electrolytic migration, and compatible with Ru-based thick-film resistor systems and cross-over dielectric materials. However, Au films are readily dissolved by Sn-bearing solders, and soldered joint strength is problematic. Ag films are considerably less expensive than Au, particularly on a volume-for-volume basis, and are not subject to severe electrolytic migration if used in hermetically sealed packages. With Ag films, however, special geometric and processing precautions must be exercised when Ag is used as electrodes for Ru-based resistor systems. In addition, the high mobility of Ag in cross-over dielectric materials seriously limits its use in multilevel package designs. To successfully resist corrosion, Ag films must be overcoated or hermetically sealed.

Cu thick films are also highly conductive and solderable, and represent the best high conductivity, low cost alternative to noble-metal films. The limitations of Cu include the necessity to fire in a nitrogen or other inert atmosphere. Additionally, protection from moisture and/or a corrosive ambient must be provided. Its thermal aging characteristics after soldering are poor due to the formation and growth of Cu-Sn intermetallic compounds.

In comparing Au, Ag, and Cu metallization systems, one of the questions addressed in the 1975 study was: What contribution does the sintered metal microstructure make in producing an adherent, useful metallization? A corollary question was also studied: How can processing and material parameters be altered to improve adhesion strength, bondability, and in-service reliability?

In the Au model ink study of 1974, it was found that the sintered Au microstructure contributes significantly to total adhesion strength with certain Au powders, glass thicknesses, and firing conditions. Considering the relative affinity for oxygen, and therefore chemical bonding potential, which increases as one shifts from Au to Ag to Cu, the microstructure contribution should become less important in Ag and Cu films. A chief aim was to identify relative microstructural effects on adhesion and thereby chart paths for the improvement of Au, Ag, and Cu films. The basic study of microstructural effects upon adhesion in 1975 was augmented by evaluation of the effects of processing conditions upon commercial Ag and Cu inks.

In 1976, RCA has added to the body of knowledge and physical test data already generated in the investigations of Au, Ag, and Cu in 1974 and 1975. The third year of study has been dedicated principally to improving the understanding of Au-Pt* inks. Au-Pt and Au inks are militarily the two most important hybrid thick-film conductor classes. The study performed in 1976 was more complex than the earlier studies because the binary alloying of the metal system added a new variable; this was further complicated by ternary systems of Pd, Au, and Pt found in many of the most popular commercial inks.

Au-Pt has achieved its broad use in military hybrids because of its good film-resistor termination capability, multilayer compatibility, properties of solderability and limited thermal adhesion degradation after soldering. Au-Pt inks have a reputation for reduced adhesion if processing varies substantially from the optimum conditions and for reduced solderability after refiring. This study is designed to investigate principally the development of the adhesion and solderability properties with the firing of Au-Pt inks on alumina substrates. The work explored the fundamental chemical and physical processes involved in the formation and segregation of the metal and binder layer phases on firing. The phase properties and their microstructural relationships were then related to the desired properties of good adhesion strength and bondability (solderability). Although a study of Au-Pt on substrates other than alumina is also needed, the program addressed only the use of 96 and 99.5 wt pct purity alumina. These, however, are the most widely used substrates in hybrid technology.

*An attempt is made in this report to list the elements constituting a conductor alloy in the order of their decreasing weight fractions.

Reactively bonded Au conductors were developed and offered for sale [3] soon after the original work [4] on frit-bonded materials. Shortly after the initial study of reactively bonded Au inks was presented [5], mixed-, frit-, and reactively bonded Au- and Ag-based conductor films [5] showed that some of the materials fire to form unusually dense, smooth, highly adherent films which are extremely conductive at low frequencies. The 1974 and 1975 contract studies have included a large number of commercial Au and Ag conductor inks. Among these, the mixed-bonded inks have yielded improved resilience to processing variations while maintaining very high adhesion strength.

Commercial reactively bonded and mixed-bonded Au-Pt inks are new, but related inks have been mentioned in the patent literature [6,7,8]. Inks of these two classes are included for study in the program along with frit-bonded Au-Pt(-Pd) inks.

Structural adhesion strength can be said to be sufficient when the bonding forces - chemical, physical, and mechanical - are greater in all cases than the forces which act to detach the film from the substrate. The major intrinsic forces acting to detach films from substrates are the internal and interfacial stresses. Interfacial stress is largely due to a thermal expansion mismatch between film and substrate. It has been judged that interfacial stresses are of little concern with Au and Ag films since the metals are very ductile. In less ductile alloy metallizations such as Au-Pt, Au-Pd, and Ag-Pd, these stresses are much more likely to be large. However, Au-Pt, Au-Pd, and Ag-Pd can have good structural adhesion when properly fired.

---

3. B. R. Smith and R. L. Dietz, "An Innovation in Gold Paste," Proc. International Soc. for Hybrid Microelec. Symp., p. 2-A-5 (1972).
4. T. T. Hitch, "Phase Morphology and Adhesion in Thick-Film Conductor Inks," Proc. International Soc. for Hybrid Microelec. Symp., p. 7-7-1 (1971).
5. T. T. Hitch, "Phase Morphology and Bondability of Reactively-Bonded and Frit-Bonded Gold and Silver Thick-Film Conductors," presented at the AIME Symposium, Preparation and Properties of Electronic Materials, Las Vegas, Nev., August 27-29, 1973; published in J. Elec. Materials 3, 553 (1974).
6. L. C. Hoffman, U. S. Patent 3,516,949 (1970) (duPont).
7. J. H. Martin, U. S. Patent 3,293,501 (1966) (Sprague Elect.).
8. L. C. Hoffman, U. S. Patent 3,516,949 (1970) (duPont).

Internal stress has been the subject of numerous experimental investigations, but its origins are still not understood. It is more generally considered to be a problem in thin-film metallizations, but it also causes problems in thick-film systems. When a diffusing species reacts with another material to form a product with a markedly different volume from the sum of the volumes of the reactants, adhesion may be strongly diminished. Because diffusion rates are exponential functions of temperature, it is unlikely that subsequent processing at moderate temperatures will influence diffusion and cause stresses *if the diffusing species was present* during the firing of the thick films. Unfortunately, the adhesive agents used to attach chips, heat sinks, and electrical contacts to the outside world may contain such species, and the film integrity at the location of chip attachment can be jeopardized by both internal stress and the extrinsic stresses applied to the connected member. It was an aim of this study to achieve a better comprehension of the reasons for the adhesion strength degradation of Au-Pt ink, and to determine guidelines for the selection of materials and processes to reduce the effects of the phenomenon.

B. THE ADHESION DEGRADATION OF Au-Pt THICK-FILM CONDUCTORS BY HIGH-TIN-CONTENT SOLDER

The principal reasons for employing Au-Pt inks in thick-film circuitry is that the Pt inhibits the dissolution of the metallizer alloy by molten solders such as 63Sn-37Pb.* The adhesion strength of Sn-based solder-coated Au-Pt metallizers has been found to degrade with time at elevated temperatures. In an early study at duPont [9], moisture was shown to accelerate the degradation. A 5 pct loss of adhesion strength was found after 600 hours of 150°C dry storage or 500 hours of 90°C storage at 95 pct relative humidity. Temperature cycling from 150° to -75°C produced no degradation.

A subsequent study by Peckinpaugh and Tuggle [10] of the effects of a military standard thermal shock (125° to -65°C) on duPont 7553 and ESL 5801

*All alloy proportions shown are percent by weight.

9. L. C. Hoffman, V. L. Bacchetta, and K. W. Fredrick, "Adhesion of Platinum-Gold Glaze Conductors," IEEE Trans. PMP-1, s-381 (1965).
10. C. J. Peckinpaugh and R. Tuggle, "Thick-Film Adhesion - Evaluation and Improvement," Proc. International Soc. for Hybrid Microelec. Symp., p. 417 (1968).

and 5800-B Au-Pt conductors demonstrated that a marked reduction in the adhesion of 62Sn-36Pb-2Ag soldered parts was caused by the thermal shocking. An underprint layer of glassy material prior to screening of the Au-Pt inks was found to reduce the degradation [10].

A thorough parametric evaluation by Gillis and Schroter [11] showed that the thermal storage and temperature cycling on adhesion strength could be related. They found that larger amounts of solder,* reduced soldering temperature, burnishing of the Au-Pt, and increased conductor thickness improved the retained adhesion strength [11]. Various Sn-Pb solders, including 10-90, 60-40, and 40-60, were compared, with 10-90 causing the least degradation. An underprint of glass followed by conventional metallization was found not to be beneficial, but a resistor material "barrier layer" used as an underprint for the Au-Pt inks gave a large improvement. The barrier layer was advocated along with optimization of the other important parameters.

Analyses of the mechanisms for adhesion degradation of Ag-based, Pd-containing and Au-Pt inks have been made. Milgram [12] studied Ag inks and showed with electron microprobe studies that the rapid degradation of these materials on thermal storage was due to Sn migration. Crossland and Hailes' classic study of Au-Pd and Ag-Pd inks also used electron microprobe mapping of the Sn, and attributed the large volume increase to the formation of $PdSn_3$ from the element, disrupting the metal film structure and reducing adhesion strength [13]. A glassy glue layer, the use of a Sn-free solder such as Cd-Pb eutectic, or a new Au-Pt ink (duPont EX8641) were studied and offered potential solutions to the problem.

*This phenomenon is probably due to a change in the test sample rigidity. It is unlikely to have any metallurgical basis.

11. T. B. Gillis and S. Schroter, "Practical Considerations Affecting Thick-Film Conductor Adherence of Solder Systems," Proc. IEEE-EIA Elec. Components Conf., p. 487 (1971).
12. A. A. Milgram, "Influence of Metallic Diffusion on the Adhesion of Screen Printed Silver Films," Met. Trans. 1, 695 (1970).
13. W. A. Crossland and L. Hailes, "Thick Film Conductor Adhesion Reliability," Proc. International Soc. for Hybrid Microelec. Symp., p. 3.3.1 (1970).

One of the better studies of adhesion degradation mechanisms in Au-Pt to date was that of Suloff [14]. Using 95Sn-5Ag and 97.5Pb-1.5Ag-1.0Sn solders and thermal storage at 85°, 125°, and 150°C, he found adhesion degradation increased with the aging time, the aging temperature, and the higher Sn-content solder. Suloff studied metallurgical cross sections of his samples using optical micrography and chemical component mapping using EDAX-equipped SEM. From this he concluded that the formation of the intermetallic $AuSn_4$ and the corresponding increase in the specific volume of the intermetallic phase over the sum of the volumes of metal components ruptured the glassy structure of the thick-film conductor and reduced its adhesion strength. From Suloff's curve of the log of intermetallic layer thickness versus 1/T, where T is the absolute temperature, activation energies can be deduced of 20.3 Kcal/mole for the Sn-Ag solder and 9.6 Kcal/mole for Pb-Sn-Ag solder.* Suloff's [14] and another recent work [15], studying the phenomenon of Au-Pt adhesion degradation, resulted in development of strength/temperature plots and formulas useful for predicting service life.

Studies [15,16] have shown that nickel has superior resistance to thermal-aging-induced adhesion degradation in the presence of Sn-based solders over Au-Pt-Pd conductors. In only one of two Au-Pt-Pd films studied in one of the two papers [15,16] could the data be fitted to an Arrhenius equation. From that fit and metallographic information, Ewell deduced activation energies of 11.7 $\pm$ 0.4 Kcal/mole for the growth of the layer adjacent to the solder and 22 $\pm$ 4 Kcal/mole for the Sn-rich layer adjacent to the unreacted conductor film. Ewell suggested that diffusion by higher velocity paths than the bulk metal was required to support these activation energies. Suloff has noted that the activation energies are not inconsistent with bulk diffusion control.*

*R. E. Suloff, private communication, January 1976.

14. R. E. Suloff, "Time Dependent Relationships in Solder Interconnections," Proc. International Soc. for Hybrid Microelec. Symp., p. 418 (1974).
15. K. B. Lasch and K. S. Lynch, "Integrity of Solder Joints Connecting Nickel Leads to Thick Film Metallization on Ceramic Substrates," Proc. International Soc. for Hybrid Microelec. Symp., p. 427 (1974).
16. G. J. Ewell, "Adhesion Degradation of Soldered Thick Film Chip Resistors During Elevated Temperature Exposure," Proc. International Soc. for Hybrid Microelec. Symp., p. 168 (1975).

No published study was found of the variation of adhesion in Au-Pt inks with substrate composition. A study has been published, however, on the effects of thermal aging and temperature cycling of Au-Pd and Ag-Pd thick films which were fired onto 92, 96, and 98 wt pct alumina substrates and soldered [17]. Substantial variations in initial adhesion strength and retained adhesion were correlated with ink-substrate combinations.

Adhesion strengths have been measured at Sandia Laboratories for two Au-Pt-type inks fired onto 96 and 99.5 wt pct alumina, with one lot each of both substrate purities purchased from each of two substrate manufacturers. Parallel gap welding attachment and peel testing as well as soldered wire tensile peel adhesion tests were used. In every case the adhesion strength data from the 99.5 wt pct alumina was lower than that from the 96 wt pct material.*

C. PROBLEMS IN THE BONDABILITY OF Au-Pt FILMS

Manufacturers of Au-Pt inks advocate their use for Au thermocompression and ultrasonic aluminum wire bonding as well as for eutectic die bonding. While Au-Pt films can be used for these applications, the bonding temperature must be raised to bond Au wires and semiconductor dice over that which is used with Au thick films, even for the most bondable Au-Pt conductors fired at optimum conditions. The higher Pt and Pd content inks require still higher bonding temperatures, and for some, bonding is not recommended except by soldering of ultrasonic methods [18]. It should be noted that Au-Pt inks are not advocated for die and wire bonding by several texts on hybrid technology.

A study of literature from several vendors indicated that a reduction in the solderability of Au-Pt inks occurs along with improved adhesion. Activated fluxes or extended times of immersion in solder are often required for the solder to wet the high-adhesion formulations. Wettability is a strong function of firing temperature and time, with wetting initially improving with increased firing temperatures and time. Extensive refiring, however, apparently requires the use of burnishing to solder Au-Pt inks, unless activated fluxes can be used.

*D. R. Johnson, private communication.

The bondability and solderability are strong functions of the amount and kind of frit used in Au-Pt inks according to several authors [6,17,18]. More particularly, they are likely to be functions of the segregation of glass to the surface of the fired films. Crossland and Hailes found no glass on the surface of their Au-Pd films using an electron microprobe [13], but that analytical method is not wholly satisfactory because glass layers that could preclude wetting by solder might be too thin to be detected.

Pt and Pd oxide formation may also reduce solderability. An x-ray diffraction technique used with Ag-Pd inks to detect oxides which reduce solderability [19] may be useful in the investigation of these materials.

17. A. C. Buckthorpe, "Degradation of Thick Film Conductor Adhesion," Proc. IERE Conf. on Hybrid Microelec., p. 57 (1973).
18. M. L. Topfer, *Thick-Film Microelectronics*, p. 47 (Van Nostrand-Reinhold Co., New York, 1971).
19. T. Kubota and T. Shinmura, "Study of Surface Oxidation and Solderability on Silver-Palladium Thick Film Conductors," Proc. International Soc. for Hybrid Microelec. Symp., p. 81 (1969).

II. MODEL INK THICK-FILM PROGRAM

A. INTRODUCTION

The model ink thick-film program examined the relationship between metallization properties and the material variations and related phenomena which affect them. These phenomena include metal powder sintering kinetics, glass-ceramic and glass-metal wetting rates, and the influence of process parameters such as peak firing temperature and time at temperature. Additional factors, while not yet fully explored, are believed to influence final metallization properties and include heating and cooling rates and atmosphere variables.

The work on Au, Ag, and Cu systems, which were studied earlier [1,2], demonstrated the large influence metal powder morophology, as well as metal and glass composition, has upon metallization adhesion strength. In addition, from the observed Cu foil-to-glaze adhesion measurements, it became evident that redox potential and atmosphere can significantly affect adhesion strength. While the exact proportion of chemical and mechanical contributions to adhesion are experimentally difficult to isolate, it is recognized that ultimately both influence metallization properties.

The current effort expanded the investigation to include multicomponent metallization systems, e.g., Au-Pt and Au-Pt-Pd. The introduction of Pt and Pd metals in thick films is necessary in hybrid circuits which are designed to attach additional devices with soldering techniques. The advantage of increased solder leach resistance in Au-Pt-Pd systems is somewhat compromised by increased electrical resistivity. In addition, the tendency of the Pt group metals to oxidize can reduce solderability. Therefore, the influence of oxidation rates must necessarily be considered in examining these systems.

B. POWDER CHARACTERIZATION

Additional Au powder MB-1 as well as initial lots of Pt MB-2 and Pd MB-3 powder were obtained for analyses. Emission spectrographic analyses of the powders as well as Pt and Pd foil are listed in Table 1. The powders, characterized by the vendor, indicate much higher specific surface areas and lower densities for Pt and Pd than for Au. For example, MB-1 Au powder is described as having a surface area of 0.66 m^2/g and a density of 6.15 g/cc,

TABLE 1. EMISSION SPECTROGRAPHIC ANALYSIS OF METAL POWDERS AND FOIL*

	Powder			Foil	
	Au MB-1	Pt MB-2	Pd MB-3	Pt	Pd
Si	0.064	0.002	0.006	0.021	0.032
Au	S***	0.003	0.003	-	0.020
Mg	0.001	0.003	0.005	-	0.001
Pb	-	0.007	-	-	-
Fe	0.002	0.006	0.009	0.009	0.006
Al	0.038	0.002	0.002	0.008	0.038
Pd	0.001	0.003	S	0.001	S
Pt	-	S	-	S	-
Cu	-	0.001	0.008	0.003	0.008
Ag	0.006	-	0.001	-	0.003
Mn	-	-	0.001	-	-
Ca	-	0.040	0.004	-	-
B	-	-	-	-	0.064
Metal**	99.89	99.93	99.96	99.96	99.83

* Elements expressed as wt pct after conversion to respective oxides

** Metal content, e.g., Au, Pt, or Pd (by difference)

*** S - Very strong signal; quantification impossible

while MB-2 Pt powder has a surface area of 14.5 m^2/g and density of 1.03 g/cc. The MB-3 Pd powder shows a slightly lower surface area of 11.1 m^2/g and density of 0.90 g/cc. As might be expected, the Pt and Pd powders contain a much larger percentage of submicron particles than the Au powder (Pt, 25 wt pct; Pd, 15 wt pct; and Au, 5 wt pct). Particle size distributions, as determined

by x-ray sedimentation analyses* and indicated in Fig. 1, are in relative agreement with the cited surface areas and bulk densities. However, the SEMographs in Figs. 2, 3, and 4 for Au, Pt, and Pd, respectively, indicate that much higher percentages of submicron particles are present in the Pt and Pd powders than indicated by x-ray sedimentation analysis. This discrepancy between directly observed particle sizes (SEM) and indirectly measured sizes (x-ray sedimentation) implies that the latter method is measuring the size of some powder agglomerate rather than thoroughly deflocculated particles. Thus, the reproducibility of x-ray sedimentation-derived particle size distributions, for high surface area powders, may not be as consistent as those for more coarse powders. It therefore appears to be necessary to monitor particle size distributions by more than one method, especially for the high surface area powders.

C. METAL POWDER SINTERING KINETICS

Similar to the procedures of previous studies of metal powder sintering kinetics [2], 0.85-g samples of the subject powders were compacted at 863-kg (1900-lb) force into 12.5-mm (0.5-in.) diameter discs, between hardened steel pins. It is important to remember at this point that ultimate powder compact density is a function of compacting pressure and material properties [20], e.g., particle size distribution and morphology, as well as metal ductility. Our main initial concern is to determine whether or not a given powder conforms to theoretical sintering behavior, i.e., exhibits a monotonic increase in fractional densification, $\Delta L/L$, as a function of time and temperature. Without establishing this conformity, little useful information can be determined about the influence of glass frit additions upon ultimate densification. This problem became evident with the MJ-2 Au powder, which began to swell (after initially shrinking) at different rates as a function of temperature [1].

A second reason for these experiments was that isothermal densification rate curves enabled us to assess approximately which metal powders will be

*Micron Data Laboratory, St. Catharines, Ontario, Canada.

20. R. M. German, "Compaction Mechanics of Submicron Palladium Powder," Int'l J. Powder Met. and Powder Tech. 11, 169,(1975).

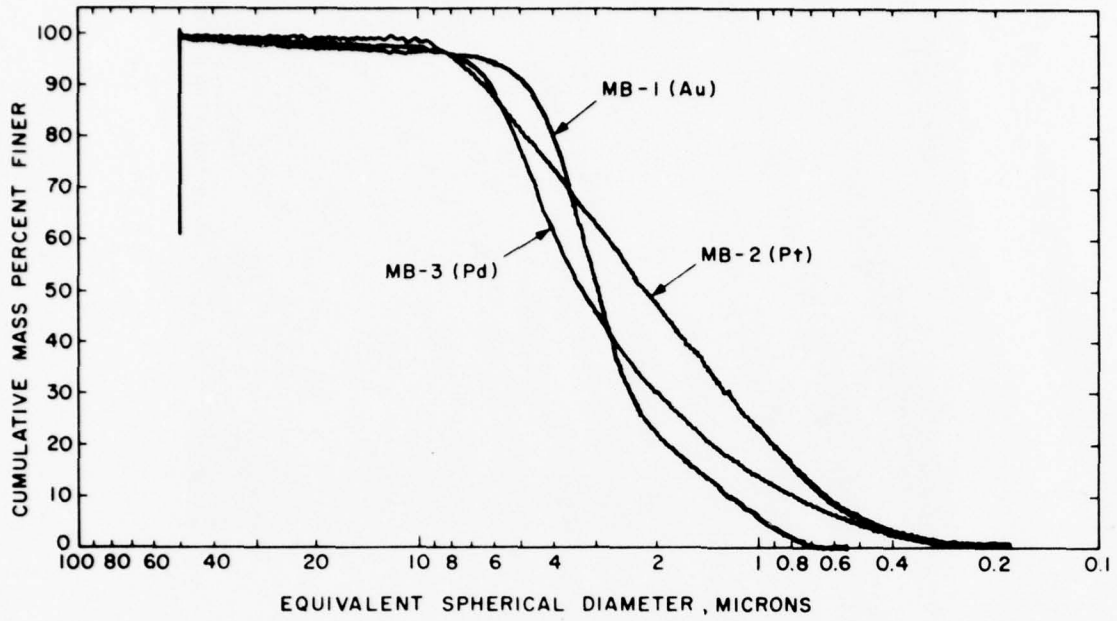

Figure 1. Metal powder particle size distributions.

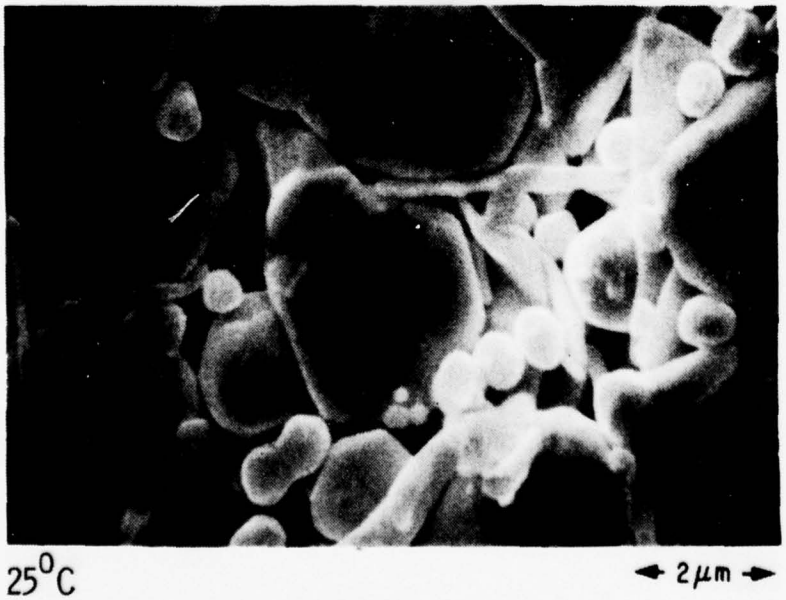

Figure 2. SEMograph of Au powder.MB-1.

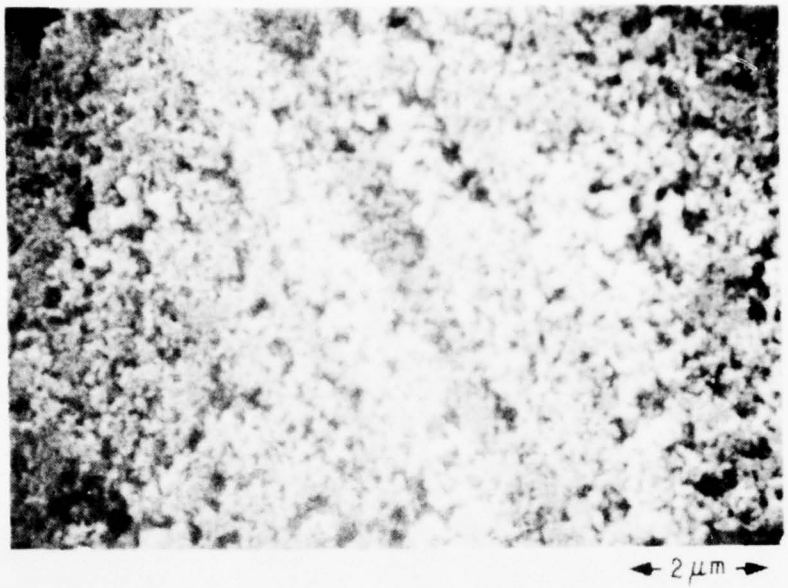

Figure 3. SEMograph of Pt powder MB-2.

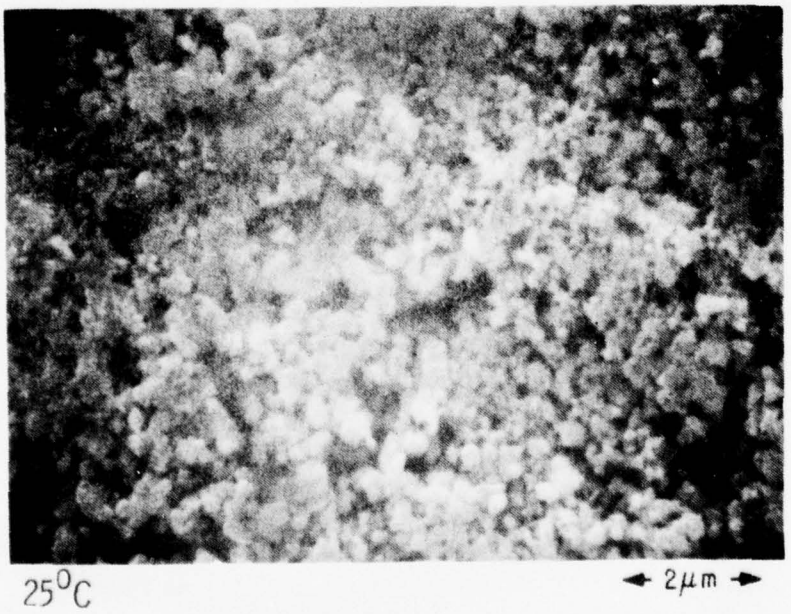

Figure 4. SEMograph of Pd powder MB-3.

compatible in terms of sintering rate uniformity. Based on the higher melting points of Pt and Pd and the fact that sintering rates are inversely related to particle size, a first approximation suggests the use of much smaller Pt and Pd particles than Au particles. This criterion has been achieved in the selection of MB-2 Pt and MB-3 Pd powders.

In Fig. 5, the isothermal densification rate curves for MB-1 Au powder are shown. These curves represent two separate lots of material and confirm both monotonic densification behavior and product uniformity. The maximum achievable fractional densification, $\Delta L/L$, is approximately 0.13 and occurs within the 500° to 900°C range. Little additional densification is observed after 5 minutes at temperature, indicating an upper useful processing time limit. The SEMographs in Figs. 6 and 7 illustrate approximately the initial and final stages of sintering, respectively. In Fig. 6, which represents Au powder heated for 2 minutes at 600°C, significant neck growth has already occurred. There is, however, a high void volume fraction observable. After 2 minutes at 1000°C, as shown in Fig. 7, the void fraction has been reduced to almost nil and considerable grain growth has already taken place.

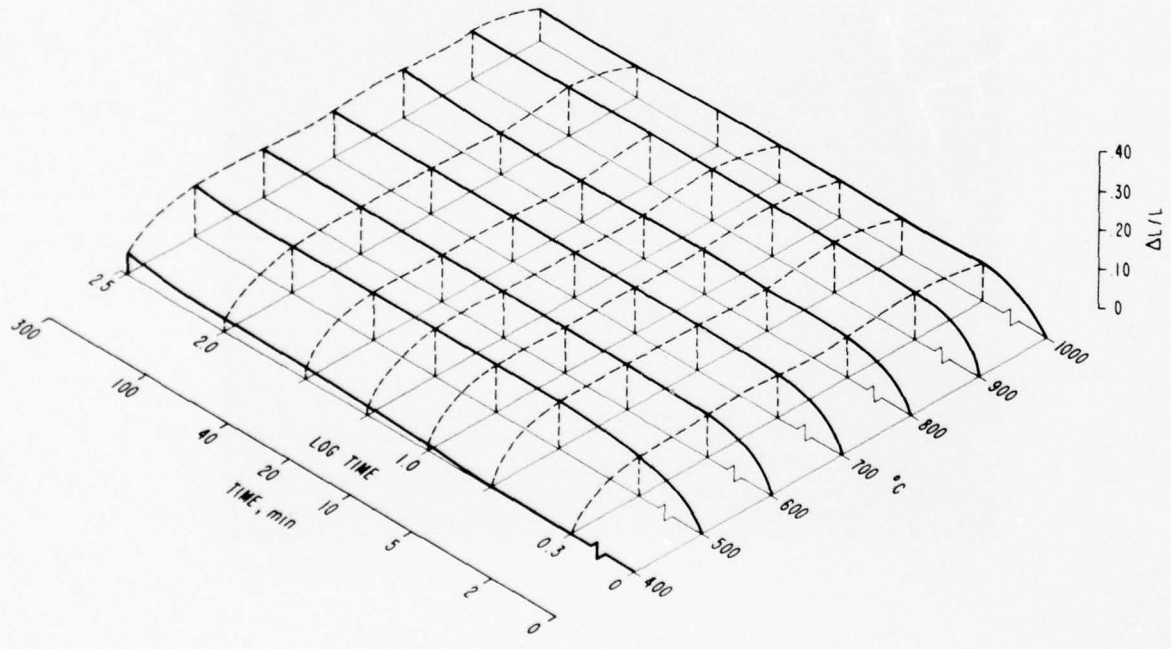

Figure 5. Isothermal densification rate curves for MB-1 Au powder

Figure 6. SEMograph of Au powder MB-1. initial stage of sintering.

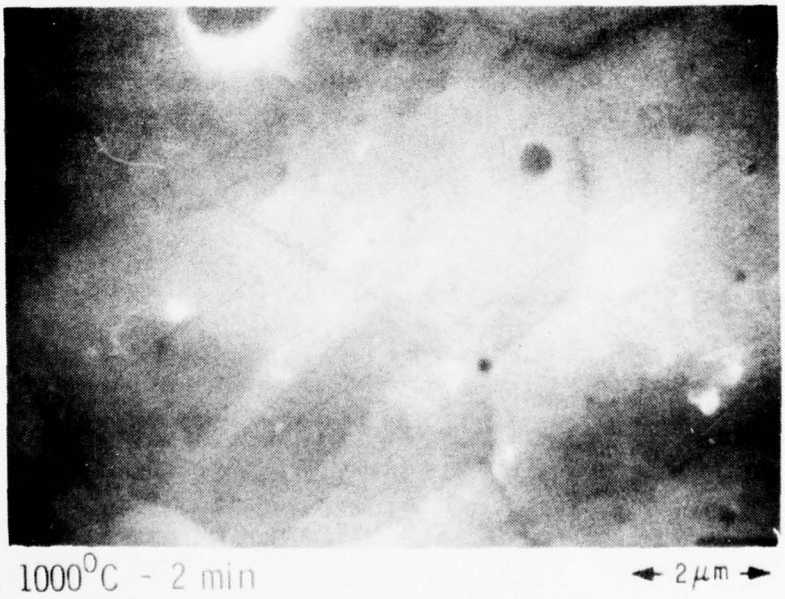

Figure 7. SEMograph of Au powder MB-1, final stage of sintering.

In contrast to Au, the Pt densification curves in Fig. 8 exhibit a more pronounced temperature dependence. Fractional densification rises rapidly between 400° and 800°C with a somewhat greater time dependence than Au. Above 800°C little additional densification is evident. The SEMograph in Fig. 9 shows a high volume fraction of voids for the 600°C-2-min-fired sample. In this case, the void sizes are much smaller, and they are more widely dispersed than in the Au powder. For the 1000°C-2-min-fired sample, the Pt powder voids are reduced dramatically in number as shown in Fig. 10. There is, however, no evidence of grain growth, in contrast to the Au powder. Both Au and Pt densify in a monotonic fashion, indicating no swelling and thus limited gas evolution.

Figures 11 and 12 illustrate the fractional densification curves and percent weight gain, respectively, for the Pd powders. During sintering of Pd pellets in air, redox reactions and diametral shrinkage are occurring, simultaneously, at different rates. Some error in measuring true diametral shrinkage was unavoidable. The oxidized pellets tended to warp as a result of

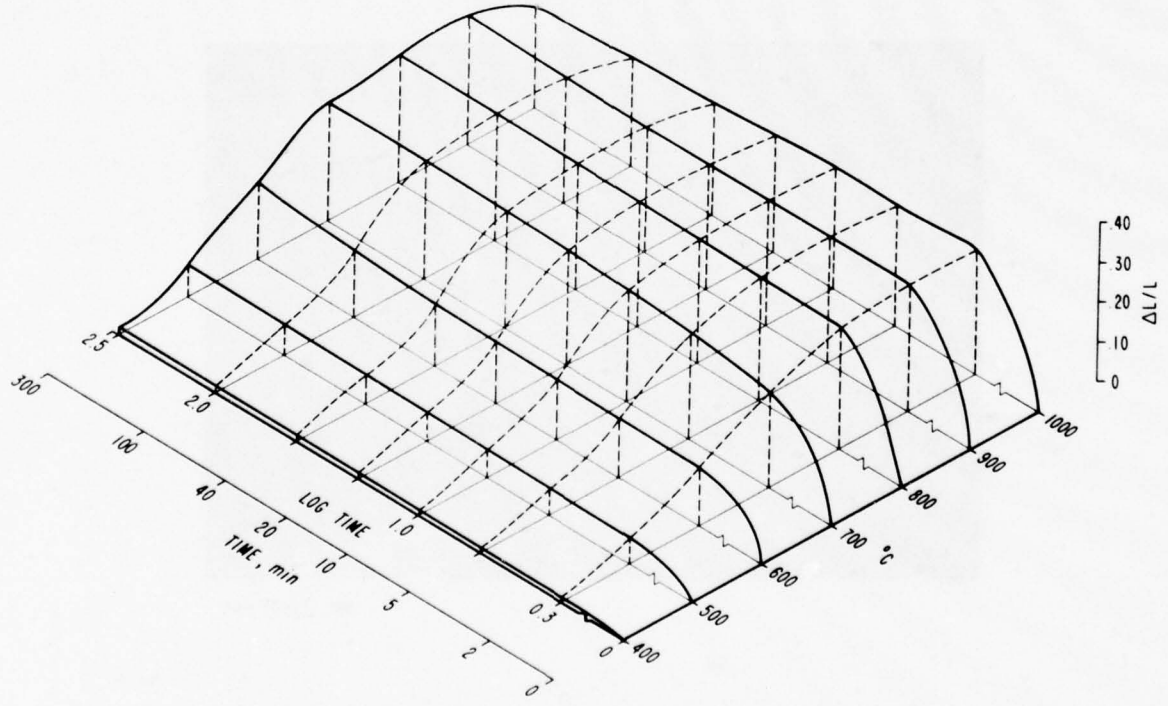

Figure 8. Isothermal densification rate curves for MB-2 Pt powder.

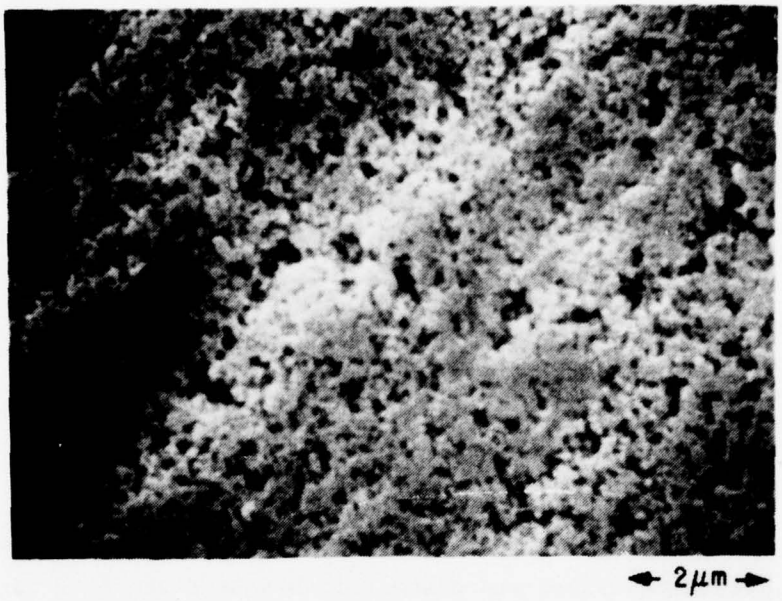

Figure 9. SEMograph of Pt powder MB-2 (600°C - 2 min).

Figure 10. SEMograph of Pt powder MB-2 (1000°C - 2 min).

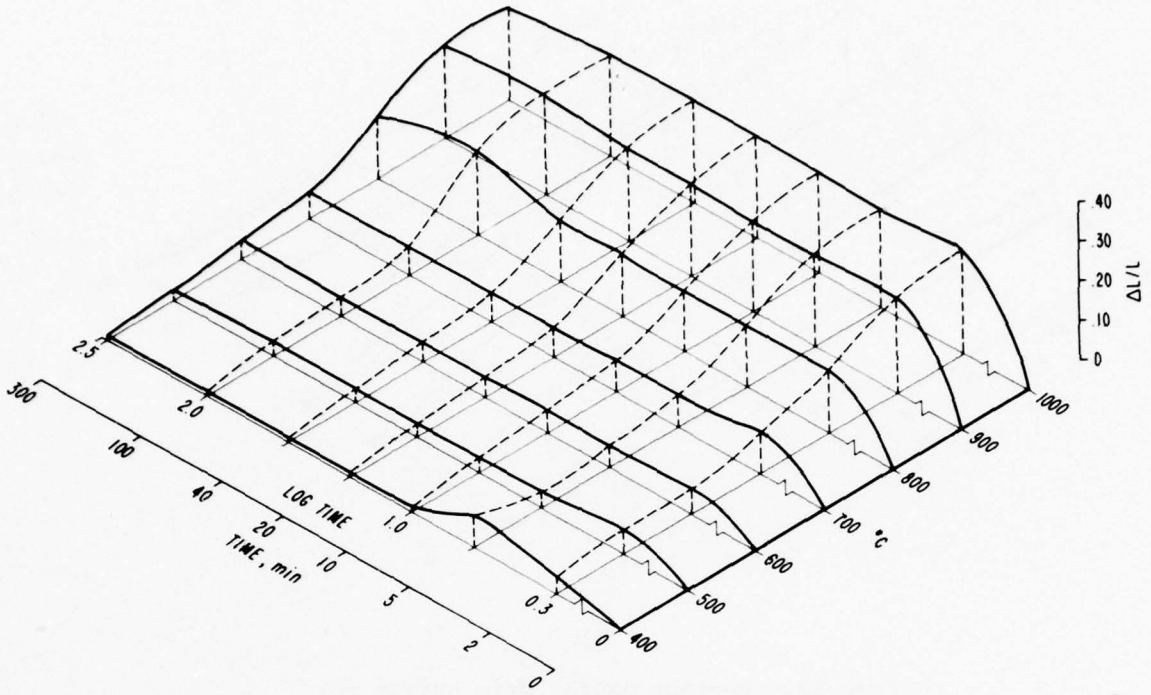

Figure 11. Fractional densification curves for MB-3 Pd powder.

the nonuniform oxidation of the top and bottom sides. This variability may account for the anomalously high fractional densification value shown for the 400°C-5-min-fired sample in Fig. 11. The uniform weight gain, i.e., Pd-to-PdO reaction, depicted in Fig. 12 suggests a more gradual and predictable oxidation. The two processes, densification and oxidation, are competitive, since a high surface area promotes both rapid sintering (densification) and oxidation.

Reaction kinetics vary with temperature for both processes. It is apparent from Fig. 11 that Pd fractional densification does not rise as rapidly as Pt (Fig. 8) in the 400° to 800°C range. From the percent weight gain curves in Fig. 12, it is obvious that Pd sintering is retarded by the Pd-to-PdO reaction below 800°C, reaching approximately 77 percent of theoretical value for PdO for the 700°C-300-min-fired sample. The corresponding decomposition of

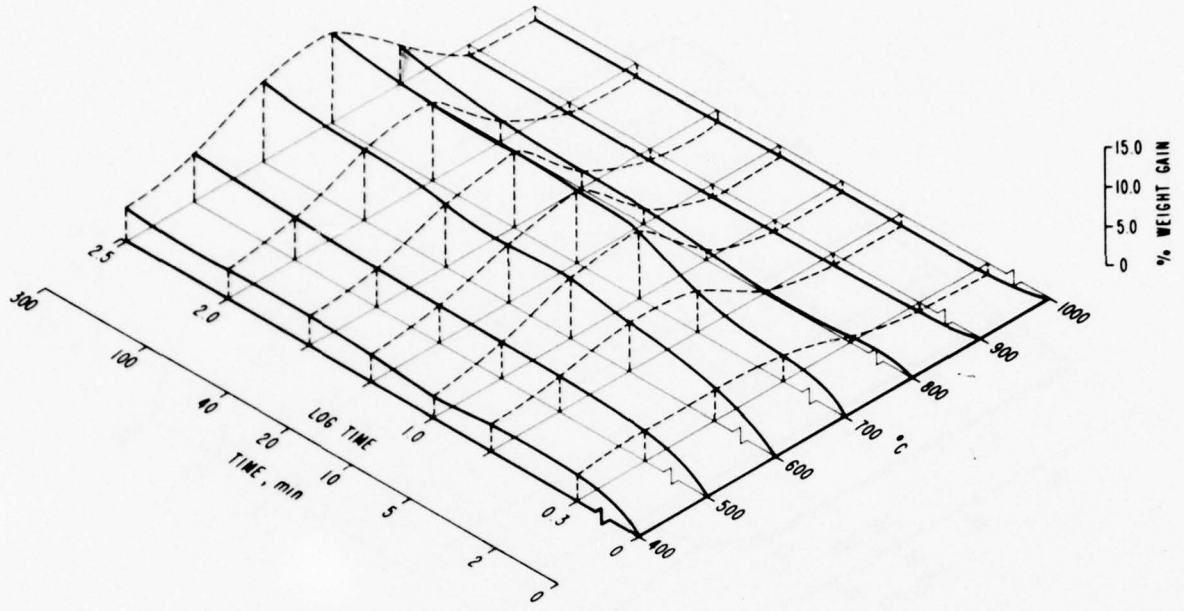

Figure 12. Percent weight gain curves for MB-3 Pd powder.

PdO is not completed, as evidenced by consistent weight loss in Fig. 12, until 900°C is reached. While the rates of oxidation-reduction and sintering will vary with pellet geometry, powder surface areas, and degree of compaction, two facts are clear. Above 800°C the powder densifies in a monotonic fashion, indicating a pure powder free from outgassing and resultant swelling (retrograde sintering). Below 800°C some portions of the pelletized Pd is oxidized and unavailable for sintering or alloying in multicomponent mixtures.

The SEMograph of the 600°C-2-min-fired Pd pellet, shown in Fig. 13, varies little in void density from the unfired compact shown in Fig. 4. However, the void volume fraction is greatly reduced for the 1000°C-2-min-fired sample illustrated in Fig. 14. In addition, grain growth has already begun, although it has not yet reached the extent found in the Au powder compact.

In summary, the powders selected appear to have sufficient purity to meet the needs of the model ink studies. The implications of Pd-PdO reactions on heating and cooling a Pd-bearing thick film through the 800°C transition region

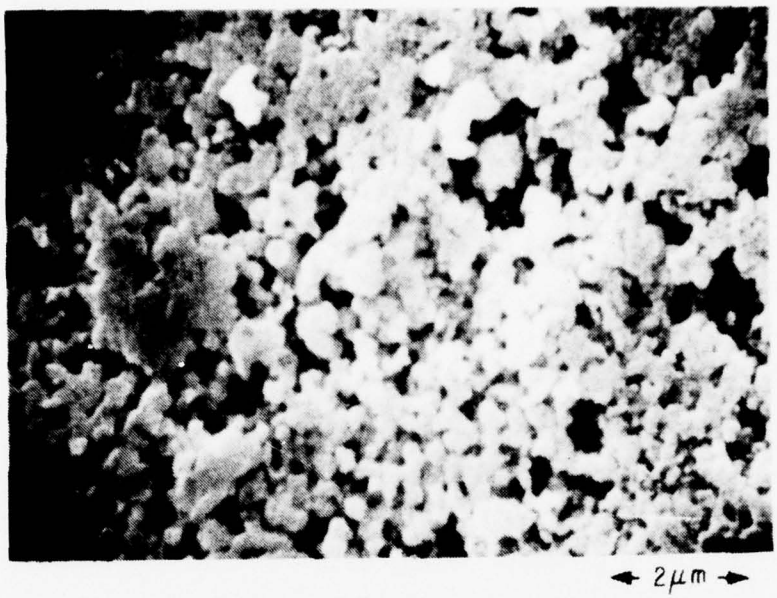

Figure 13. SEMograph of Pd powder MB-3 (600°C - 2 min).

Figure 14. SEMograph of Pd powder MB-3 (1000°C - 2 min).

are at least twofold. Alloying reactions, e.g., among Au, Pt, and Pd, which can be expected to occur on firing, may not be completed if the thick film is fired below 800°C. Secondly, some portion of the Pd in a Pd-bearing thick film will oxidize on cooling through 800°C-to-room-temperature region. This oxide formation can have a potentially adverse effect on solderability while possibly improving adhesion. The latter may result from the availability of additional oxygen atoms (from PdO) acting as a link between the glaze and Pd metal and/or Pt and Au.

D. GLAZE SPREADING RATES ON Pt AND Pd FOIL

Samples of Drakenfeld E1527 glass frit, with and without 20 wt pct CuO admixed, were compacted into 4-mm-diam pellets weighing 0.085 g and fired for various times and temperatures on the Pt and Pd foil. The spreading rates for 800°, 875°, and 950°C are presented along with the data for Au, Ag, Cu, and alumina (96 wt pct) in Figs. 15, 16, and 17 for heating times of 30, 300, and 1000 s, respectively. At the highest temperature, 950°C, the spread rates are greatest on Ag and alumina. With the exception of the receding glaze drop on Cu (Fig. 17, 950°C), the glaze spreading rate is approximately the same for the remainder of substrate materials, i.e., Au, Pt, and Pd. In every case, the added CuO accelerated the spreading rate, indicating that significant influence on adhesion and bondability can be achieved by altering binder composition.

E. METAL FOIL-TO-E1527 GLAZED CERAMIC ADHESION STRENGTH

Samples of Pd and Pt foil measuring 0.04 in. (∿1 mm) wide by 0.625 in. (∿16 mm) long by 0.002 in. (∿0.05 mm) thick were bonded to E1527-glazed alumina (96 wt pct) in a manner similar to that used for Au [1], Ag [2], and Cu [2] and fired for 10 min at 950°C in air. The foil was subsequently peeled from the glaze in an Instron tensile test machine, and the summary for all metal-to-glaze adhesion strengths is presented in Table 2. With the exception of the Cu which was fired in nitrogen, the Au, Pt, and Pd adhesion strengths are roughly comparable to each other, but considerably less than that for Ag. When considered in conjunction with the spreading rate information and metal solubility data in Table 3, which shows Pt, Pd, and Au to be considerably less soluble than Ag

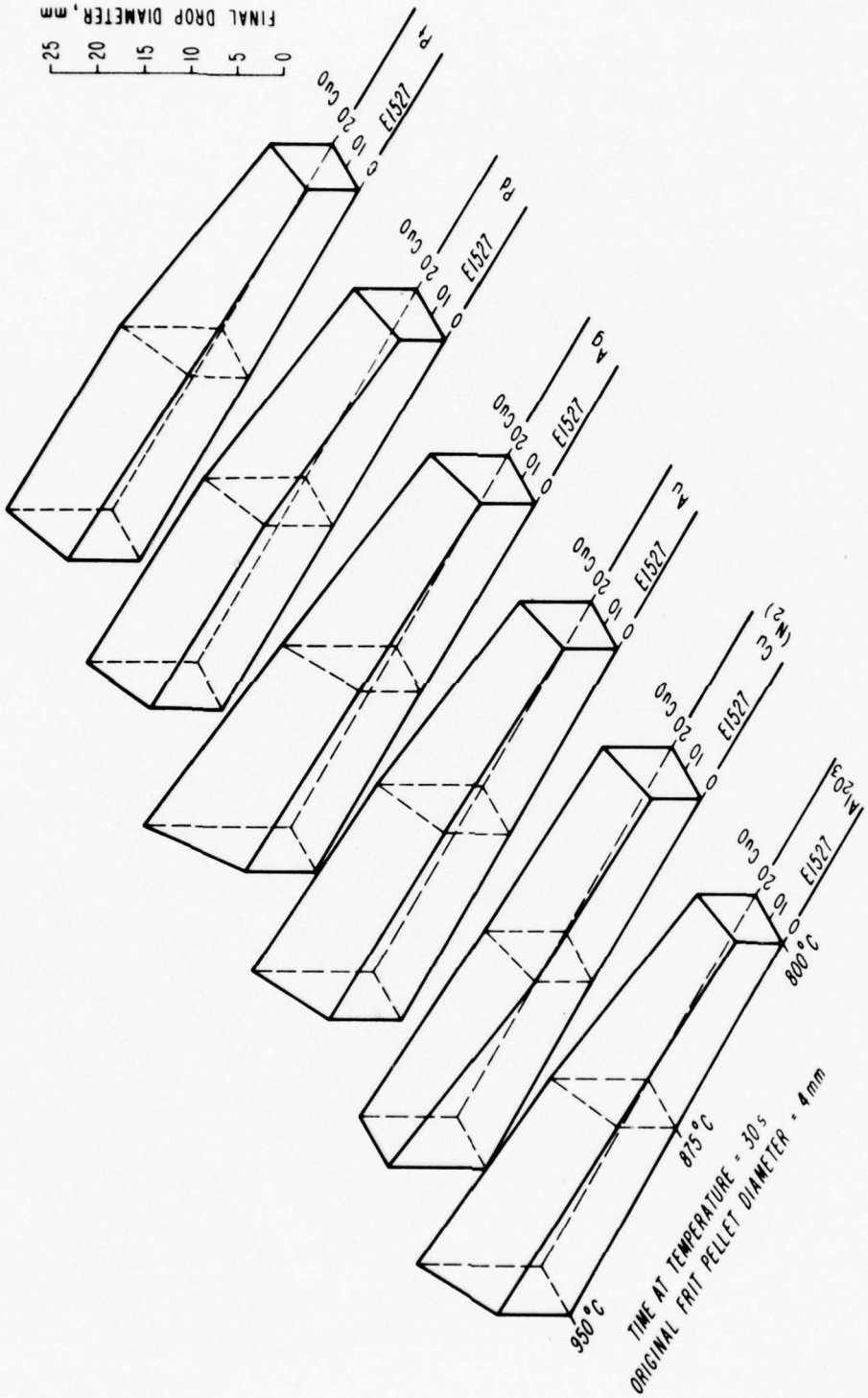

Figure 15. Glaze spreading rates in various substrates, heating time = 30 s.

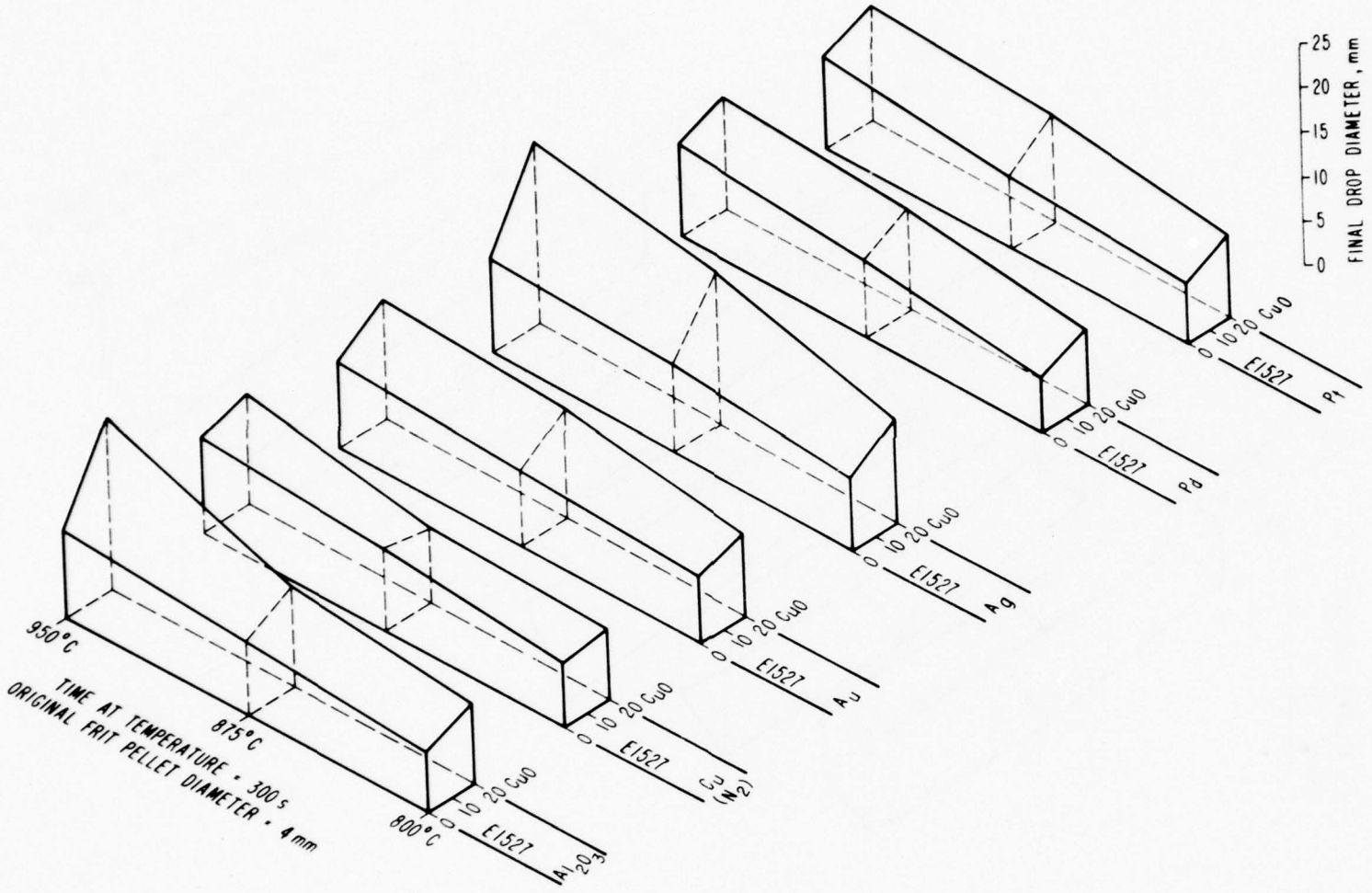

Figure 16. Glaze spreading rates on various substrates, heating time = 300 s.

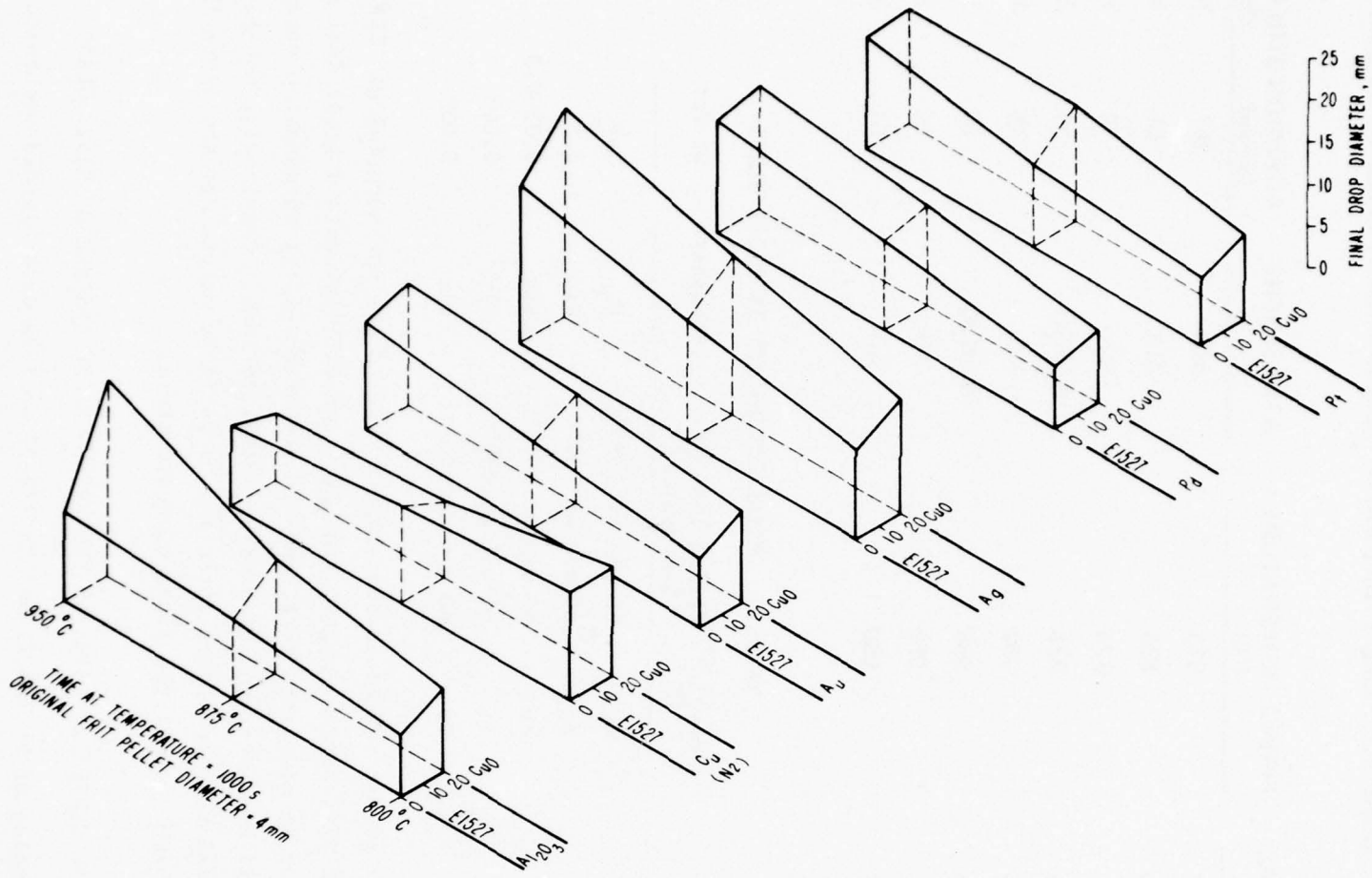

Figure 17. Glaze spreading rates on various substrates, heating time = 1000 s.

TABLE 2. METAL FOIL-TO-E1527 GLAZED CERAMIC ADHESION STRENGTH

METAL	FIRING TEMPERATURE (°C)	ATMOSPHERE	ADHESION STRENGTH (g/mm)	(%V)
Ag	875	AIR	267	10
Au	875	AIR	56	30
Cu	875	N_2	14	39
Cu	875	N_2-H_2O	31	29
Cu	950	N_2	15	27
Cu	950	N_2-H_2O	39	11
Pt	950	AIR	66	18
Pd	950	AIR	51	32

TABLE 3. METAL SOLUBILITY IN E1527 GLASS

Metal	Firing Time and Temperature	Atmosphere	Wt Pct
Cu	60 min at 1050°C	N_2	5.8
Ag	60 min at 930°C	air	3.5
Au	60 min at 1030°C	air	0.03-0.3
Pt	60 min at 950°C	air	0.005
Pd	60 min at 950°C	air	0.038

in E1527 glass, the adhesion strength results are not surprising. The marked strength differences suggest that Ag films will tolerate a great deal more variation in microstructure, and its attendant effect on adhesion strength, than will Au-, Pt-, and Pd-bearing metallizations. Conversely, non-Ag-bearing films will require closer attention to particle morphology and sintering kinetics which control the final microstructure.

F. METAL SINTERING RATES IN THE PRESENCE AND ABSENCE OF E1527 GLASS

Samples of Pt (MB-2) and Pd (MB-3) powders were blended mechanically with sufficient E1527 glass powder to make the final glass volume fraction equal to

10 percent, assuming complete densification. Both the glass-bearing and pure metal powders were then compacted into 12.7-mm (0.5-in.)-diam discs weighing 0.85 g, as previously described [2]. The samples were then fired at 900°C for times ranging from 2 to 300 min. The diametral densification, $\Delta L/L$, data are presented in Fig. 18 for Pt and Pd powders as well as for Au, Cu, and Ag which were previously tested. With the exception of Ag, none of the powders showed improved densification in the presence of glass. In fact, Au, Pt, and Pd all exhibited retrograde sintering or swelling with the extended heating at 900°C. The MJ-3 Ag powder was the only material to show evidence of liquid-phase-assisted densification, despite the appearance of some short-term swelling. Since both Ag and Cu are highly soluble in E1527 glass, there is some question as to why densification in the Cu powder did not improve with the glass addition. The one notable difference, in this powder vs the others, is a rather large median particle size of 10 μm. All of the other powders tested had median particle sizes ranging from 1.5 to 3.0 μm, approximately. Theoretically, liquid-phase transport of Cu or any metal will be reduced as particle size increases.

The densification curves for the MB-1 Au powder indicated that the bulk of the densification occurred at a temperature as low as 500°C. Earlier electrical sheet conductivity measurements of metallizations made with this powder and various volume fractions of E1527 glass added to it showed that maximum conductivity was delayed until the temperature exceeded 500°C; i.e., until the glass was sufficiently fluid to be extruded out of the way by the sintering Au microstructure [1]. Since neither bulk densification, electrical conductivity, nor surface bondability are improved by adding glass directly to the sintering powder, it seemed logical to test the performance of layered structures, i.e., metal over glaze as depicted in Fig. 19, more thoroughly.

G. LAYERED METALLIZATION RESISTIVITY RATIOS

Matthiessen's rule [21] states that the electrical resistivity of a metal is the summation of temperature-dependent and temperature-independent contributions, i.e.,

$$\rho_T = \rho_i + \rho_{ii} \qquad (1)$$

21. N.F. Mott and H. Jones, *The Theory of the Properties of Metals and Alloys* (Dover Publications, N.Y., 1958), p.288.

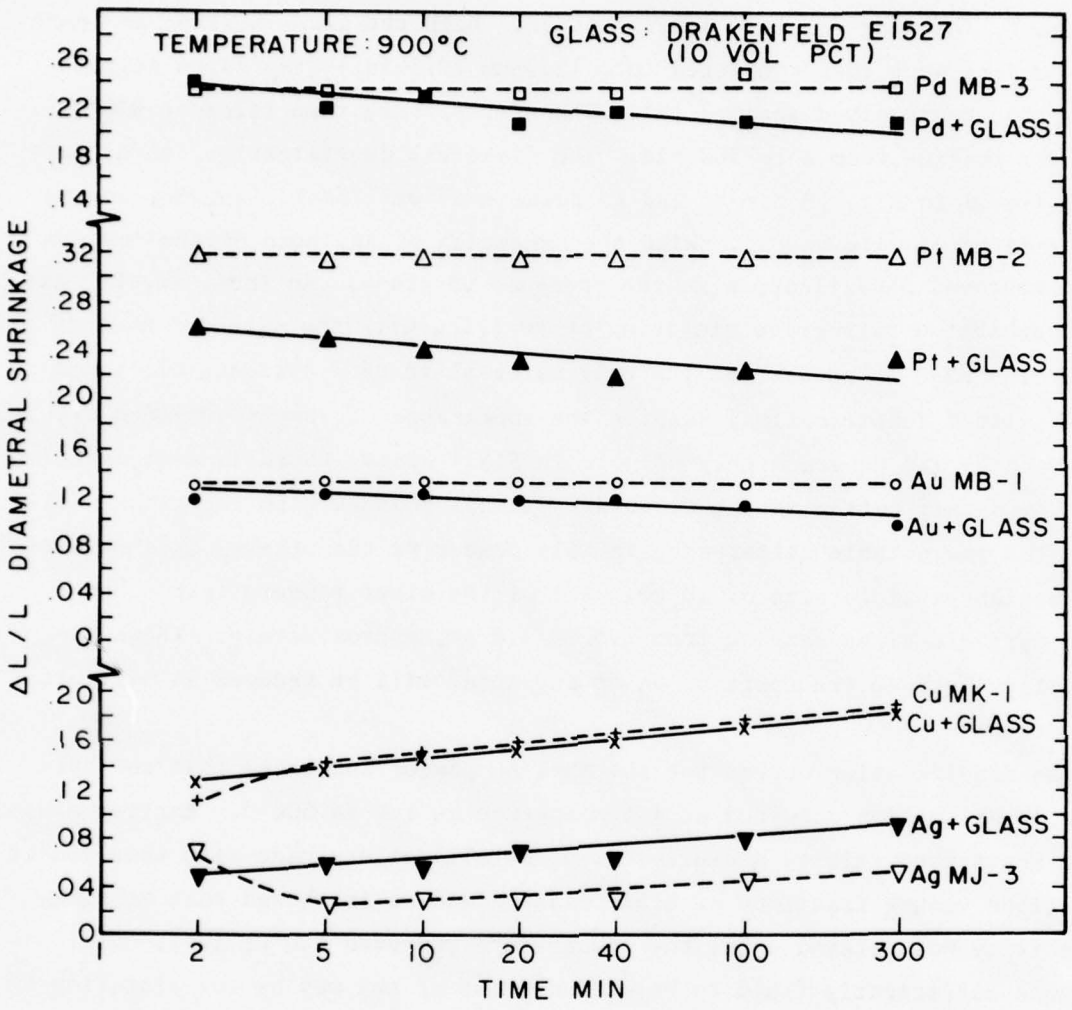

Figure 18. Glass-bearing and metal powder diametral densification data.

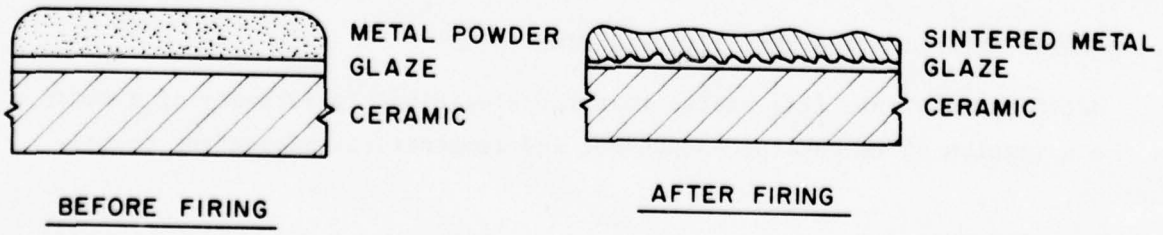

Figure 19. Thick-film layered metallization.

where ρ_i is the temperature-dependent contribution and ρ_{ii} is the temperature-independent contribution. The temperature-dependent contribution results from electron scattering around thermally activated metal atom vibrations, while the temperature-independent contribution is caused by lattice defects, vacancies, solute atoms, grain boundaries, etc. For pure, annealed Au, the resistivity ratio, $R_{300°K}/R_{77°K}$, is approximately 5.1 [22]. This ratio must decrease as lattice defects, grain boundaries, and solute atom impurity concentrations increase.

In order to clarify the reactions occurring between the metal and binder phases of layered metallization, samples were prepared to test the tendency toward impurity level buildup in the Au film. MB-1 Au powder was formulated with VF-1 vehicle and screen-printed onto (a) unglazed alumina (96 wt pct), (b) alumina preglazed with E1527 glass, and (c) alumina preglazed with E1527 glass with 20 wt pct CuO added. Samples of the layered structures were then fired at temperatures of 500°, 750°, and 900°C for 10 minutes each. As shown in Fig. 20, the resistivity ratio increased from approximately 4.5 for samples fired at 500°C to 4.8 when fired at 900°C, for both the unglazed and preglazed alumina substrates. This increase in ratio confirmed that high-temperature annealing decreased the temperature-independent contributions, i.e., sufficient grain growth occurred to substantially reduce lattice defects and grain boundaries. Conversely, the CuO-doped glazed samples showed a distinct decline in the $R_{300°K}/R_{77°K}$ ratio from 4.2 to less than 3.0 when fired at 500° and 900°C, respectively. Therefore, despite the annealing and grain growth which occurred, the temperature-independent contribution increased from alloying between Cu and Au. Since the CuO was presumably reduced and diffused into the Au film, it is then free to diffuse throughout the film. At a lower temperature, as Cu diffuses to the top bonding surface the Cu may reoxidize due to exposure to air, producing a poor bonding surface.

To observe the extent of alloying between Pt and Au, samples containing 75Au(MB-1)-25Pt(MB-2) were prepared and fired on preglazed alumina similar to the pure Au. The sheet resistances and resistivity ratios, presented in Fig. 21, indicate that the alloying is essentially completed at 900°C, but a minimum in

22. G. T. Meaden, *Electrical Resistance of Metals* (Plenum Press, N.Y., 1965), p. 15.

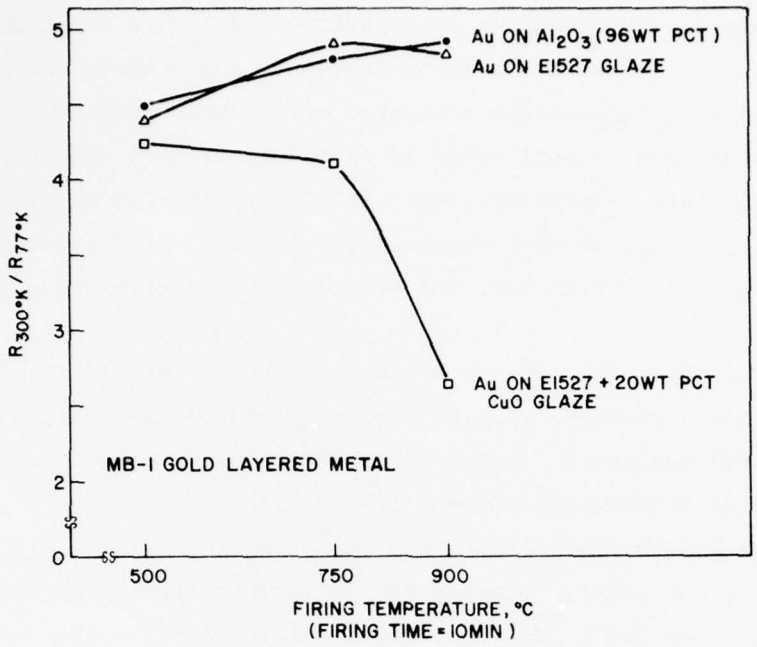

Figure 20. Resistivity ratio data.

sheet resistance occurs in the 700°C-fired samples. The apparently anomalous sheet resistance minimum is better understood by examining the difference in microstructure for the 600°C- and 900°C-fired samples. The photomicrograph of the 600°C-fired microstructure, as shown in transmitted light in Fig. 22, is fairly dense with only occasional voids apparent. Conversely, in the photomicrograph of the 900°C-fired sample, shown in Fig. 23, gross voids are present which result in a more discontinuous network and, therefore, higher electrical resistance. The minimum in sheet resistance could be shifted to higher firing temperatures by preparing Pt powder of sufficiently larger particle sizes so as to reduce the excessive shrinkage which occurs with the MB-2 Pt.

H. SURFACE SOLDERABILITY OF LAYERED METALLIZATION

Prior to determining the adhesion strength of layered alloy metallizations, it is necessary to examine the influence of film thickness and glaze penetration upon surface solderability. The commercial films generally require burnishing, i.e., mechanically abrading the metallization surface to remove surface

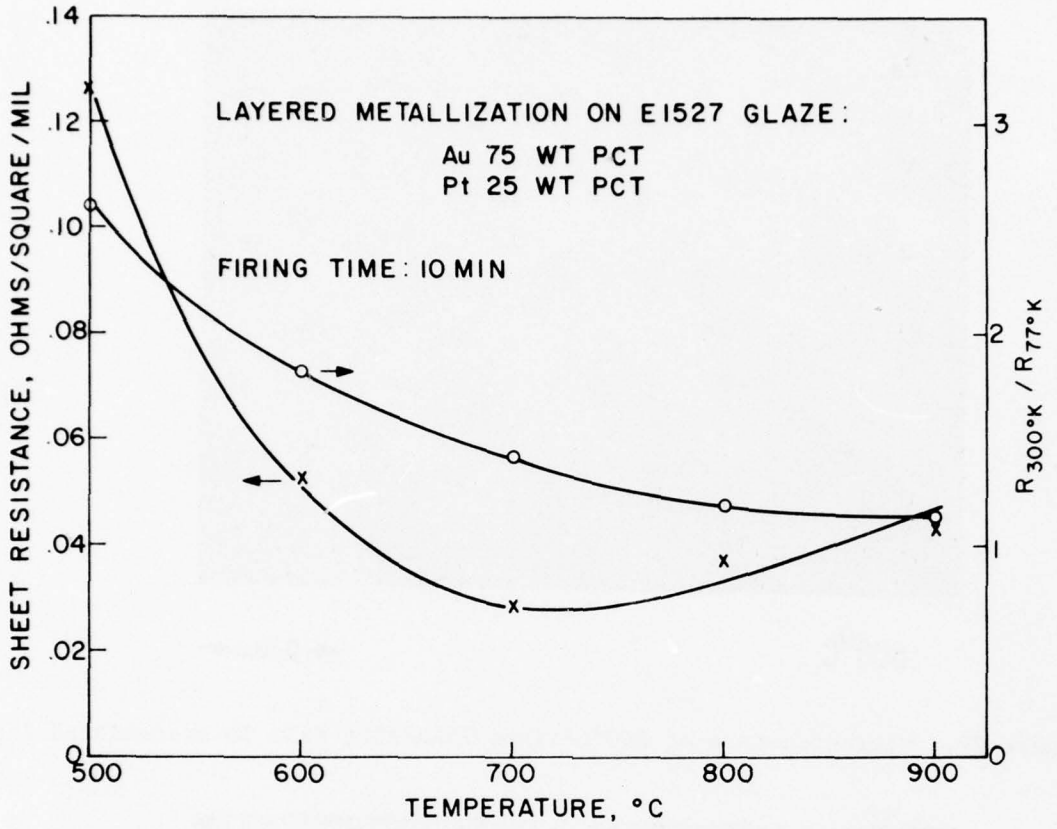

Figure 21. Sheet resistance and resistivity ratio data.

glaze and/or to smear metal over the glaze. This act must influence the apparent adhesion strength by imposing high stresses at localized sites on and beneath the metallization surface.

If the true adhesion strength between metal powders and glazes is to be accurately determined, it must be accomplished without uncontrolled mechanical stressing of the film prior to the actual test. By providing a layered structure of appropriate thickness, surface solderability can be maintained, while avoiding the customary burnishing operation. However, where thick-film, conductor alloying during firing is necessary in metallizations which are to be soldered, in order to avoid undesirable dissolution of soluble constituents in the solder, the required firing time and temperature to accomplish this may be excessive in terms of glaze migration to the soldering surface. Prolonged heating will result in an overglazing of the metallization, and, as a result, solderability will be reduced.

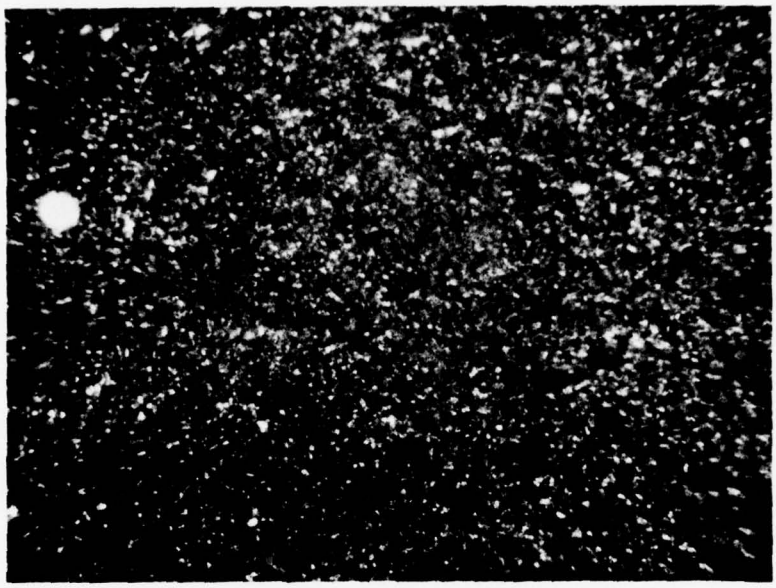

Figure 22. Microstructure of 600°C-fired 75Au-25Pt film in transmitted light.

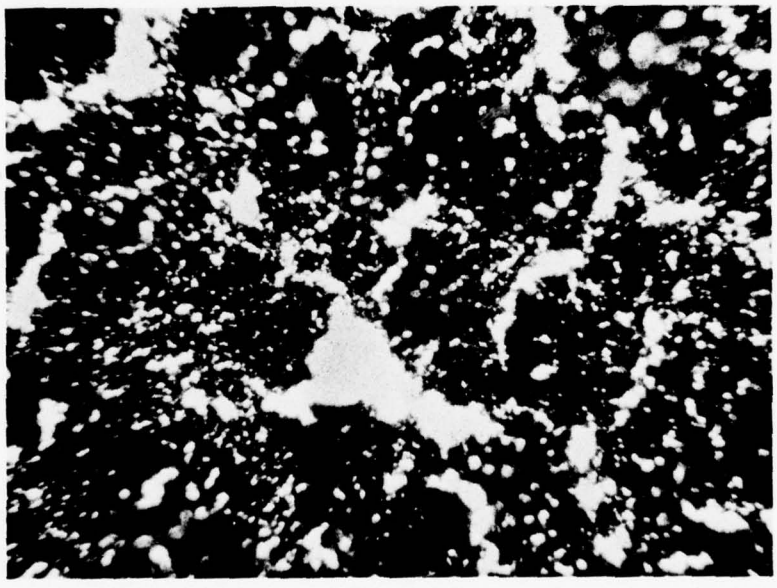

Figure 23. Microstructure of 900°C-fired 75Au-25Pt film in transmitted light.

As a preliminary test for solderability, small samples of 60Sn-40Pb solder were cut from solid wire [0.8-mm (0.032-in.)-diam] stock to a weight of 0.008 g. The sample weight spread was approximately 2.5 percent of the average weight. These solder samples were dipped into Kester 1544 solder flux (activated resin) and applied to the center of 0.5-mm (0.020-in.)-wide line on the Au-Pt layered metallization test substrates. These assemblies were then placed on a hotplate at a temperature of 216° ± 4°C. Upon reaching the solder liquidus temperature (generally 30 to 40 s after contact), a 5-s exposure to the 216°C hotplate was permitted before quickly transferring the sample to a cold brass block. Contact angles and length of solder spread were then determined.

The 500°C-fired samples were all quickly dissolved by the Sn-Pb solder, leaving the preglazed underlayer exposed. This result is attributed to the minor degree of sintering and alloying between the Au and Pt powders. Since a high surface area accelerates dissolution rates, the solder was capable of reacting very rapidly with the available metal. The 600° to 900°C samples were not dissolved by the solder. In fact, wetting of the metallizations became progressively more difficult for samples fired at temperatures above 600°C, as shown in Table 4. This loss of wetting coincides with the overglazing which results when the layered structure is heated to temperatures high enough for the glass to be sufficiently fluid to wet the adjacent metal film.

TABLE 4. WETTABILITY OF SOLDER ON Au-Pt LAYERED METALLIZATION AND ALUMINA

Substrate	Firing Temperature (°C)	Contact Angle (degrees)	Solder Spread (mm)
Metallization	500	-	-
Metallization	600	16	8.8
Metallization	700	65	2.1
Metallization	800	143	0.6
Metallization	900	136	0.6
Alumina (96 wt pct)		147	0.7

X-ray diffraction determinations of lattice constants for Au-Pt and Au-Pt-Pd alloys, shown in Table 5, indicate that higher temperatures are needed to complete the alloying reactions in reasonable times, e.g., 10 min. From the resistivity ratio curve, shown in Section II.G, which leveled off at 900°C, and the x-ray diffraction results, it is clear that films have to be fired at 900°C or more in order to produce an alloy resistant to dissolution by solder. It is believed that commercial inks are also composed of mixtures of precious metals, so the same alloying requirements pertain to them.

To determine the required metal film thickness as a function of firing temperature on E1527-glazed substrates, additional contact angle measurements were made. Films of variable print thickness were fired between 600° and 900°C on 4-μm-thick E1527-glazed alumina (96 wt pct) substrates for 10 min. The contact angles were determined after developing a solder reflow process which utilized hot air, Kester 1544 flux, and 60Sn-40Pb solder balls measuring 1.02 mm (0.040 in.) in diameter. A 25.4-cm (10-in.)-diam aluminum disc (rotating at 0.6 rpm) was used as the support fixture for the fluxed solder ball and substrate.

TABLE 5. X-RAY DIFFRACTION DETERMINATION OF LATTICE CONSTANTS FOR POWDER COMPACTS*

	80Au-20Pt		80Au-10Pt-10Pd	
	600°C	900°C	600°C	900°C
Phase (1)	4.077 Å 99Au-1Pt**	4.047 Å 79.7Au-20.3Pt	Same as (1) in 80Au-20Pt	4.032 Å cubic alloy
Phase (2)	4.043Å 77Au-23Pt	-	Same as (2) in 80Au-20Pt	
Phase (3)	3.9231 Å Pt Intensity 1/4 to 1/5 of (2) and (3)	3.9231 Å Pt 5 pct or less of total volume	Pt	
(4)	PdO Pt and PdO are weaker than (1) and (2)			

*Fired for 10 min at temperature.

**Table compositions are in atomic pct and are deduced from Vegard's law which hold for substitutional solid solutions, i.e., the stated alloy is implied from the noted lattice constant.

A Sylvania* serpentine gas heater (Part No. 114682, 470 W) with 8.4-mm (0.330-in.)-diam orifice was used to heat the air which was directed orthogonally to the substrate bearing the solder ball. The following parameters, achieved after several trials, produced reasonable flow of the solder ball on the metallized surface:

Gas heater orifice-to-substrate distance	:	3.5 mm
Air flow rate (SCFH)	:	5
Variac voltage	:	90
Air temperature at heater exit orifice	:	817°C
Number of passes under heater	:	1

Examples of solderable and non-solderable surfaces, shown in Figs. 24 and 25, respectively, illustrate the dramatic change in contact angle which occurs on surfaces with little and large amounts of overglazing, respectively.

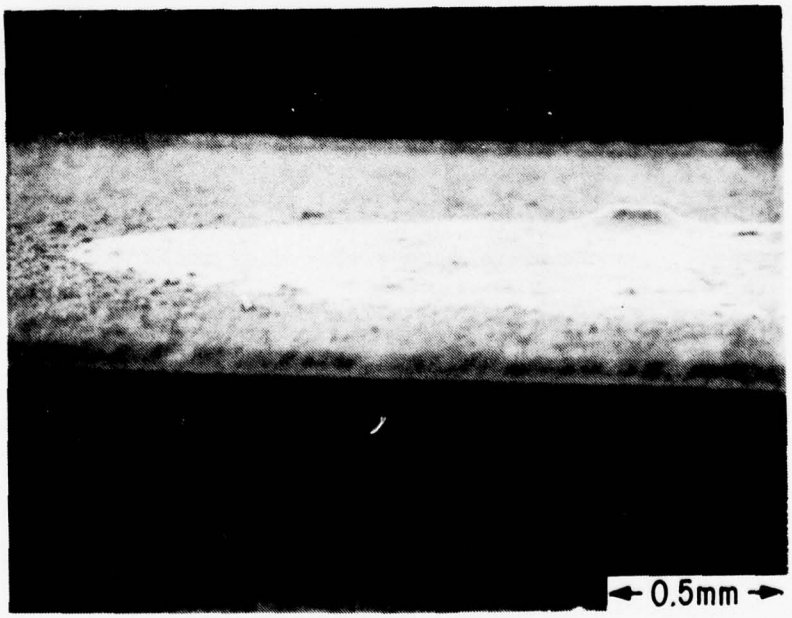

Figure 24. Reflowed solder on 75Au-12.5Pt-12.5Pd layered metallization fired at 600°C for 10 min. and cooled rapidly. Extremely high solderability is indicated by low contact angle.

*GTE Sylvania, Inc., Exeter, N.H.

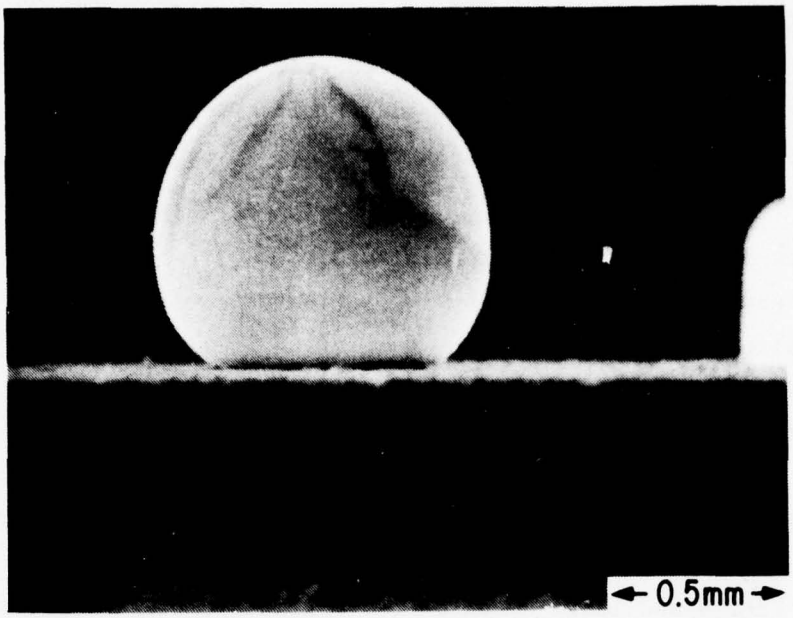

Figure 25. Reflowed solder on 75Au-12.5Pt-12.5Pd layered metallization fired at 900°C for 10 min and cooled rapidly. Extremely poor solderability is indicated by high contact angle.

Two metallization compositions were prepared by mechanically blending the appropriate powders, e.g., MB-1 Au, MB-2 Pt, and MB-3 Pd. The 75Au-25Pt and 75Au-12.5Pt-12.5Pd mixtures were then dispersed in a proprietary vehicle, Code No. VF-1, and screen printed to achieve variable fired thicknesses on the E1527-glazed alumina (96 wt pct) substrates. The Pt and Pd concentrations, were increased in each system over that listed in Table 5 to amplify the tendency for oxides to form during firing. While a particular alloy may be thermodynamically stable and have achieved equilibrium within 10 min at temperature, some portions of the oxidizable metal may oxidize on cooling from the peak firing temperature. The rate of cooling and alloy composition would then determine the degree to which oxides would form. Initially, these compositions were fired from 600° to 900°C on unglazed ceramic, cooled rapidly from the tube furnace, and found to be completely wettable by solder. At the extreme temperatures, i.e., 600° and 900°C, some of the alloy was dissolved by the solder. Apparently, the 600°C-fired material contained unalloyed gold and was

readily attacked by the molten solder. The 900°C-fired material, sintered in the absence of glaze, delaminated from the substrate. Thus in poor thermal contact with the alumina substrate, the solder reached higher temperatures, i.e., approaching the hot air temperature of 800°C, and the solder was able to dissolve some of the thick films under these conditions. Under the same cooling rate on the glazed ceramic substrates, however, solderability rapidly deteriorates with increasing firing temperature as shown in Figs. 26 and 27, for 75Au-25Pt and 75Au-12.5Pt-12.5Pd metallizations, respectively. Thus, whatever oxide, e.g., PdO, that may have formed on cooling was easily reduced

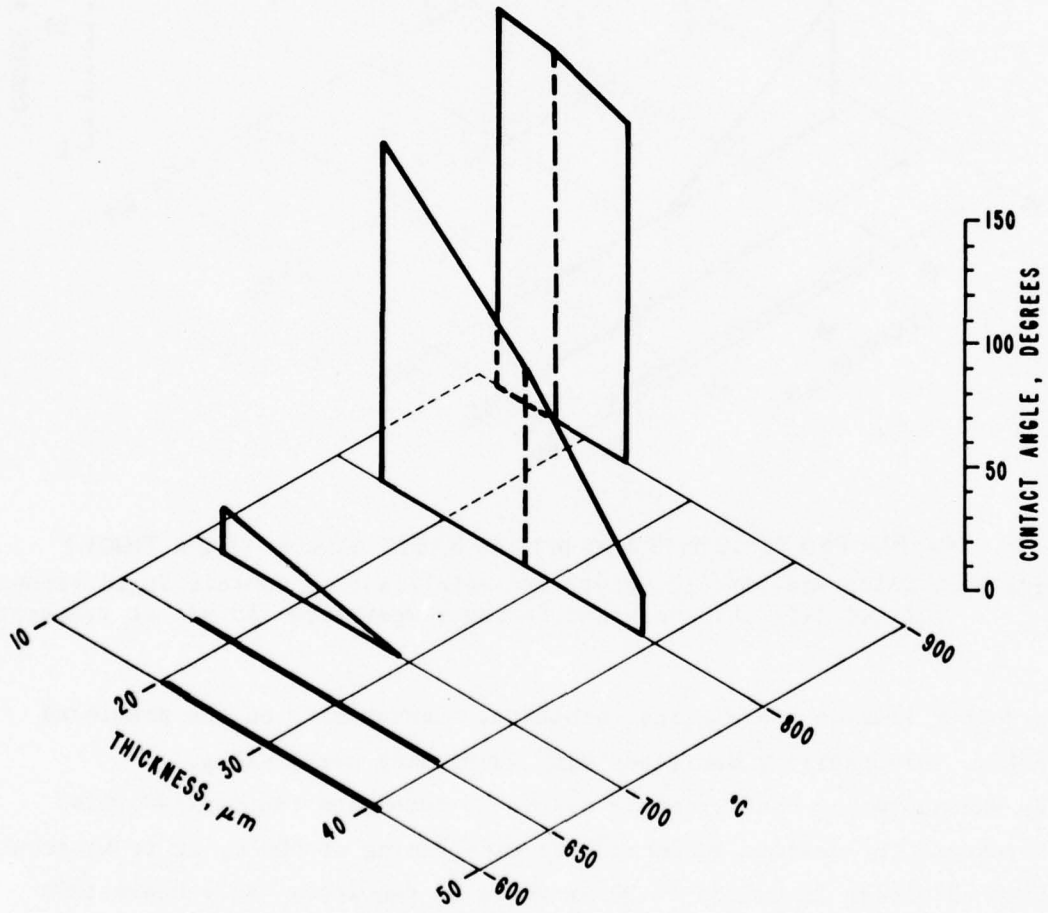

Figure 26. Solder-to-75Au-25Pt metallization contact angle versus fired film thickness and firing temperature (10 min at temperature).

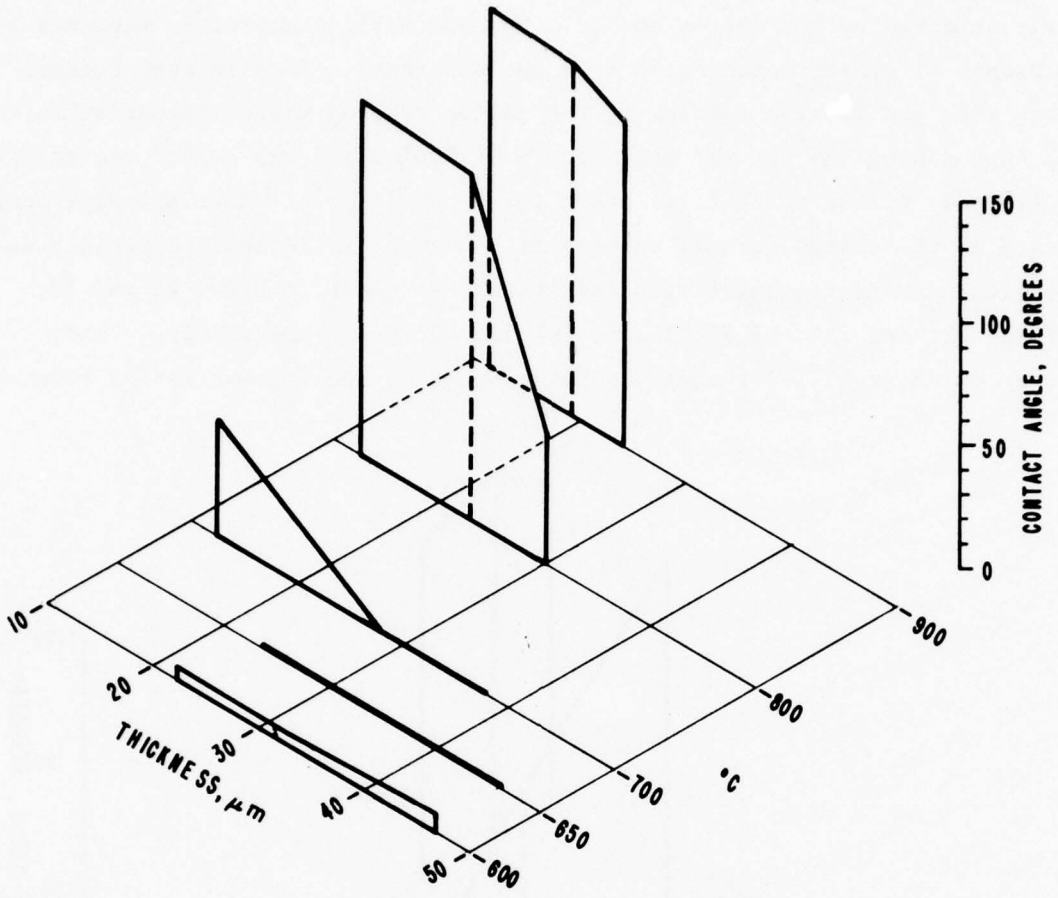

Au-Pt-Pd (75-12.5-12.5 wt pct) on E1527 GLAZE (4 μm THICK)

Figure 27. Solder-to-75Au-12.5Pt-12.5Pd metallization contact angle versus fired film thickness and firing temperature (10 min at temperature).

by the solder flux on the alumina substrate. Conversely, on the preglazed substrates, solderability decreased with increasing overglazing.

By extrapolating contact angle slopes to determine the desired metal film thickness for maximum solderability with firing at 900°C, it is apparent that film thickness in excess of 50 μm would be required. To achieve this fired thickness, dried print thickness must exceed 0.1 mm (0.004 in.). Alternatively, a modified glaze composition with higher viscosity at 900°C could be utilized, and this approach is discussed in Sections II.J and II.K below.

I. METALLIZATION MICROSTRUCTURES

The metallization microstructure, which is chiefly responsible for adhesion strength variations, differs in the two metallizations 75Au-25Pt and 75Au-12.5Pt-12.5Pd, as shown in Figs. 28 and 29, respectively. Note that the Au-Pt-Pd film is slightly less dense, as indicated in Fig. 29 by the greater number of pores, than the Au-Pt film. The contact angles for solder on Au-Pt-Pd metallization were slightly higher than those of the Au-Pt films. This decreased solderability is attributed to the greater number of pores present in the Au-Pt-Pd film, since more channels are available for glass migration to the top surface. The decreased density in the Au-Pt-Pd metallization may be attributed to two possible causes: (a) the tendency for Pd to oxidize below 800°C, which would retard densification as shown in the isothermal densification curves in Fig. 11, and (b) decreased interdiffusion rates, i.e., higher activation energies for the three species in the alloyed solid state, since liquid-phase assisted densification is not operative with these metals.

In either case, Pd appears to slow the densification process somewhat, and this retardation results in a more open, porous microstructure. Defining

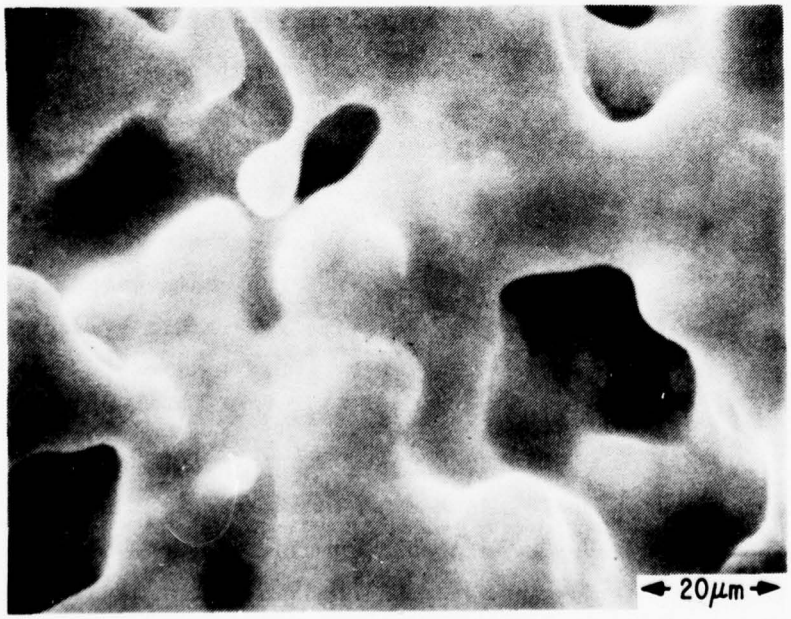

Figure 28. Top surface of 75Au-25Pt metallization fired at 900°C for 10 min.

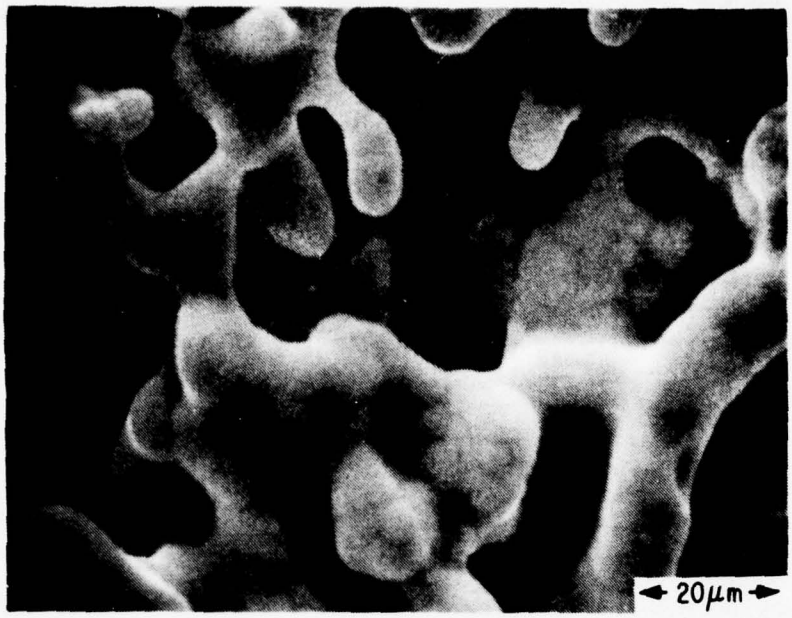

Figure 29. Top surface of 75Au-12.5Pt-12.5Pd metallization fired at 900°C for 10 min.

the optimal microstructure-adhesion strength relationship depends upon producing a solderable surface with reasonable thickness.

J. LAYERED METALLIZATION ADHESION STRENGTH - PRELIMINARY TEST WITH MODIFIED GLAZE

Because of the inability to obtain a fully solderable surface fired at the 900°C alloying temperature with the E1527 glaze, the glaze composition was modified by adding alumina to increase the viscosity and retard glaze migration. An initial addition of 5 wt pct Al_2O_3 to E1527 glass frit was mechanically blended, dispersed in a proprietary vehicle, screen printed, and fired on alumina (96 wt pct) substrates. Glazing temperatures of 900° and 950°C were tried with firing times of 1, 5, and 10 minutes. Alumina dissolution in the E1527 glass was enhanced by utilizing a particularly fine particle size material, i.e., 0.05 μm, Linde "B" metallographic polishing powder. While complete homogenization of the melt was not expected under these conditions, the alumina addition provided sufficient upward adjustment in glaze viscosity to enable soldering to the 75Au-25Pt metallization without burnishing.

After glazing 2-mm (0.080-in.)-diam dots onto the ceramic substrates 1-mm (0.040-in.)-diam 75Au-25Pt metallization dots were screen printed and fired at 900°C for 1, 2, and 5 min. A tensile test was utilized to determine adhesion strength and was accomplished by joining a 0.8-mm (0.032-in.)-diam copper pin orthogonally to the metallization dot. The 1-mm (0.040-in.)-diam 60Sn-40Pd solder balls were first reflowed on the metallization dots using the hot air flow method with the following parameters:

Gas heater orifice-to-substrate backside distance, mm	:	5
Air flow rate (SCFH)	:	10
Turntable, rpm	:	0.6
Variac voltage	:	100
Number of passes by heater	:	2

Subsequently the copper pins were attached, also by reflow soldering, while held in a brass jig which retained pin perpendicularity within 0.6°. Heating parameters were identical to the contact angle solder ball reflow described above with two exceptions: (a) air flow was from the front side and aimed at the pin-solder ball interface at an angle of 45° to the substrate, and (b) heater orifice-to-target distance was 10 mm. After removal of the soldering jig, hooks were bent in the free ends of the copper pins, and the tensile loads to induce failure were determined in an Instron Tensile Test Machine at a strain rate of 12.5 mm (0.5 in.)/min.

Preliminary results which represent averages for three samples or less, are presented in Table 6 for the glaze and metal firing combinations examined. The highest strengths occur at the longest metal firing time, i.e., 5 minutes, on both of the 900° and 950°C glazed substrates, being 2.9 and 3.4 kg/mm^2, respectively. Since it is known that the metal microstructure forms in less than 5 min at 900°C, based on the isothermal densification curves determined earlier, the strength increase that occurs with time must be related to the amount of glaze penetration into the microstructure.

Future evaluations should use identical glaze and metal dot diameters, since a portion of the periphery of each metal dot was overglazed due to the thinner edge and greater quantity of glass at this junction. As a result, the

TABLE 6. ADHESION STRENGTH OF 75Au-25Pt ALLOY ON E1527 + 5 wt pct Al_2O_3 GLAZE

	Metal Firing Time at 900°C					
	1 Minute		2 Minutes		5 Minutes	
Glaze Firing Time at 900°C	Film Thickness (μm)	kg/mm^2 (ksi)	Film Thickness (μm)	kg/mm^2 (ksi)	Film Thickness (μm)	kg/mm^2 (ksi)
1 minute	21	*	19	1.57 (2.23)	18	*
5 minutes	22	1.42 (2.02)	16	2.58 (3.67)	19	2.39 (3.40)
10 minutes	19	1.52 (2.16)	16	2.71 (3.85)	20	2.89 (4.11)
Glaze Firing Time at 950°C						
1 minute	19	2.45 (3.48)	19	2.04 (2.90)	18	2.56 (3.64)
5 minutes	21	2.36 (3.35)	18	3.03 (4.31)	17	*
10 minutes	20	2.85 (4.05)	20	2.69 (3.82)	18	3.35 (4.76)

*Off scale, loads not recorded.

apparent strengths contain a cohesive component caused by tearing of the metallization at the soldered-metal-to-unsoldered-metal interface. This region is depicted in Fig. 30, which shows a portion of the glazed dot overlaid by the remaining portions of the torn metallization.

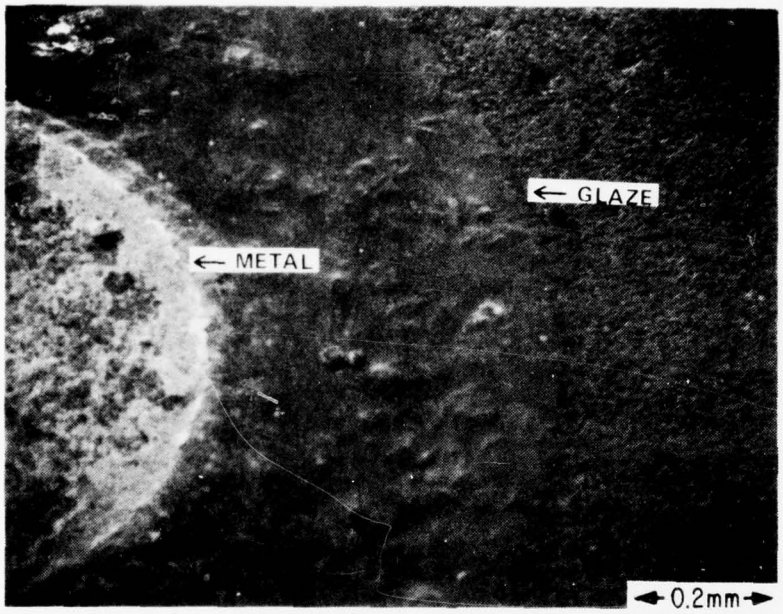

Figure 30. Portions of layered metallization tensile test dot on substrate glazed with E1527 + 5 wt pct Al_2O_3.

K. MODIFIED GLAZE EFFECTS ON SOLDERABILITY AND ADHESION STRENGTH

The effects upon solder wetting of 5 wt pct Al_2O_3 additions to the E1527 glaze were examined on both metallization systems, i.e., 75Au-25Pt and 75Au-12.5Pt-12.5Pd. However, two preglazing times, i.e., 5 and 10 minutes, were used in conjunction with metal firing times of 1, 2, and 5 minutes, respectively. Solder ball contact angles were again observed and found to differ for the two metal systems as shown in Table 7. Au-Pt appears to be less rapidly overglazed than Au-Pt-Pd. Furthermore, extended preglazing time tends to improve solder wetting for the longer metal firing times. This result was expected, since longer preglazing time provides for more dissolution of alumina

TABLE 7. SOLDER WETTING OF METALLIZATION AS FUNCTION OF FIRING CONDITIONS ON E1527 + 5 wt pct Al_2O_3 PREGLAZED SUBSTRATES

Glaze fired at 950°C for	1 Minute				2 Minutes				5 Minutes			
	75Au-25Pt		75Au-12.5Pt-12.5Pd		75Au-25Pt		75Au-12.5Pt-12.5Pd		75Au-25Pt		75Au-12.5Pt-12.5Pd	
	Thickness, μm	Contact angle, degrees	Thickness, μm	Contact angle, degrees	Thickness, μm	Contact angle, degrees	Thickness, μm	Contact angle, degrees	Thickness, μm	Contact angle, degrees	Thickness, μm	Contact angle, degrees
5 minutes	27	7	21	31	24	19	19	106	20	74	21	128
10 minutes	25	8	21	37	22	20	19	76	21	32	17	126

and the resultant increase in glass viscosity. With increased glass viscosity, penetration into the metal microstructure is retarded.

The effect of additions of alumina, i.e., 5 and 10 wt pct to E1527 glass was examined for the Au-Pt-Pd system, which was the most readily overglazed one. Table 8 shows higher initial alumina concentrations generally result in improved wetting. Some discrepancy exists for the longer firing time, highest alumina concentration samples, however, and is not yet understood.

A partial test matrix based on preglazing and metal firing times as well as glaze composition was completed to determine the effect of these variables on Au-Pt-Pd adhesion strength. Table 9 shows the results of this phase of the study. At first glance it appears that higher initial alumina content improves the adhesion strength. However, upon computing R, which is the ratio of the difference between the sample means to the standard error of the difference* [23], it was shown (see Table 10) that the strength differences are statistically insignificant.

* $R = \left(\bar{x}_1 - \bar{x}_2\right) \Big/ \left(\sigma_1^2/n_1 + \sigma_2^2/n_2\right)^{1/2}$

where $\bar{x}_1$ and $\bar{x}_2$ are sample means,
σ_1^2 and σ_2^2 are variances, i.e., the squares of the standard deviation,
n_1 and n_2 are sample sizes;
when $R < 2$, not significant
$R > 2$, probably significant
$R > 3$, definitely significant

23. M.J. Moroney, *Facts from Figures* (Penguin Books, New York, 1975), p.220-221.

TABLE 8. SOLDER WETTING OF 75Au-12.5Pt-12.5Pd METALLIZATION AS A FUNCTION OF FIRING CONDITIONS AND Al_2O_3 CONCENTRATION IN E1527 GLAZE

		Metal Fired at 900°C for					
		1 Minute		2 Minutes		5 Minutes	
Preglazed at 950°C for	% Al_2O_3 in E1527	Thickness, µm	Contact angle, degrees	Thickness, µm	Contact angle, degrees	Thickness, µm	Contact angle, degrees
5 minutes	5	20.8	31	19.2	105.5	21	128
	10	19.8	<2	25.8	5.3	21.8	26.5
	15	31.6	<2	25.6	23.5	22.5	88.6
10 minutes	5	20.7	37	19.3	75.5	16.7	125
	10	26.1	<1	21.4	6.5	25	26.5
	15	24.8	3.5	27.0	17.7	23.7	43.8

TABLE 9. ADHESION STRENGTH OF 75Au-12.5Pt-12.5Pd METALLIZATION AS A FUNCTION OF FIRING CONDITIONS AND Al_2O_3 CONCENTRATION IN E1527 GLAZE

		Metal fired at 900°C for					
		1 Minute		2 Minutes		5 Minutes	
Preglazed at 950°C for	% Al_2O_3 in E1527	Thickness, µm	Adhesion Strength, kg/mm^2 (ksi)	Thickness, µm	Adhesion Strength, kg/mm^2 (ksi)	Thickness, µm	Adhesion Strength, kg/mm^2 (ksi)
1 minute	5	17.2	0.79 (1.12)	17.2	1.38 (1.96)	15.2	1.55 (2.20)
	10					19.7	2.64 (3.75)
	15					21.6	2.00 (2.84)
5 minutes	5	22.2	0.79 (1.12)	20.7	1.43 (2.03)	16.5	1.36 (1.93)
	10					21.3	1.80 (2.56)
	15					21.6	2.00 (2.84)
10 minutes	5	22.5	1.15 (1.63)	22.0	1.60 (2.27)	18.3	2.04 (2.90)
	10					21.7	2.02 (2.87)
	15					17.5	2.20 (3.13)

TABLE 10. ADHESION STRENGTH R VALUES, E1527 + 10 wt pct Al_2O_3 AND E1527 + 15 wt pct Al_2O_3, AND PREGLAZING TIME vs 75Au-12.5Pt-12.5Pd ON E1527 + 5 wt pct Al_2O_3

Preglazing Time, Minutes	E1527 + 10 wt pct Al_2O_3	E1527 + 15 wt pct Al_2O_3
1	0.7	2.1
5	0.4	0.7
10	0.02	0.1

It was also found that greater concentrations of dissolved alumina tended to produce what appeared to be a devitrified deposit. Therefore subsequent sample preparation and testing was limited to a glass consisting of E1527 plus 5 wt pct Al_2O_3.

L. THERMAL AGING EFFECTS ON METALLIZATION ADHESION STRENGTH

In designing a test matrix with 5 wt pct Al_2O_3 added to the E1527 glass, some attempt was made to compensate for the overglazing tendency by double printing the metal deposit; i.e., the deposition sequence was print, dry, print, dry and fire. Samples of both 75Au-25Pt and 75Au-12.5Pt-12.5Pd were screen printed onto 96 wt pct alumina substrates preglazed for 10 min at 950°C with the E1527 + 5 wt pct Al_2O_3 composition, which was nominally 4 μm thick when fired. The metal deposits were subsequently fired at 500°C for 2 min (for binder burnout) plus 5 min at 900°C. Copper pins were soldered to the 1-mm (0.040-in.)-diam metallization dots as previously described. Both soldered and unsoldered metallization dots were aged for 10 and 500 h at 150° ± 1°C in an environmental chamber* with circulating air. Metallization adhesion strength was determined as previously described and the fracture interfaces examined to assess the amount of metallization remaining on the substrate.

*Delta Design, Inc., Model MK 3900, La Mesa, Calif.

Tables 11 and 12 summarize the tensile test values of adhesion strength for the Au-Pt and Au-Pt-Pd films, respectively. In comparison, the R values (Table 13) show the adhesion strength differences between the adhesion of Au-Pt and Au-Pt-Pd to be generally statistically insignificant. In the one case, i.e., single print, aged 10 h without solder, where a significant difference does occur, the 85 percent greater strength for the Au-Pt-Pd film (Table 14) appears to be related to a 34 percent greater film thickness, as shown in Table 15. Unaged adhesion strength appears to be less sensitive to thickness variation, of the same magnitude, since an equivalent thickness difference, 36 percent, in the single-print sample showed insignificant strength differences.

TABLE 11. 75Au-25Pt THERMALLY AGED ADHESION STRENGTH

Time, hours	Single Print: Adhesion Strength kg/mm^2 (ksi)	Single Print: %V/n	Single Print: Film Thickness, μm	Double Print: Adhesion Strength kg/mm^2 (ksi)	Double Print: %V/n	Double Print: Film Thickness, μm
Aged with Solder						
0	1.81 (2.57)	48.2/6	11.8	2.52 (3.58)	32.1/8	19.6
10	2.06 (2.93)	21.1/9	12.7	2.29 (3.26)	24.2/9	19.7
500	0.79 (1.12)	53.7/10	12.7	0.83 (1.18)	40.7/10	19.7
Aged without Solder						
0	1.81 (2.57)	48.2/6	11.8	2.52 (3.58)	32.1/8	19.6
10	1.34 (1.91)	25.6/6	12.2	2.89 (4.12)	20.2/8	20.9
500	0.76 (1.08)	73.6/9	13.8	2.07 (2.94)	29.7/9	20.9

* %V = 100 x (standard deviation/mean); n = sample size.

TABLE 12. 75Au-12.5Pt-12.5Pd THERMALLY AGED ADHESION STRENGTH

Aged with Solder

Time, hours	Single Print: Adhesion Strength, kg/mm^2 (ksi)	Single Print: %V/n*	Single Print: Film Thickness, µm	Double Print: Adhesion Strength, kg/mm^2 (ksi)	Double Print: %V/n	Double Print: Film Thickness, µm
0	2.00 (2.85)	37.7/12	16	2.39 (3.40)	26.6/12	22.5
10	2.16 (3.07)	19.1/11	15.6	1.87 (2.67)	32.3/12	22.7
500	0.50 (0.71)	76.4/8	13.9	0.48 (0.68)	89/8	20.3

Aged without Solder

0	2.00 (2.85)	37.7/12	16	2.39 (3.40)	26.6/12	22.5
10	2.48 (3.53)	31/9	16.4	2.82 (4.01)	22.8/12	21.9
500	0.65 (0.93)	66.4/7	14.4	1.32 (1.88)	70.6/8	19.9

*%V = 100 x (standard deviation/mean); n = sample size.

TABLE 13. ADHESION STRENGTH R VALUES 75Au-25Pt vs 75Au-12.5Pt-12.5Pd

Time, hours	Aged with Solder: Single Print	Aged with Solder: Double Print	Aged without Solder: Single Print	Aged without Solder: Double Print
0	0.5	0.4	0.5	0.3
10	0.5	1.7	3.9	0.3
500	1.5	1.9	0.4	1.9

TABLE 14. ADHESION STRENGTH DIFFERENCES IN PERCENT BASED ON 75Au-25Pt VALUES

Time, hours	Aged with Solder		Aged without Solder	
	Single Print	Double Print	Single Print	Double Print
0	+ 10.0	- 5.2	+ 10.0	- 5.2
10	+ 4.9	- 18.3	+ 85.1	- 2.4
500	- 37.0	- 42.2	- 14.5	- 36.2

TABLE 15. FILM THICKNESS DIFFERENCES IN PERCENT BASED ON 75Au-Pt VALUES

Time, hours	Aged with Solder		Aged without Solder	
	Single Print	Double Print	Single Print	Double Print
0	+ 35.6	+ 14.8	+ 35.6	+ 14.8
10	+ 22.8	+ 15.2	+ 34.4	+ 4.8
500	+ 9.4	+ 3.0	+ 4.3	- 4.8

However, when comparing adhesion strength losses as a function of aging time, significant changes are evident for both metal systems as seen in Tables 16 and 17 for Au-Pt and Au-Pt-Pd, respectively. Aging with solder and without solder produces significant strength losses at 500 h, but not 10 h. Furthermore, Au-Pt-Pd strength losses are more significant than the Au-Pt losses at this aging time, with and without solder. In comparing metal remaining on the substrate after tensile testing (Table 18), the aged-without solder Au-Pt-Pd films always showed less metal remaining on the substrate than the Au-Pt films. This relationship was also true even for the 10-h-aged-with-solder films. Only with the extreme 500-h-aged-with-solder samples does metal removal show equal amounts for both film compositions.

In analyzing the significance of aging with and without solder, Table 19 shows aging with solder produces a generally significant loss in adhesion for the double print or thicker deposits of both films. For the thinner, single-print films the change is generally insignificant. Since both single and double print films approach a common minimum adhesion strength upon aging

TABLE 16. R VALUES OF ADHESION STRENGTH CHANGE FROM TIME ZERO FOR 75Au-25Pt vs AGING TIME

Time, hours	Aged with Solder		Aged without Solder	
	Single Print	Double Print	Single Print	Double Print
10	0.7	0.7	1.2	0.9
500	2.7	5.5	2.6	1.1

TABLE 17. R VALUES OF ADHESION STRENGTH CHANGE FROM TIME ZERO FOR 75Au-12.5Pt-12.5Pd vs AGING TIME

Time, hours	Aged with Solder		Aged without Solder	
	Single Print	Double Print	Single Print	Double Print
10	0.6	2.1	1.4	1.6
500	5.9	8.0	5.0	2.8

TABLE 18. VISUAL ESTIMATE OF METAL REMAINING ON CERAMIC IN PERCENT AFTER TENSILE TEST

	Aged with Solder				Aged without Solder			
	Single Print		Double Print		Single Print		Double Print	
Time, hours	75Au-25Pt	75Au-12.5Pt-12.5Pd	75Au-25Pt	75Au-12.5Pt-12.5Pd	75Au-25Pt	75Au-12.5Pt-12.5Pd	75Au-25Pt	75Au-12.5Pt-12.5Pd
0	93	23	39	23	93	23	39	23
10	28	6	7	1	97	28	44	15
500	1	1	1	1	92	75	52	12

TABLE 19. ADHESION STRENGTH R VALUES - AGED WITH SOLDER vs AGED WITHOUT SOLDER

Time, hours	Single Print		Double Print	
	75Au-25Pt	75Au-12.5Pt-12.5Pd	75Au-25Pt	75Au-12.5Pt-12.5Pd
10	3.6	1.1	2.2	3.3
500	0.1	0.7	5.4	2.3

(0.5 kg/mm^2 for Au-Pt-Pd and 0.8 kg/mm for Au-Pt), the statistical significance accruing to the thicker deposits merely derives from the higher initial strengths over the thinner deposits.

The above comparisons confirm that in these experiments Pd-bearing Au-Pt films were found to be more prone to adhesion strength loss than non-Pd-bearing Au-Pt films. Indeed strength losses are evident even in the absence of solder when aged in circulating air at 150°C. These non-solder-dependent adhesion losses suggest other mechanisms than Sn diffusion (Refs. 13 through 17) are operative in causing adhesion loss and subsequent delamination of the bulk of the film. These mechanisms can include low-temperature oxidation of Pd with subsequent volumetric expansion and separation at the metal-glass interface as well as low-temperature annealing processes or strain relief which cause localized disruption at the metal-glass boundary. Furthermore, compositional inhomogenities may cause metal migration to occur via fast diffusion paths such as free surfaces, and probably, glass/metal phase boundaries. If the metal interdiffusion coefficients differ sufficiently, voids may appear at various sites in the microstructure, including glass-metal interfaces.

Since there is an economic advantage to substituting Pd for Pt in solderable metallizations, attention should be devoted to improving the understanding of failure mechanisms related to Pd-bearing systems. Specific consideration should be given to solder- and non-solder-dependent influences. It is conceivable that pre-alloying the compositions, not simply coprecipitating metal powders, may eliminate the compositional heterogeneities which are believed to be responsible for some of the non-solder-dependent component of adhesion loss.

It is also plausible to assume improvements can be attained in minimizing solder-dependent adhesion loss by refinements in powder particle size and shape distributions. By balancing the open microstructure needed to maximize adhesion strength with the need to minimize such rapid diffusion paths to retard Sn migration, improvements in adhesion strength retention may be expected. Study of the sintering kinetics and porosity of various metal powders will probably be one of the most fruitful areas for product improvement.

Finally, but not least in importance, adhesive agent composition must continue to be studied. As the commercial ink studies show in Section III, the industry has be no means standardized on the optimum adhesive agent composition. It is worth mentioning that a systems approach must be utilized in evaluating any

material. Since much of the value of a material depends upon its compatibility with related manufacturing processes, improvements in any one material must be weighed against these extraneous demands upon its performance.

III. COMMERCIAL INK STUDIES

A. SURVEY OF AVAILABLE INK MATERIALS

In order to examine a large number of Au-Pt inks without incurring high expense, e.g., ~$500 per trial lot x 20 trial lots, samples of more than 20 different Au-Pt and related ink types were obtained fired on 96 wt pct, standard grade alumina from seven ink manufacturers. The conductor test patterns were requested to contain $(0.10\text{-in.})^2$ pads and to be fired to give optimum adhesion strength. Where samples with $(0.080\text{-in.})^2$ pads were furnished, they were used without any attempt to normalize the data.

1. Chemical Analysis

X-ray fluorescence spectrometry (XRFS) was the technique applied to determine the chemical constituency of the fired films. For the noble-metal elements, the data taken can be converted semiquantitatively to wt pct of Au, Pt, and Pd in the metal phase of the conductor film. Standards were prepared to permit this. When analyzing film patterns, the presence of glass, flux, and ceramic additions can be detected in the films only when they are present in significantly greater amounts than appear in the surface of the substrate. Thus, a single significant figure is shown where the concentration of binder phases are presented. The analyses of the conductor films are shown along with other data in Table 20.

In addition to the problem of interference of the signal from the substrate, substantial segregation of the metal and the binder phases can occur on firing the conductors, and this has rendered the analyses less quantitative. Substantial errors in the Pd data of Table 20 are suspected and may be due to segregation of Pd to the film surfaces to form PdO_x during firing.

The analytic procedure used is described in Appendix A. The calibration procedure and details of the XRFS method developed are presented in Appendix B.

TABLE 20. SEMIQUANTITATIVE X-RAY FLUORESCENCE CHEMICAL ANALYSES, ADHESION STRENGTH AND OTHER DATA FOR Au-Pt-Pd-TYPE CONDUCTOR INK SAMPLES SUPPLIED FIRED BY INK VENDORS.

Ink No.	Wt pct ratios of other elements with gold**							Initial Adhesion Strength		Thermal Aged Adhesion Strength		Special Advertised Properties
	Pt/Au	Pd/Au	Bi/Au	Pb/Au	Cu/Au	Cd/Au	Ni/Au	(lb)/N	Fbt*/N	(lb)/N	Fbt*/N	
1	0.20	-	0.1	-	-	-	-	-	Yes/1	2.5/1		bondability
2	0.16	0.20	0.1	-	-	-	-	3.5/3	Yes/3	3.1/2		fine line
3	0.23	0.057	0.1	0.04	-	-	-	4.2/4		2.6/2		resistance to solder leaching
4	0.22	-	0.06	0.01	0.01	-	-	4.1/3		3.6/3		solderability without active flux
5	0.18	0.085	0.05	0.05	-	-	-	3.8/4	Yes/1	4.0/6	Yes/1	wide firing range
6	0.21	0.080	0.2	0.05	0.001	-	-	4.4/13		4.2/1		thermal shock resistance, adhesion str
7	0.18	0.074	0.06	0.02	-	0.01	0.01	4.6/4		2.5/1	Yes/1	Pb-Sn solderability
8	0.19	0.12	0.1	0.04	-	-	-	5.6/3		2.5/3	Yes/1	
9	0.15	-	-	-	0.01	0.006	-	8.0/5		5.0/5		reactively bonded, bondability
10	0.16	0.068	0.1	0.02	-	-	-	6.1/3		3.2/1	Yes/3	resistance to solder leaching
11	0.17	-	0.2	0.02	-	-	-		Yes/4	2.2/1	Yes/4	
12	0.085	0.13	0.2	0.01	0.01	-	-	5.0/4		4.0/4		
13	0.13	-	0.06	-	-	-	-		Yes/6		Yes/5	
14	0.12	0.12	0.2	0.03	0.01	-	-	4.9/4		3.9/2	Yes/2	
15	0.12	-	0.1	-	0.001	-	-					bondability
16	0.10	0.081	0.1	0.04	0.01	-	-	4.7/4		3.6/1	Yes/3	
17	0.082	0.22	0.09	-	-	-	-		Yes/4		Yes/1	fine line
18	0.18	0.15	0.2	0.02	0.01	-	-	6.6/8		4.1/8		
19	0.085	0.12	0.08	-	-	-	-		Yes/4		Yes/4	fine line
20	0.10	-	-	0.03	-	-	-	7.7/4		2.9/4		
21	0.075	-	-	0.02	-	-	-	6.6/8		3.9/8		
22	***							6.7/16		4.6/16	Yes/4	Ag-Au based, low cost, bondability

*Failed before testing.
**Elements found in significant amounts in 96 wt pct alumina substrates are omitted from these analyses.
***XRFS technique described in Appendix B is only qualitative for this high-Ag content material.

2. Adhesion Strength

The adhesion strength of the pads was measured using a soldered-wire tensile peel method quite similar to that described in subsection IV.B.2. of Ref. 2. Thermal aging was performed before adhesion testing on approximately half the parts from each lot obtained from the ink vendors. The aging was performed in an oven powered by a heavily damped (no temperature overshoot), RCA-proprietary temperature controller using a platinum-resistance bulb sensor. The aging time-temperature history was monitored by a chart recorder. Aging was carried out for 250 h at 150° $\pm$ 1°C. The oven was opened briefly a few times to remove parts, check temperature sensor positions, etc., but no effect of thermal shocking should have resulted since the samples were lying on heavy aluminum trays.

In several cases when cutting the wires between pads (see description of test method in Appendix C) was performed after aging, the test pads broke off the substrate. With other samples, the test pads were too poorly adherent to withstand this preparation for testing even before aging. The adhesion test data and the number of samples destroyed in preparation for testing are shown in Table 20.

B. PARAMETRIC PROCESSING EFFECTS ON SIX SELECTED Au-Pt-TYPE INKS

From the commercial ink materials investigated in the survey described in subsection III.A, six inks were selected for further study on the basis of their adhesion strength properties and their chemical analyses shown in Table 20.

The data presented here describe an investigation of the properties of the six Au-Pt-class inks, two substrates (96 and 99.5 wt pct alumina), four firing profiles (750°, 850°, 925°, and 1025°C peak temperature), three print thicknesses (165, 200, and 325 mesh), thermal aging with and without solder (500 h in air at 150°C), and the effect of thermal shock [15 cycles in accordance with Mil Std 883 - Method 1011, Schedule C (-65° to 150°C)].

1. Chemical Analyses of Selected Inks

Because of the limitations of chemical analyses by XRFS of fired thick-film conductor patterns, thorough chemical analyses were made of the six ink materials purchased for more intensive study. The data shown in Table 21 are

TABLE 21. COMPLETE CHEMICAL ANALYSES OF SIX INKS SELECTED FOR THE STUDY OF EFFECTS OF PARAMETRIC PROCESSING VARIATIONS

Constituents of Inorganic Ink Solids (wt pct)

Noble Metals	Ink Code Nos.					
	3	9	10	18	21	22
Ag	0.03	0.03	0.03	0.03	0.03	70.
Au	65.1	75.1	65.0	65.2	74.1	8.8
Pd	2.62	0.01	2.71	10.3	0.005	0.01
Pt	19.0	16.8	20.0	12.4	11.2	9.5
Rh	0.002	-	0.002	0.01	0.03	0.001
Glass-Active Metal Oxides [24]						
Al_2O_3	0.4	0.09	0.4	0.09	0.2	0.09
B_2O_3	0.2	0.003	0.1	0.06	0.6	0.01
BaO	0.01	-	0.01	-	0.003	-
CaO	0.3	0.004	0.3	-	0.04	0.04
CdO	0.01	1.2	0.01	0.01	0.11	1.1
MgO	0.05	0.01	0.05	0.02	0.005	0.02
PbO	2.8	0.005	2.6	1.5	8.8	0.003
SiO_2	0.4	0.06	0.4	0.4	0.4	0.2
SnO_2	0.004	-	0.004	0.006	-	-
SrO	0.002	0.004	0.002	0.002	0.004	-
TiO_2	0.008	0.005	0.008	0.3	0.08	0.002
V_2O_5	-	0.09	-	-	-	-
ZnO	-	-	-	-	1.2	-
ZrO_2	0.01	-	0.01	-	0.007	-
Other Metal Oxides						
Bi_2O_3	4.9	0.001	5.0	5.6	0.003	0.12
CuO	0.15	0.59	0.15	1.7	0.012	2.6
Fe_3O_4	0.08	0.008	0.08	0.08	0.02	0.02
NiO	-	-	-	0.01	-	-
Sb_2O_3	-	0.001	-	0.004	-	-
Mn_2O_3	0.01	0.0001	0.01	0.03	0.001	0.003

24. W. D. Kingery, *Introduction to Ceramics* (John Wiley and Sons, New York, 1960), p. 148.

the results of those analyses. The origin of the data can be determined by the number of significant figures given for each constituent; i.e., three significant figures indicate wet chemical analysis, two significant figures are the result of atomic absorption spectrometry, and one significant figure signifies data from optical emission spectrometry.

2. First Parametric Adhesion Strength Study (200 Mesh Prints)

To study all the variables in a single matrix would be most difficult; accordingly, the first matrix dealt only with 200 mesh prints. The adhesion test* data for the six inks are shown in Figs. 31 to 36.

All the data presented result from specimens made with a *10-second heating after the solder melts* cycle, except the slow-cooled and the fast-cooled specimens which were both made with the *7-second heating after solder melts* cycle described in Appendix C.

Except where noted, the failure mode of the test specimen lot was the "A" mode, the wire and solder pad were pulled from the substrate by testing on the Instron, and took with them virtually all of thick-film conductor material. Many samples were too weak to permit cutting of the wires or loading the specimens into the Instron. When no specimen was testable, a zero adhesion strength was plotted for the material/process combination. In other lots, if any specimens were testable, their adhesion strengths were averaged to give the data shown.

At high failure loads, several modes besides "A" failures were observed. In "B" mode failures, the solder is removed by the wire, but the thick-film pad remains attached to the substrate and is nominally intact.

A "C" mode failure is identified by finding most of the solder remaining on the thick-film pad after the wire has pulled out the solder. Mixed mode failures were seen, and, where indicated, imply that a substantial fraction of the surface of the test pads had the appearance of each of the failure modes noted.

*The adhesion test method is described in Appendix C.

(a) Substrate A

(b) Substrate B

Figure 31. The adhesion strength of frit-bonded Au-Pt-Pd ink, Code No. 3 as a function of processing and environmental stressing.

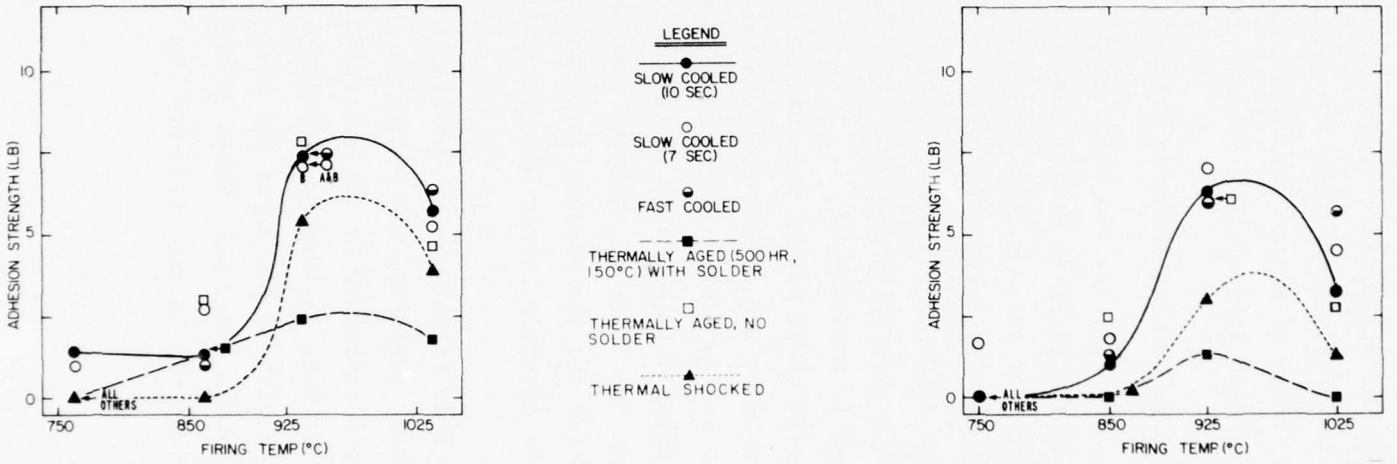

(a) Substrate A - 96 wt pct alumina

(b) Substrate B - 99.5 wt pct alumina

Figure 32. The adhesion strength of reactively bonded Au-Pt ink, Code No. 9 as a function of processing and environmental stressing.

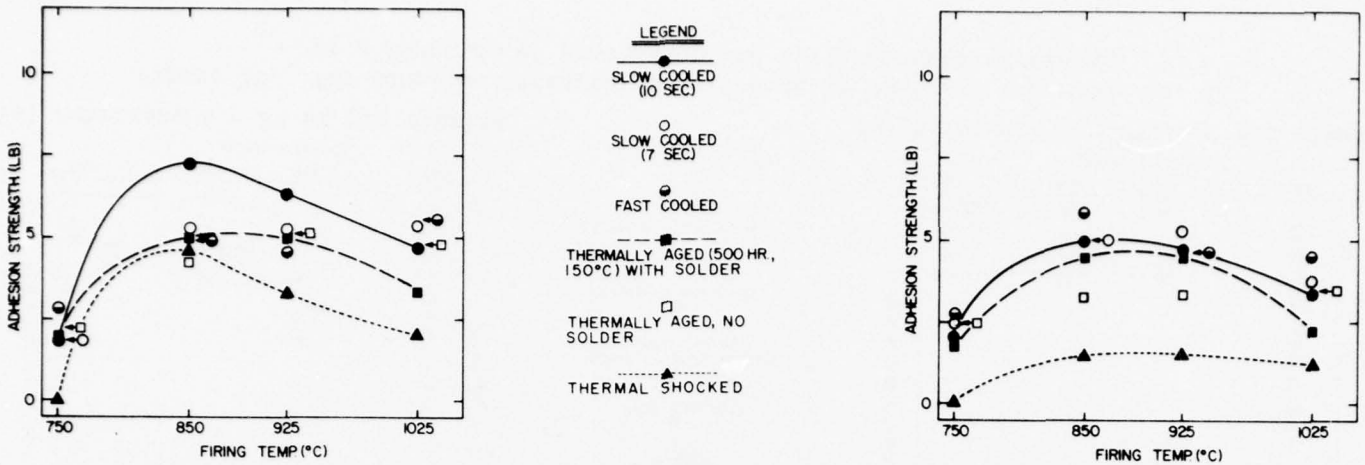

(a) Substrate A

(b) Substrate B

Figure 33. The adhesion strength of frit-bonded Au-Pt-Pd ink, Code No. 10 as a function of processing and environmental stressing.

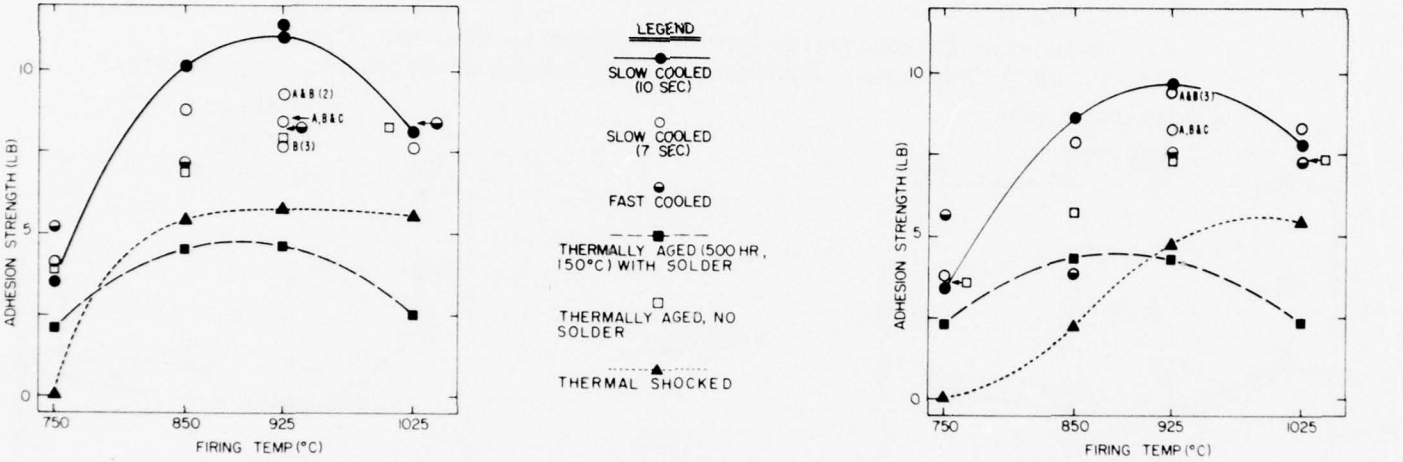

(a) Substrate A - 96 wt pct alumina

(b) Substrate B - 99.5 wt pct alumina

Figure 34. The adhesion strength of mixed bonded Au-Pt-Pd ink, Code No. 18 as a function of processing and environmental stressing.

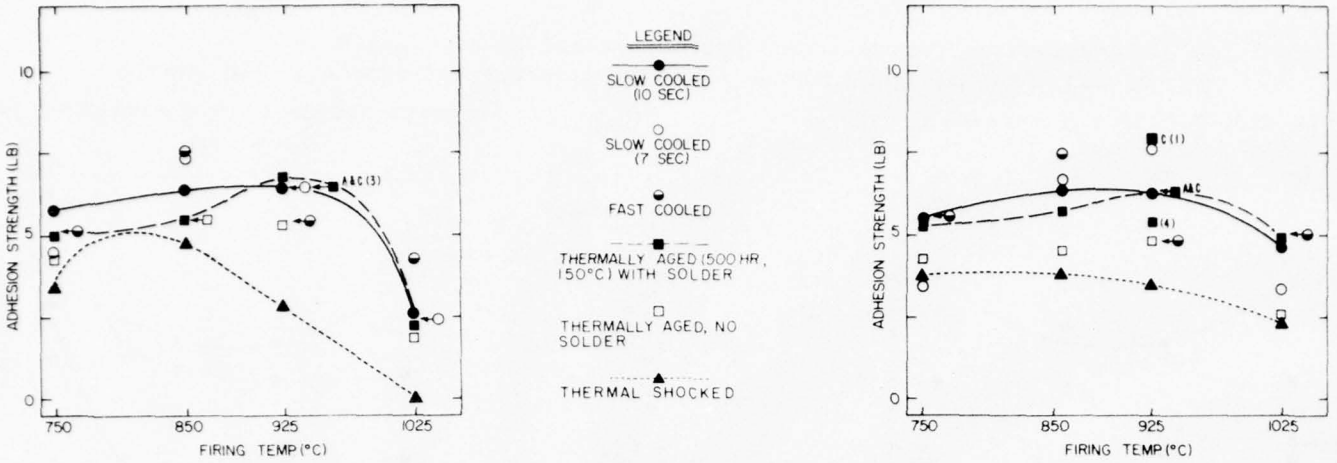

(a) Substrate A

(b) Substrate B

Figure 35. The adhesion strength of frit-bonded Au-Pt ink, Code No. 21 as a function of processing and environmental stressing.

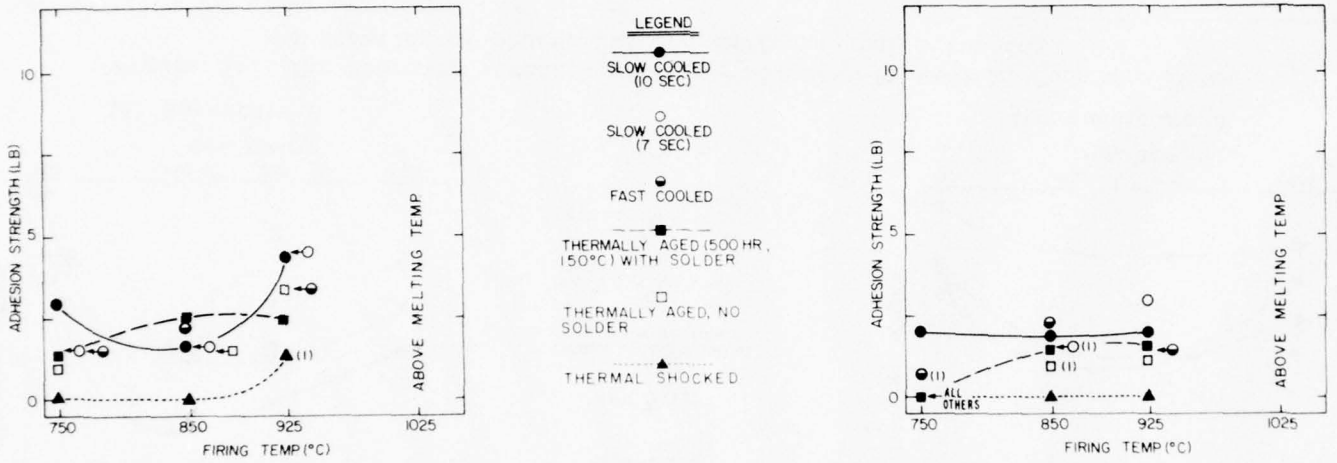

(a) Substrate A - 96 wt pct alumina

(b) Substrate B - 99.5 wt pct alumina

Figure 36. The adhesion strength of frit-bonding Ag-Pt-Au ink, Code No. 22 as a function of processing and environmental stressing.

Twelve adhesion test pads were prepared for each point with the A substrates; eight were prepared for the B substrates. Where a very small number of pads were testable, the number contributing to the data point is shown beside it in parentheses.

3. Discussion

It was projected that most of the adhesion strength data from differently prepared specimens would be similar except for the thermally aged with solder and the thermally shocked samples. In general this was the case. No clear trend was found between the adhesion strengths of fast-cooled specimens (140° $\pm$ 10°C/min*, except the 750°C specimens which were cooled at 103°C/min) and similarly prepared slow-cooled (52° $\pm$ 2°C/min) specimens. (All the specimens in the study were fired with flat-top profiles and 10 min at peak temperature as in our NASC study of thick-film Au conduct [1]. Only the fast-cooled samples were not cooled at $\sim$50°C/min.)

For most of the material/firing temperature combinations, the variations in preparation of as-fired specimens produced only small changes in the adhesion strength. Changing the soldering cycle from 10- to 7-s heating after the solder melts, as described in Appendix C, appears to make little difference. Fast cooling produced an irregular, but larger, effect. Thermal aging without solder appeared to moderately reduce the adhesion strengths of some specimen lots.

In contrast to the as-fired data, typified by the slow-cooled (7-s) data, markedly reduced adhesion was caused by the thermally aging with solder and thermal shock environmental stresses on several material/firing combinations. This is predicted by the work of several authors [9-16]. In other combinations no effect of environmental stressing could be detected.

In several of the materials there is a significant difference between the relative amounts of adhesion degradation induced by thermal aging with solder and thermal shock, i.e., in the form of the data curves as a function of temperature. Considering the mechanism of adhesion this should not be surprising,

*The time for the profiling thermocouple to cool from 700° to 300°C was measured and divided into 400°C to obtain these cooling rates.

i.e., cracks probably are initiated by mechanical stresses resulting from differential thermal expansion in the alumina, Au-Pt, solder, and wire and degrade the adhesion strength of thermally shocked specimens. On the other hand, thermally activated Sn diffusion is believed to degrade the adhesion in soldered and thermally aged specimens. For poorly adherent material/process combinations, either of these strongly adhesion degrading environmental stresses lowers the adhesion strength so drastically that the specimens either fail spontaneously or are too weak to permit loading into the Instron fixturing for testing.

It should be noted that the thermally aged samples had not had the wires cut from between the pads during thermal aging with solder. On removing these specimens from the 150°C oven to allow them to cool, many of the soldered thick-film pads broke off the ceramic. The wires on the thermally shocked parts were cut before imposition of the environmental stressing. In retrospect, cutting the wires of the thermally aged parts would have been desirable, and oven cooling from 150°C would probably have provided still more testable parts.

4. Second Parametric Adhesion Strength (Variation of Print Thickness)

Adhesion strengths for sample lots of the matrix of 6 inks x 2 substrates x 3 print thicknesses x 4 firing temperatures were measured with specimens fabricated using the *7-second heating after solder melts* schedule described in Appendix C. A sample lot size of 12 test pads was again taken for the Code A substrates and 8 test pads for the B substrates. Figures 37 to 42 indicate the adhesion strengths of the combinations of firing temperature and print thickness for the six inks each on the two substrates.

As has been observed [1,2,5], the adhesion strengths of reactively bonded inks are strong functions of the firing temperature, and this is borne out by ink No. 9 in Fig. 38. It is unusual, however, for Ag- or Au-based reactively bonded inks to suffer a marked loss in adhesion strength with increased firing temperature, and this occurrence in ink No. 9 should receive further study. Frit-bonded inks Nos. 3 and 10 are reported by their manufacturer to have identical composition; ink No. 10 is the improved version. Their behaviors are rather similar, according to Figs. 37 and 39.

Mixed-bonded ink No. 18 had the highest Pd content and a substantial Pt content also. It is believed that the reasons this material exhibited the

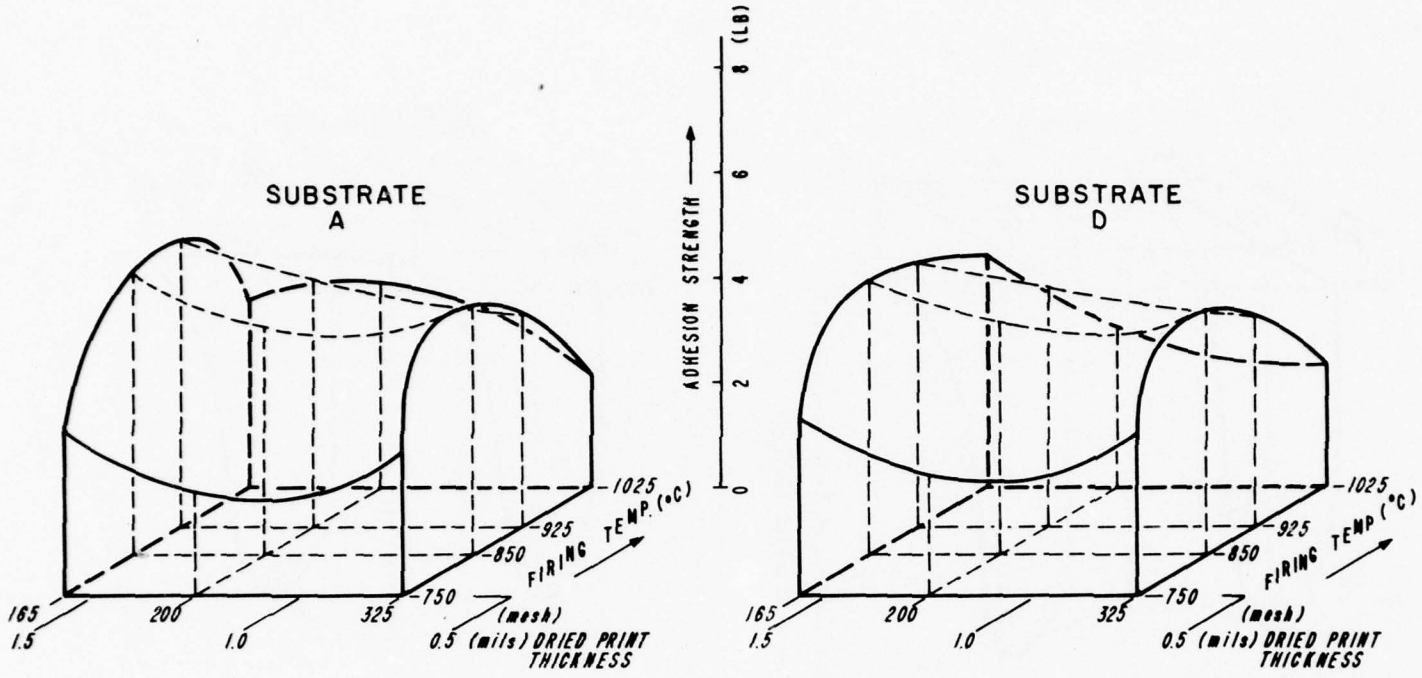

Figure 37. Adhesion strength of frit-bonded Au-Pt-Pd ink, Code No. 3 as a function of film thickness and firing temperatures.

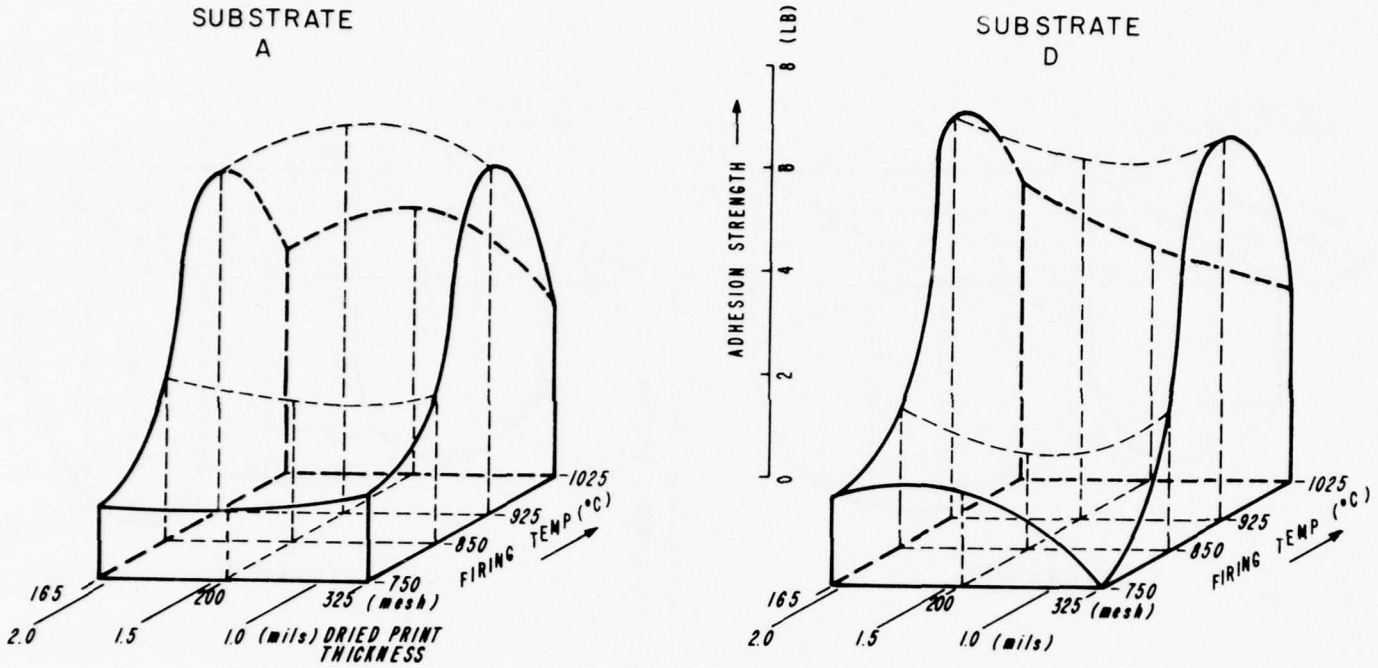

Figure 38. Adhesion strength of reactively bonded Au-Pt ink, Code No. 9 as a function of film thickness and firing temperatures.

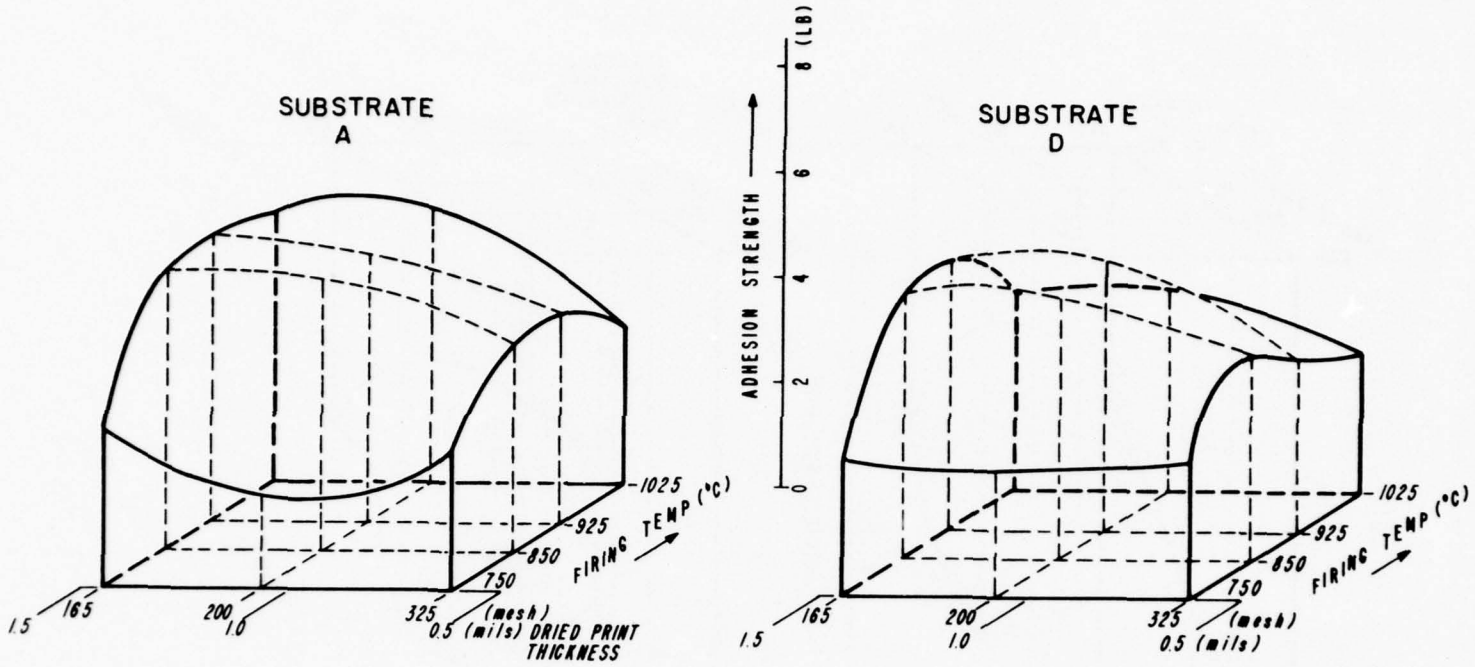

Figure 39. Adhesion strength of frit-bonded Au-Pt-Pd ink, Code No. 10 as a function of film thickness and firing temperatures.

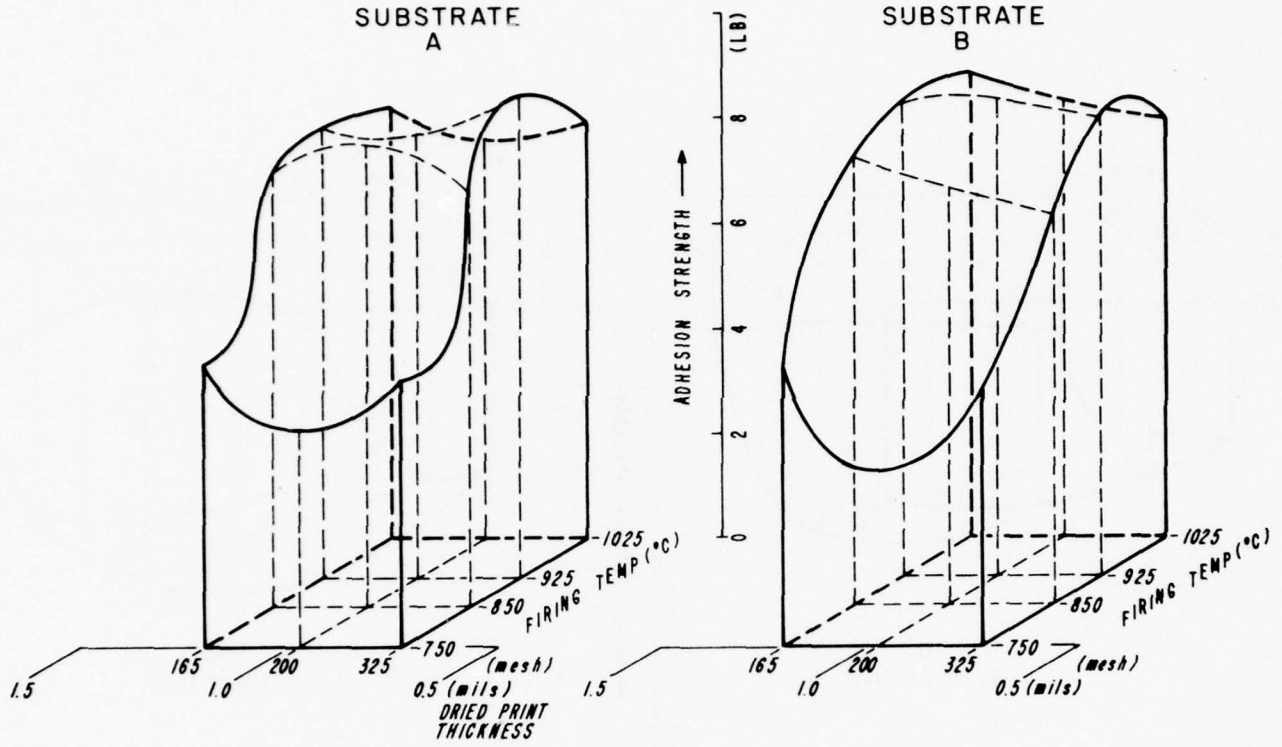

Figure 40. Adhesion strength of mixed bonded Au-Pt-Pd ink, Code No. 18 as a function of film thickness and firing temperatures.

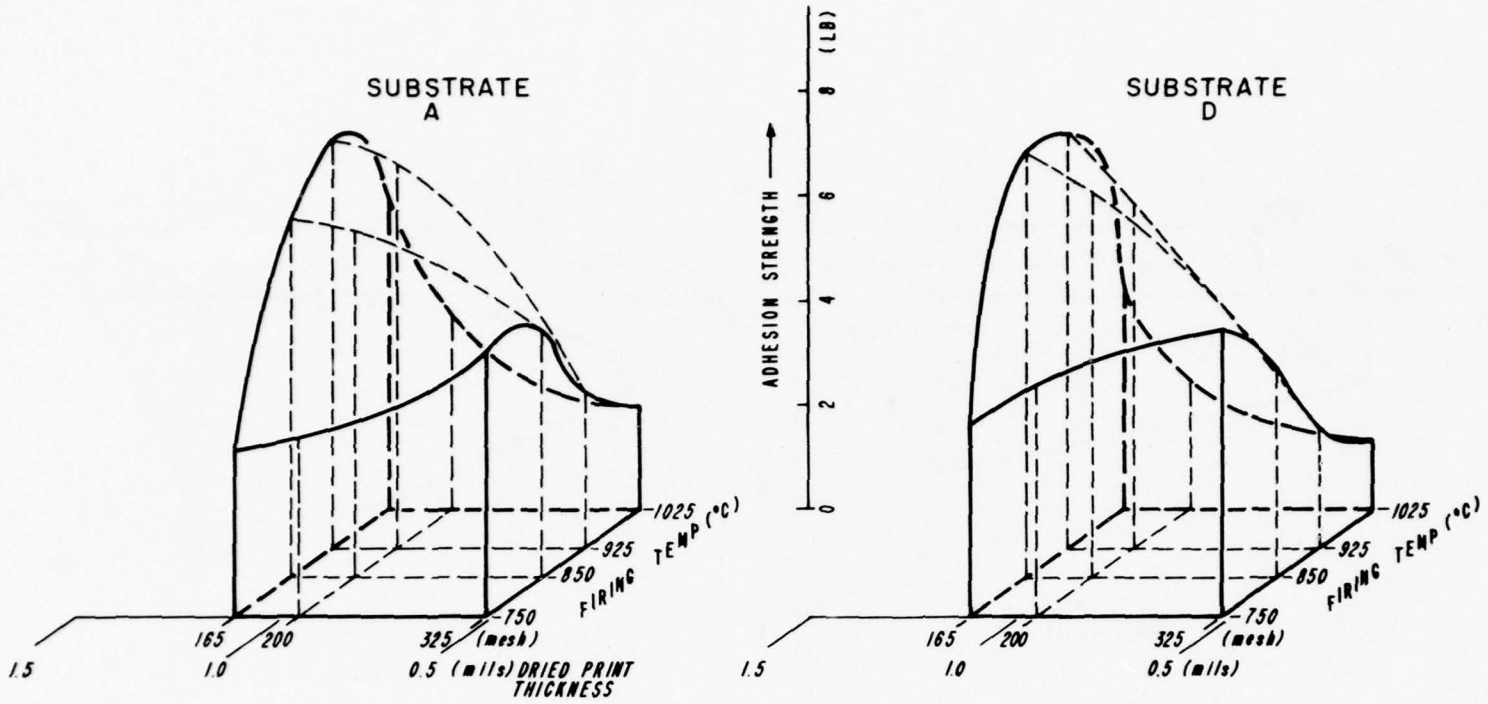

Figure 41. Adhesion strength of frit-bonded Au-Pt ink, Code No. 21 as a function of film thickness and firing temperatures.

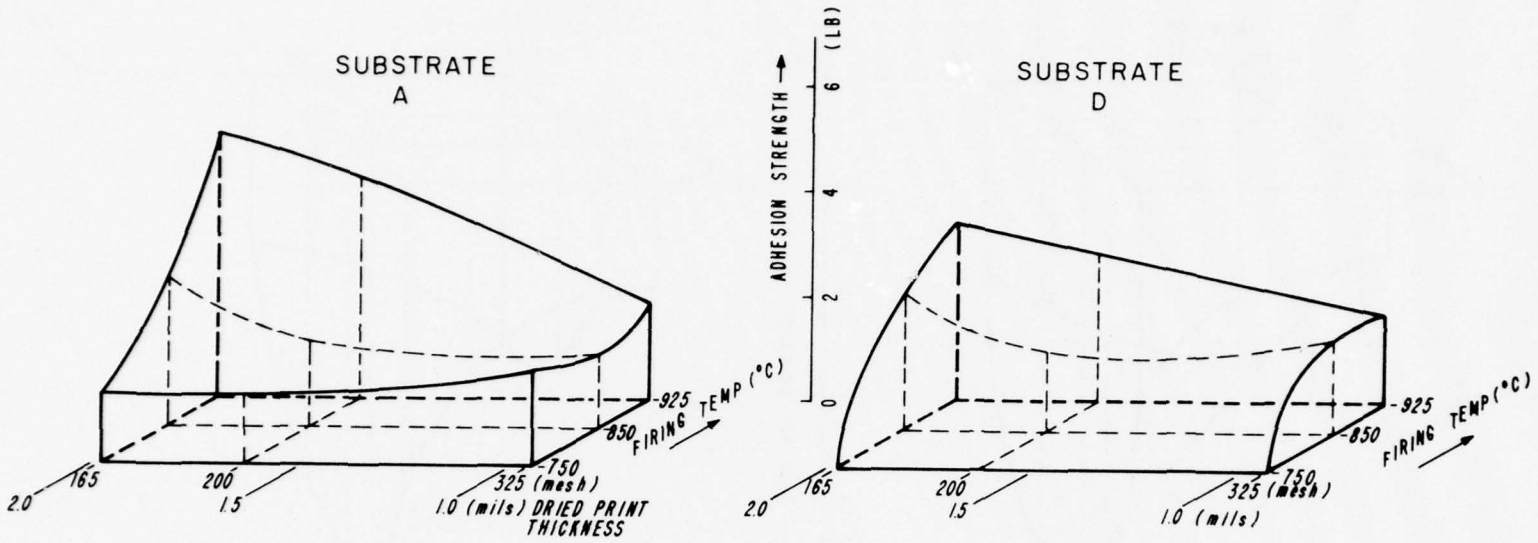

Figure 42. Adhesion strength of frit-bonded Ag-Pt-Au ink, Code No. 22 as a function of film thickness and firing temperatures.

highest adhesion strength of all the materials studied include the mixed-bonding and the high Pd content. Although the adhesion strength of this material is reduced by thermal aging with solder, the strength remaining after 500 h at 150°C is greater than for many of the materials as-fired.

With the lowest Pt content of the six Au-Pt(-Pd) inks selected for detailed study, ink No. 21 demonstrated moderate to good adhesion strength over a wide range in firing temperature, as can be seen from Fig. 41. It can also be noted that ink No. 21 demonstrated rather poor adhesion strength with 325 mesh print thickness, but the 325 mesh prints for this ink were thinner than those for any of the other inks.

The adhesion strength of ink No. 22, shown in Fig. 42, was disappointing. The material holds promise as a low cost, high performance material but had poor adhesion strength (except at 925°C with thicker prints, particularly on A substrates). The material is projected to have reduced Ag migration and resistor termination effects compared with the high Ag inks and improved wire bondability over Au-Pt inks. A material of this type may permit one conductor to do work for which two are required now, and thus the material may still be considered for high-reliability military hybrids if an optimized firing temperature (between 925° and 1025°C) would produce greatly improved adhesion performance. An additional requirement is that the retained fraction of adhesion strength after thermal aging with solder also improve with higher firing temperatures.

An analysis of the statistical significance of a difference between the adhesion strengths of two points (in the second parametric study) indicates that for A substrates and mean failure loads above 3 lb, a 15 percent difference is probably significant (95 percent confidence level of Student t) [25]. Approximately twice that amount (i.e., 30 percent differences) between similar data are required of the B substrate data because of the smaller number of samples and higher standard deviation in the data relative to the mean adhesion strengths.

---

25. M. J. Moroney, op. cit., pp. 227-230.

5. Solder Wettability Measurement

The six conductor materials selected for detailed study were fabricated into Meniscograph specimens by screening with a 200 mesh screen and firing at 750°, 850°, 925°, and 1025°C. Kester 1544 soldering flux was used with 62Sn-36Pb-2Ag solder held at a set point of 230°C. Further details of the specimens' preparation and test method are described in Appendix D. The wetting curves are shown in Figs. 43 through 48. A higher curve between 0 and 10 s indicates better solder wettability. All the curves shown are the averages of data for three or four slow-cooled specimens. Fast-cooling-rate furnace profile fired specimen lots were also tested, but their behaviors were not significantly different from specimens of the same inks fired at the same peak temperatures but slow-cooled.

6. Correlation of the Wettability and Adhesion Strength

This discussion is pertinent to the selection of Au-Pt-Pd-class inks for use without burnishing. If burnishing is required in a manufacturing process, the wettability data that applies is that of burnished, not as-fired, specimens. Three of the inks offer promise of good performance in a manufacturing process which requires soldering but precludes both strongly activated fluxes and burnishing.

Ink No. 10 is one of the two Au-Pt(-Pd) inks which demonstrated high as-fired solderability for the same firing temperatures where it showed high adhesion strength in both the as-fired and thermally aged conditions. Ink No. 3, with a similar inorganic composition to No. 10, had significantly poorer wettability than No. 10. Ink No. 9 demonstrated good as-fired adhesion strength with only a limited range of firing temperatures. For that range, however, the solderability was good. Ink No. 22 is not a Au-Pt(-Pd) conductor material, but contains mostly Ag. As noted earlier, the material needs further study to be seriously considered, but the solderability of samples fired at 925°C was excellent. No measure of solderability after many refirings was made in this study. Such measurements will be required to fully qualify the material for most manufacturing processes involving soldering without burnishing.

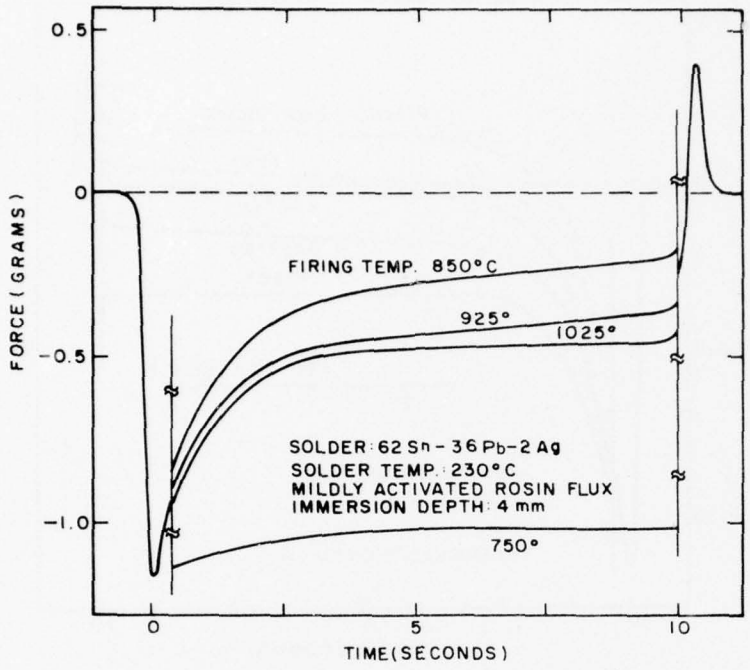

Figure 43. Meniscograph solder wettability as a function of firing temperature for frit-bonded Au-Pt-Pd ink No. 3.

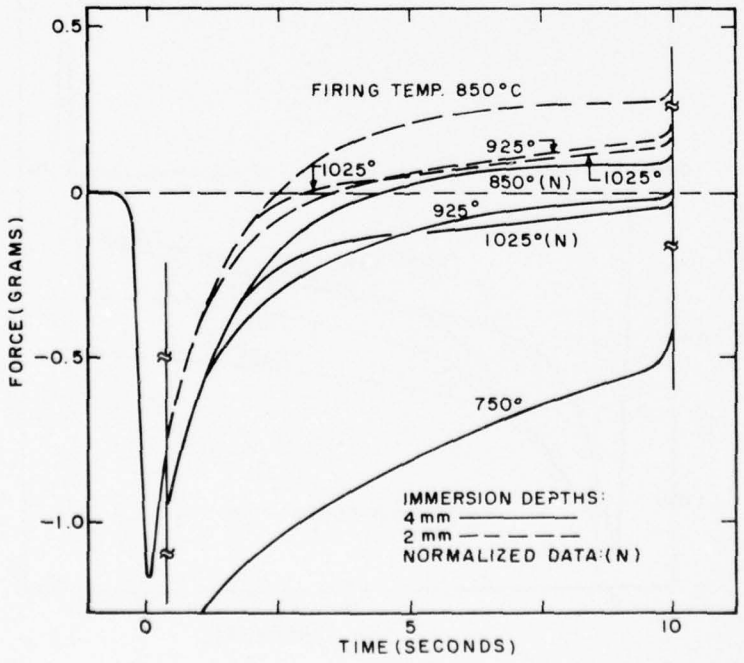

Figure 44. Meniscograph solder wettability as a function of firing temperature for reactively bonded Au-Pt ink No. 9.

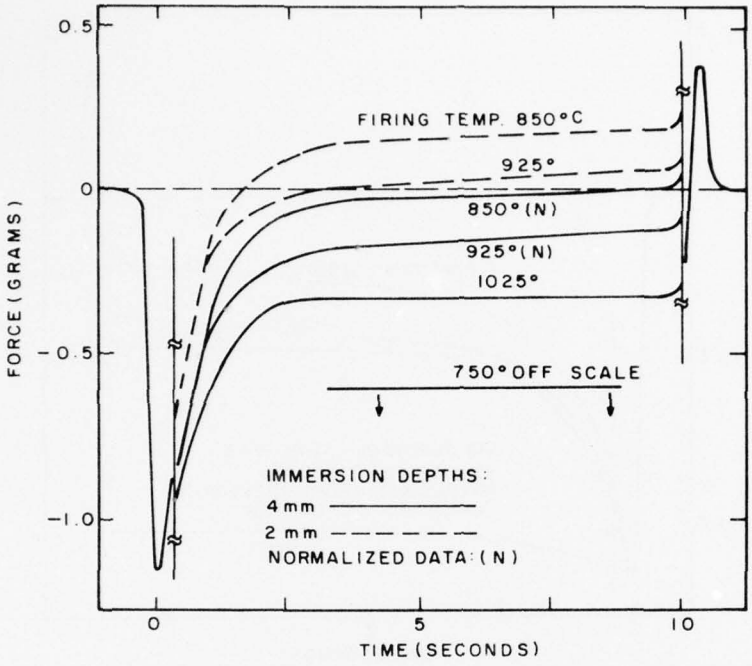

Figure 45. Meniscograph solder wettability as a function of firing temperature for frit-bonded Au-Pt-Pd ink No. 10.

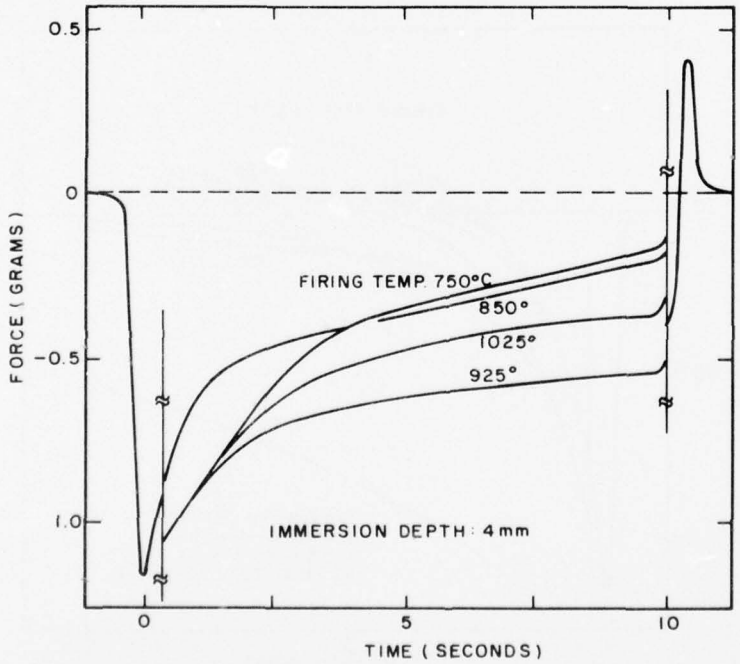

Figure 46. Meniscograph solder wettability as a function of firing temperature for mixed-bonded Au-Pt-Pd ink No. 18.

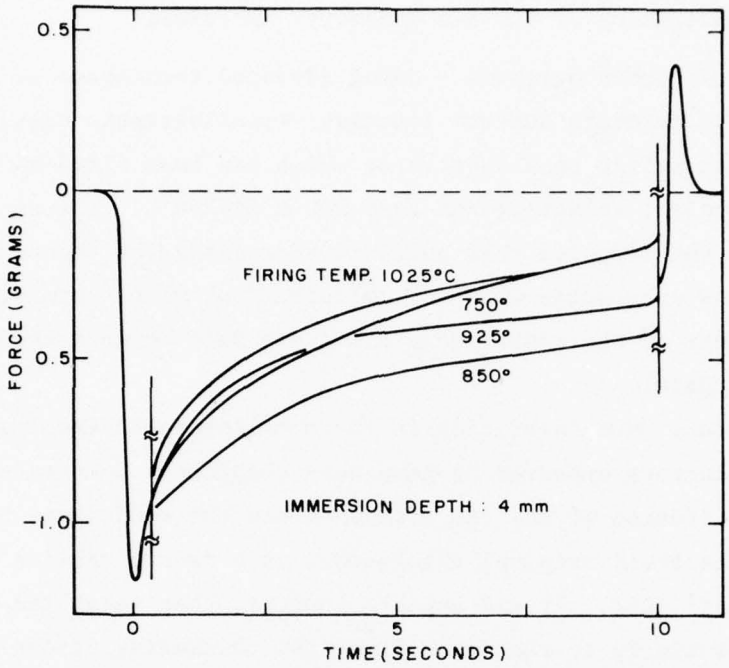

Figure 47. Menisograph solder wettability as a function of firing temperature for frit-bonded Au-Pt ink No. 21

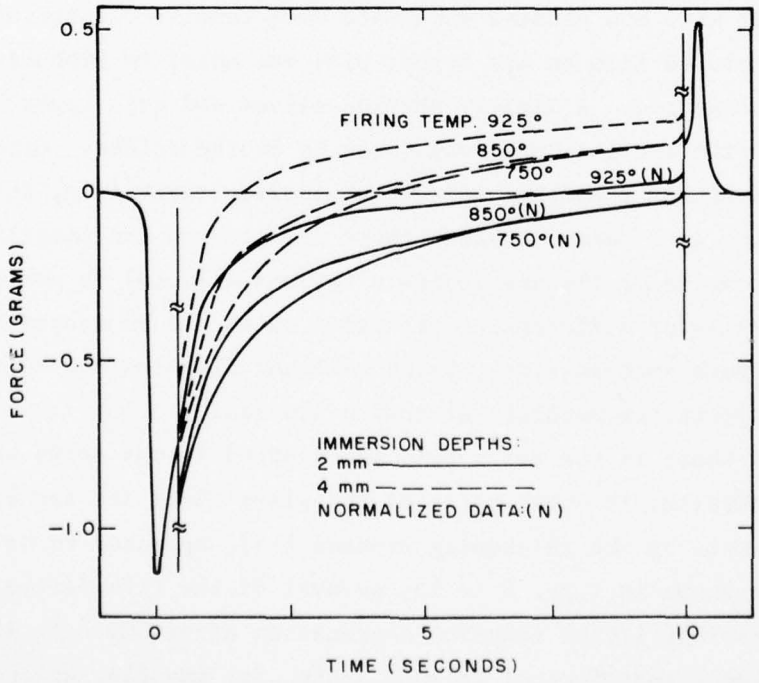

Figure 48. Meniscograph solder wettability as a function of firing temperature for reactively bonded Ag-Pt-Au ink No. 22.

7. Other Investigation of the Six Conductor Materials

a. Metallurgical Cross Sections - Using advanced techniques of sample mounting and polishing to maintain surface flatness, metallographic cross sections were made of 200-mesh prints on A substrates which had been fired at 750°, 850°, and 1025°C; slow cooled; soldered; and aged 500 h at 150°C. The sections were made to cut through the adhesion test pull wires crossing the thick-film pads. Other pads on the same substrates were not soldered (but were thermally aged, of course), and some of the comparisons drawn are made between the soldered and the unsoldered pads.

Several areas were identified in the metallographic examination. All the thick-film conductors appeared to have been completely penetrated by, presumably, the diffusion of Sn. As a consequence the conductors had thickened to several times their original thicknesses in a manner similar to that described by Suloff [14]. It did appear, however, that where the copper wire was in close proximity to the thick film, the thickening effect was reduced. This reduction is believed to occur because of the reduced availability of Sn under the wire.

The copper wire and alumina substrate were readily identified. A dense, thin, silver-colored film on the copper wire was noted to probably be a Cu-Sn intermetallic compound. A lightly mottled silver and grey layer between the swollen thick film and the $CuSn_x$ was taken to be the solder. Often between the solder and either the $CuSn_x$ and/or the swollen thick film, dull layers containing voids were seen. Whether these dull layers are constituted principally of voids or include separate intermetallic(s) is not known. They may be the results of differential diffusion rates and be caused by phases in the microstructure such as glass, which will not dissolve Sn, Au, etc., and thus cannot support the metallic diffusion process.

The glass phase in the thick film was studied in the cross sections, and the Suloff mechanism, in which parts of the glass phase are transported far from the substrate by the thickening process [14], appeared to have been operating. As shown in Figs. 8 to 13, several of the film/firing temperature combinations exhibit little adhesion degradation after 500 h at 150°C. It is possible, however, that further thermal aging, for example, an additional

500 h, might produce substantial reductions in the adhesion strength of film/firing temperature combinations that showed good adhesion retention after the first 500 h at 150°C.

b. Mercury Vapor Leaching - Samples were leached, using Hg vapor, of combinations of the six selected conductors which were fired at temperatures that produced substantial adhesion strength as well as some combinations which exhibited lower adhesion strength. It was found immediately that leaching was slower on the Pt and Pd containing films of inks Nos. 3, 9, 10, 18, and 21, compared with Au- and Ag-based thick films. In some cases Hg stopped wetting the films before leaching was completed. In other cases there was a question as to whether the higher temperatures and extended leaching times might have damaged the frit phase structure, but on the whole, the leaching was considered successful. Leached specimens were baked at 150°C for 24 h into a mercury diffusion pumped system to remove residual mercury from their surfaces. A discussion of the findings of the micrographic examination follows.

Ink No. 3 showed the most extensive interlocking phase structure of all the materials for specimens fired at temperatures corresponding to good adhesion strength. Its compositional twin, ink No. 10, was found to have a more poorly developed interlocking structure, despite its sometimes superior adhesion strength. The microstructures of ink Nos. 3 and 10 were substantially different.

Ink No. 18 showed some surface projections after Hg-vapor leaching, but they are considered to have been an insufficient micromechanical interlock with the metal phase to cause the high adhesion strength. A green tinge was in evidence under the Hg-vapor-leached pads and was ascribed to copper, which was found in high levels in this ink.

At the magnification employed in the micrographic examination, only minor features were found on the surfaces of the reactively bonded ink specimens Nos. 9 and 22. The results of re-examination at higher power will be reported elsewhere.

c. Physical Analysis of the Inorganic Ink Solids - In order to study the physical makeup of the solids of the six commercial inks selected for extensive testing, two techniques were employed. The first method was oxygen baking of

dried ink samples followed by SEM investigation, as described earlier [1,2]. This technique revealed that a hexagonal and triangular shaped platelet powder very similar to that seen in our earlier investigations [1] and used in our model ink studies, i.e., Au MB-1 could be observed in ink Nos. 9, 18, and 21. Also, the particle shape and size make-up of ink Nos. 3 and 10 were found to substantially different. The complexity of the SEMographs, resulting from the number of metal and binder powders in these inks, precluded any further conclusions from being drawn by the use of this technique.

The second method of studying the powder particle characteristics of the inks was to remove the organic constituents by successively dispersing the inks in solvents, centrifuging the mixtures, and decanting the solvents along with any dissolved ink vehicle constituents. Each ink sample was dispersed two times in $\sim$50 cm^3 of methylethyl ketone and once in a similar volume of trichlorethylene. Several features of these inks were identified by this investigation. Macroscopic observation showed that each of the inks, but one, formed a top (slowest settling) layer of powder that was black with a fine particle size. This layer is believed to consist of the Pt and Pd powders, probably mixed with the glass particles, CuO, and other low density constituents. Ink No. 10 had a light colored top layer of unknown origin. Ink Nos. 9, 18, and 21 appeared to include a flake Au layer, verifying the oxygen bake/SEM study results. The flake Au formed a sediment, which was the bottom layer in Nos. 9 and 21 and the second layer in No. 18. Ink No. 22 appeared to sediment into three distinct metal layers with two silver-colored layers below a Au layer. It should be noted that a single powder such as Au MB-1, which consists of a mixture of small spheres and larger platelets, might readily yield two layers in sedimentation.

Further work will be necessary to make additional correlations of the results of the findings of this section with the physical data for the six fired thick-film conductors.

IV. DISCUSSION

The adhesion of solderable thick-film metallizations is inextricably linked to the ambient thermal stresses and compositional reactions which occur both during soldering and while thermal aging. Therefore, any discussion of metal-to-ceramic adhesion requires one to address the corollary factors which affect adhesion, i.e., solder acceptance (solderability), metal oxidation, thermally induced stresses in the film, phase formation rates, and the fundamental material properties that apply. The latter include diffusion or migration rates of reacting species such as oxygen, tin, and metal film constituents, volume changes from phase formation and intrinsic adhesion strength changes from the intrusion of new species to an interface. Investigation of such phenomena are further complicated because physical factors such as metal and glass particle sizes, size distribution and shape variation, obfuscate already complicated phenomena.

It is hoped, in a field presently crowded by much art of mixed quality, that an impartial assessment of the aforementioned factors will result in a greater understanding of the phenomena and improved materials. Preliminary steps have been taken in the work described here to replace art with scientific understanding.

For example, it was shown in the model ink study that alloyed metallizations can be soldered without burnishing, provided sufficient effort is taken to separate the binder and metal phases. This fact holds true even for high Pd-bearing metallizations which are more readily oxidized than film alloys containing only Au and Pt. Furthermore, the initial adhesion strength of the Pd-bearing film did not differ dramatically from that of the Au-Pt metallization. The comparable adhesion strengths were readily predictable, based on the similarity of chemically-derived adhesion between metal foils and glaze, provided metallization microstructures were identical. Difficulty exists, of course, in quantitatively defining differences in microstructure. Based on solder-to-metallization contact angle measurements, the Pd-bearing film appeared to have poorer solderability. One might suspect that the more porous microstructure observed by SEM led to more rapid overglazing of the Pd-bearing film. This conclusion assumes, however, that glaze spreading rates on the elements are identical for the alloys and this has not yet been evaluated.

The commercial ink study has amply demonstrated that there are numerous differences in binder composition, metal morphology, and noble-metal alloy compositions present in the industry. These variations, of course, account for the wide disparity in performance, i.e., initial and aged adhesion strength and solderability. Within the ink systems, a coincidence of highest adhesion strength and acceptable as-fired solderability with the same peak firing temperature was not widely found. In most of the systems examined, adhesion strength was rather sensitive to peak firing temperature, and more modestly sensitive to film thickness, and still less sensitive to cooling rate. Only ink No. 10 combines reasonable adhesion strength and solderability with modest sensitivity to peak firing temperature. Thus, most inks possess rather limited processing ranges, when intended for use without burnishing to enhance the solderability.

With regard to thermally aged adhesion strength retention, the model ink study showed significant strength losses when films were aged both with and without solder. The commercial inks were less sensitive to aging without solder, but strength losses were still evident. Therefore, the pertinent factors in both cases, i.e., aging with and without solder, need to be more clearly defined.

Since aged-without-solder strength losses were significant for Au-Pt and Au-Pt-Pd model inks, oxidation and thermally derived stresses are both processes which bear closer scrutiny. The thermal shock tests on the commercial inks vividly focuses on the latter.

Aged-with-solder strength losses are directly related to the new phases which form during aging. Phase growth, evidenced by the microstructure studies in the commercial inks and the nearly complete removal of the thick-film metallization during tension testing the model inks after 500-h aging, suggests that the high diffusivities of phase constituents are dependent upon microstructural and compositional differences.

V. CONCLUSIONS

An initial study of the composition and properties of multicomponent model ink materials and commercially available inks has been completed. Model inks based on Au-Pt and Au-Pt-Pd were formulated after characterizing metal powder composition, morphology, and sintering kinetics in the presence and absence of glass. Measurements of E1527 glass and E1527 glass plus 20 wt pct CuO glaze spreading rates on Pt and Pd foil were obtained to complement the values previously determined for Au, Ag, Cu, and alumina (96 wt pct Al_2O_3). The studies showed the glaze spreading rates were comparable on Au, Pt, and Pd.

Analyses of reaction rates between Au-Pt and Au-CuO, were conducted by utilizing electrical resistivity ratio measurements. By this method and x-ray diffraction studies, the minimum firing temperature, 900°C, to achieve a solderable metallization from the mixed powders was determined. The Au-CuO electrical resistivity ratio test indicated that even in layered structures, i.e., metal over glazed ceramic, Cu (from CuO) could migrate very rapidly to the upper bonding surface. This fact is more critical to non-soldered metallizations where reducing agents may not be used.

From the study of solder-to-metallization contact angles, it was learned that layered metallizations, based on E1527 glaze, would have to be inordinately thick to achieve a surface capable of being soldered without burnishing. Consequently, the glass viscosity was raised by adding 5 wt pct alumina, thereby retarding the tendency to overglaze at the 900°C firing temperature. With the changed glass composition, soldering was possible with fired film thicknesses as low as 12 um for 75Au-25Pt and 16 um for 75Au-12.5Pt-12.5Pd films. The more porous microstructure observed in the 75Au-12.5Pt-12.5Pd film is believed to account in part for the more rapid overglazing.

Adhesion strengths, measured by a tensile test, showed insignificant differences for the initial values of 75Au-25Pt vs 75Au-12.5Pt-12.5Pd. Upon aging, at 150°C for 500 h, both with and without solder present, adhesion strength losses were significant in both cases, with the Pd-bearing film showing greater changes in this regard.

The commercial ink studies again elucidated the wide compositional and morphological differences with respect to both metal and binder constituents. Selected inks of the frit-, mixed-, and reactively bonded types were examined

for variations in initial and aged adhesion strength, thermal shock resistance, and solderability as a function of fired film thickness and firing parameters. For the most part, film properties, e.g., adhesion strength and solderability, showed a large sensitivity to peak firing temperature. The systems were generally less sensitive to film thickness or to the cooling rate following the peak firing temperature. In only one ink, No. 10, did a reasonably broad processing range exist in terms of both adhesion strength and solderability.

Improvements in physical adhesion testing were made by refinements in the peel test and the introduction of a tensile test for soldered metallizations. Analytical procedures, employing x-ray fluoresence spectroscopy (XRFS), were developed and show promise as a means for rapidly determining variations in inorganic ink constituents. These tests provide improved aids for in-process control of thick-film metallizations.

APPENDICES

REFERENCES

1. T. T. Hitch and K. R. Bube, *Basic Adhesion Mechanisms in Thick and Thin Films*, Final Report, NASC Contract No. N00019-74-C-0270, 31 January 1975.
2. T. T. Hitch and K. R. Bube, *Basic Adhesion Mechanisms in Thick and Thin Films*, Final Report, NASC Contract No. N00019-75-C-0145, 31 January 1976.
3. B. R. Smith and R. L. Dietz, "An Innovation in Gold Paste," Proc. International Soc. for Hybrid Microelec. Symp., p. 2-A-5 (1972).
4. T. T. Hitch, "Phase Morphology and Adhesion in Thick-Film Conductor Inks," Proc. International Soc. for Hybrid Microelec. Symp., p. 7-7-1 (1971).
5. T. T. Hitch, "Phase Morphology and Bondability of Reactively-Bonded and Frit-Bonded Gold and Silver Thick-Film Conductors," presented at the AIME Symposium, Preparation and Properties of Electronic Materials, Las Vegas, Nev., August 27-29, 1973; published in J. Elec. Materials 3, 553 (1974).
6. L. C. Hoffman, U. S. Patent 3,516,949 (1970) (duPont).
7. J. H. Martin, U. S. Patent 3,293,501 (1966) (Sprague Elect.).
8. L. C. Hoffman, U. S. Patent 3,516949 (1970) (duPont).
9. L. C. Hoffman, V. L. Bacchetta, and K. W. Fredrick, "Adhesion of Platinum-Gold Glaze Conductors," IEEE Trans. PMP-1, s-381 (1965).
10. C. J. Peckinpaugh and R. Tuggle, "Thick-Film Adhesion - Evaluation and Improvement," Proc. International Soc. for Hybrid Microelec. Symp., p. 417 (1968).
11. T. B. Gillis and S. Schroter, "Practical Considerations Affecting Thick-Film Conductor Adherence of Solder Systems," Proc. IEEE-EIA Elec. Components Conf., p. 487 (1971).
12. A. A. Milgram, "Influence of Metallic Diffusion on the Adhesion of Screen Printed Silver Films," Met. Trans. 1, 695 (1970).
13. W. A. Crossland and L. Hailes, "Thick Film Conductor Adhesion Reliability," Proc. International Soc. for Hybrid Microelec. Symp., p. 3.3.1 (1970).
14. R. E. Suloff, "Time Dependent Relationships in Solder Interconnections," Proc. International Soc. for Hybrid Microelec. Symp., p. 418 (1974).
15. K. B. Lasch and K. S. Lynch, "Integrity of Solder Joints Connecting Nickel Leads to Thick Film Metallization on Ceramic Substrates," Proc. International Soc. for Hybrid Microelec. Symp., p. 427 (1974).
16. G. J. Ewell, "Adhesion Degradation of Soldered Thick Film Chip Resistors During Elevated Temperature Exposure," Proc. International Soc. for Hybrid Microelec. Symp., p. 168 (1975).
17. A. C. Buckthorpe, "Degradation of Thick Film Conductor Adhesion," Proc. IERE Conf. on Hybrid Microelec., p. 57 (1973).
18. M. L. Topfer, *Thick-Film Microelectronics*, p. 47 (Van Nostrand-Reinhold Co., New York, 1971).
19. T. Kubota and T. Shinmura, "Study of Surface Oxidation and Solderability on Silver-Palladium Thick Film Conductors," Proc. International Soc. for Hybrid Microelec. Symp., p. 81 (1969).
20. R. M. German, "Compaction Mechanics of Submicron Palladium Powder," Int'l J. Powder Met. and Power Tech. 11, 169, (1975).
21. N. F. Mott and H. Jones, *The Theory of the Properties of Metals and Alloys* (Dover Publications, N.Y., 1958), p. 288.
22. G. T. Meaden, *Electrical Resistance of Metals* (Plenum Press, N.Y., 1965), p. 15.
23. M. J. Moroney, *Facts from Figures* (Penguin Books, New York, 1975), p. 220-221.
24. W. D. Kingery, *Introduction to Ceramics* (John Wiley and Sons, New York, 1960), p. 148.
25. M. J. Moroney, op. cit., pp. 227-230.

APPENDIX A

CHEMICAL ANALYSIS OF THICK-FILM CONDUCTOR INKS AND FILMS

A. FIRED FILMS ANALYZED IN THE SURVEY OF AVAILABLE MATERIALS

The analytical procedure used with the vendor furnished, fired conductor patterns was as follows:

(1) The backsides of two typical substrates were analyzed by x-ray fluorescence spectrometry (XRFS), and the elemental origin of each spectral peak was identified to be coming either from the chromium target x-ray tube or from elements expected in 96 wt pct alumina substrates (see Appendix E of this report and Appendix E of Ref. A-1).

(2) The thick-film conductor metallized sample surfaces were analyzed with XRFS, and the peaks on the resulting chart that corresponded to those of the substrate and x-ray tube were deleted from further analysis.

(3) The remaining peaks were ascribed to Au, Pt, Pd, Pb, Bi, Ni, Cu, Cd, Ag, and other elements.

(4) On each chart of diffractometer position vs x-ray intensity, background base lines were drawn and at least one spectral peak height for each element was measured, in accordance with the procedures used with the calibration standards and described in Appendix B. The backgrounds of all the charts were reasonably consistent in magnitude and shape, implying nominally reproducible operation of the XFRS apparatus.

(5) The selected peak height for each of the elements (from the background base line) was divided by the peak height for the Au line, and the ratio used, as described in Appendix B, to derive the analytical data shown in Table 20 in the main body of this report.

A-1. T. T. Hitch and K. R. Bube, *Basic Adhesion Mechanisms in Thick and Thin Films*, Final Report, Naval Air Systems Command Contract No. N00019-74-C-0270, January 31, 1975.

APPENDIX B

CHEMICAL ANALYSIS OF Au-Pt-Pd THICK-FILM INKS BY X-RAY FLUORESCENCE SPECTROMETRY

A method of chemical analysis for Au-Pt-Pd thick-film pastes using x-ray fluorescence spectrometry (XRFS) has been developed as a nonrequired part of this contract. The anticipated usefulness of such a method and the way it should complement the technique of optical emission spectrometric analysis have been considered in Appendix F of Ref. B-1. The value of the method in the quantitative chemical analysis of these complex mixtures of materials has not yet been proven. However, the procedure that was developed is presented here to describe our progress. It is hoped that time will permit further work to perfect and prove the method.

RCA is currently using elements of the method, i.e., sample preparation techniques, x-ray exposure values, and the selections of the best characteristics spectral peaks, to monitor the lot-to-lot variation of thick-film inks purchased from several lots of vendors. Substantial differences in composition have been detected in several cases and correlated with changes in the performance of materials, which were purchased using identical manufacturers' type numbers.

A. STANDARD PREPARATION

Calibration standard inks were prepared from premixed and pure metal powders, Drakenfeld E1527 glass, and bismuth oxide. These were blended into inks using a commercial thick-film vehicle. The form of the standards was a 1-in.-diam circle of dried thick-film paste on a 1-in. x 1-in. x 0.025-in. alumina substrate. Sufficient thickness (infinite to the x-rays) was attained by printing twice with a 63-S mesh Nytex screen, and the layer was smoothed by printing twice with an 80-mesh, 0.002-in.-diam wire stainless-steel screen. The screens were fabricated by Microcircuit Engineering, Mount Holly, New Jersey. The standards were not fired. They were dried after each printing.

B-1. T. T. Hitch and K. R. Bube, *Basic Adhesion Mechanisms in Thick and Thin Films*, Final Report, Naval Air Systems Command Contract No. N00019-75-C-0145, January 30, 1976.

B. CALIBRATION OF THE ANALYTICAL METHOD

The object of the calibration was to enable the conversion of the specific characteristic x-ray spectral peak-height ratio for each element with Au into a ratio of weight fractions. It is known that such a calibration is straightforward when the amount of a single element in a matrix of fixed composition must be determined [B-2]. The thick-film conductors studied in the survey of Au-Pt-class films contained several elements which varied in amount, but the matrices were principally Au. For a large proportion of the Au-Pt inks, the Pt-to-Au ratio was similar, and the amount of Pd and binder constituents, such as Cd, Pb, and Bi were small enough that their effects on the analysis for the other should be small.

Table B-1 shows the design compositions of the standards. It can be seen that larger proportions of Pd have been treated as thoroughly as larger proportions of Pt. This was done for two reasons. First, the method should be suitable for Au-Pd inks, which are still in wide use in the industry. The second is that the form of the calibration curves is better developed by a wide range of proportions rather than a narrow group centered on the concentrations of principal interest. The range of binder constituents covered by the standards is limited but provides a good starting point for the design of further calibration standard compositions.

C. THE CALIBRATION CURVES

Table B-2 shows the angles for the characteristic spectral lines used and considered for use in the analyses, in terms of goniometer position (2θ), where θ is the Bragg angle of the PET analyzing crystal. Possible interferences are obvious by the close juxtaposition of indicated peaks and from the comments. The data were taken with the apparatus previously described in Appendix F of Ref. B-1; the chromium target x-ray tube was operated at 32 kV and 37.5 mA.

Primarily it was desired that the Pt-to-Au ratio be determined by the method. To reduce the possibility of differential enhancement or absorption, the Au and Pt peaks selected for measurement should have close 2θ values to

---

B-2. E. P. Bertin, *Principles and Practice of X-ray Spectrometric Analysis* (Plenum Press, New York, 1970), ed. 1, pp. 392-393.

AD-A045 831 RCA LABS PRINCETON N J F/G 9/5
BASIC ADHESION MECHANISMS IN THICK AND THIN FILMS.(U)
JAN 77 K R BUBE, T T HITCH N00019-76-C-0256
UNCLASSIFIED PRRL-77-CR-2 NL

2 OF 2
ADA045831

END
DATE FILMED
11-77
DDC

TABLE B-1. WEIGHT PERCENT RATIOS OF COMPONENTS OF CALIBRATION STANDARDS

Calibration Standard	Au/Pt	Au/Pd	Bi_2O_3 / (Au + Pt + Pd)	Bi_2O_3 / Au	E 1527 / (Au + Pd + Pt)	E 1527 / Au
1A	1.00	-	-	-	-	-
1D	1.00	-	0.042	0.084	0.038	0.076
2A	0.25*	-	-	-	-	-
2B	0.250	-	0.080	0.100	-	-
2C	0.250	-	-	-	0.090	0.113
2D	0.250	-	0.044	0.055	0.040	0.050
3A	0.0526	-	-	-	-	-
3D	0.0526	-	0.044	0.046	0.040	0.042
4A	0.23	0.023	-	-	-	-
4D	0.23	0.023	0.044	0.055	0.040	0.050
5A	0.023	0.23	-	-	-	-
5D	0.023	0.23	0.045	0.061	0.049	0.056
6A	0.12	0.12	-	-	-	-
6D	0.12	0.12	0.047	0.059	0.043	0.053
7A	-	0.25	-	-	-	-
7B	-	0.250	0.920	0.115	-	-
7C	-	0.250	-	-	0.102	0.128
7D	-	0.250	0.044	0.0555	0.049	0.060
8A	-	1.00	-	-	-	-
8D	-	1.00	0.058	0.116	0.053	0.106

*Where only two significant figures are shown, the calibration standards were made using pre-alloyed powders, nominally 80Au-20Pt and 80Au-20Pd (wt pct). A check of the alloy accuracy is underway for these materials.

TABLE B-2. CHARACTERISTIC PEAKS USED AND CONSIDERED FOR USE IN THE ANALYSES

PET 2θ (deg)	Element	X-ray Peak*	Relative Intensity**	Remarks
14.2	Au	$L\beta$	∿250	see Pt $L\beta$
14.7	Pt	$L\beta$	75	some overlap with Au $L\beta$
15.0	Bi	$L\alpha$	15	some overlap with Pt $L\beta$
16.8	Au	$L\alpha$	∿600	see Pt $L\alpha$(1)
17.3	Pt	$L\alpha$	∿150	some overlap with Au $L\alpha$(1)
20.3	Cu	$K\alpha$	∿ 15	best Cu line
21.9	Ni	$K\alpha$	∿ 15	best Ni line
25.6	Fe	$K\alpha$	-	X-ray tube contaminant line
27.6	Cr	$K\beta$	∿200	tube line
30.4	Cr	$K\alpha$	∿1000	tube line
33.4	Ti	$K\beta$	3.5	useful check on identity of Ti $K\alpha$
34.0	Au	$L\alpha$(2)	100	best Au line for analyses
35.0	Pt	$L\alpha$(2)	25	best Pt line to relate to Au $L\alpha$(2)
36.7	Ti	$K\alpha$	25	best Ti line
37.0	Ba	$L\alpha$	∿ 15	rarely seen
41.4	Ca	$K\beta$	0.7	useful check on identity of Ca $K\alpha$
45.2	Ca	$K\alpha$	5	best Ca line, interference from Pt $L\beta$(3) 45.2°
50.7	K	$K\alpha$	∿ 15	rarely seen
53.8	Cd	$L\alpha$	10	best Cd line, Pd interference usually negligible
56.6	Pd	$L\beta$	10	overlaps with Cr $K\beta$ (3)
57.0	Cr	$K\beta$(3)	25	tube line
60.0	Pd	$L\alpha$	15	best Pd line, minor overlap with Au $L\beta$(4)
63.2	Cr	$K\alpha$(3)	110	tube line used to monitor excitation power
68.3	Bi	$M\beta$	10	best Bi line, see Pb $M\beta$
71.0	Pb	$M\beta$	4	overlaps with Bi $M\beta$
71.7	Bi	$M\alpha$	25	overlaps with Au $L\alpha$(4) 71.5° and Au $M\alpha$ 72.1°
74.4	Pb	$M\alpha$	10	best Pb line
80.1	Au	$M\beta$	200	empirically less useful than Au $L\alpha$(2)
83.8	Au	$M\alpha$	∿350	too strong
87.5	Pt	$M\alpha$	65	used with Au $M\beta$
109.2	Si	$K\alpha$	10	best Si line

*Parenthetic numbers are diffraction orders.

**Relative intensity data were taken from the XRFS chart of calibration sample 4D (see Table B-1). Intensities for characteristic lines used in the study but not present in 4D are designated by values estimated for the presence of the element at a level of 0.01 wt ratio with Au.

preclude interfering absorption edges of common thick-film ink constituents from falling between them. The selected peaks should have moderate relative intensities to facilitate intensity comparisons with primary peaks from elements present in lesser amounts. Accordingly, two pairs of Au and Pt lines appeared suitable. The calibration curves resulting from the measurement of the peak heights of these lines on the x-ray intensity vs 2θ traces for the standards are shown in Figs. B-1 and B-2. Considering data from the standards which contained only metal, i.e., with no binder constituents, one can note that the curve of the Pt $L\alpha(2)$/Au $L\alpha(2)$ is a better fit to the data than that of Pt $M\alpha$/Au $M\beta$, indicating that the former is the better choice for analyzing Pt concentrations in Au matrices. It can be noted further that the presence of up to 10 wt pct Pd does not appear to have a large effect on the Pt calibration curve. See Table B-1 for the compositions of the samples from which the numbered data points arose in Fig. B-1.

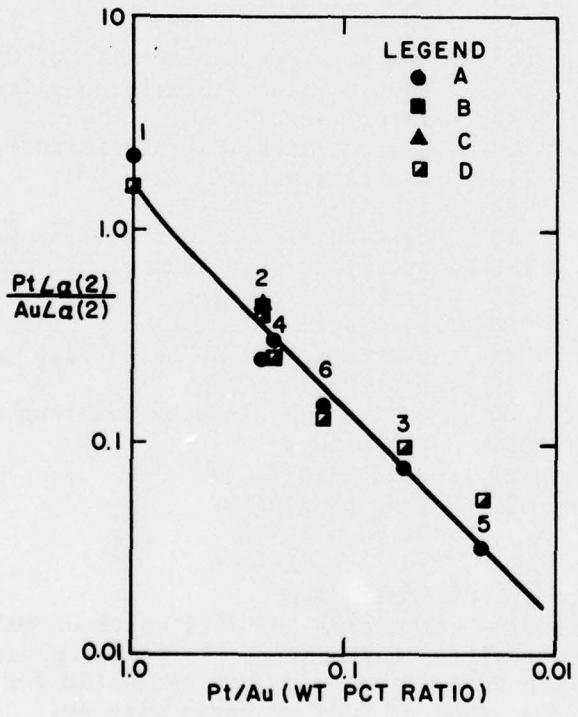

Figure B-1. XRFS calibration curve for Pt (preferred).

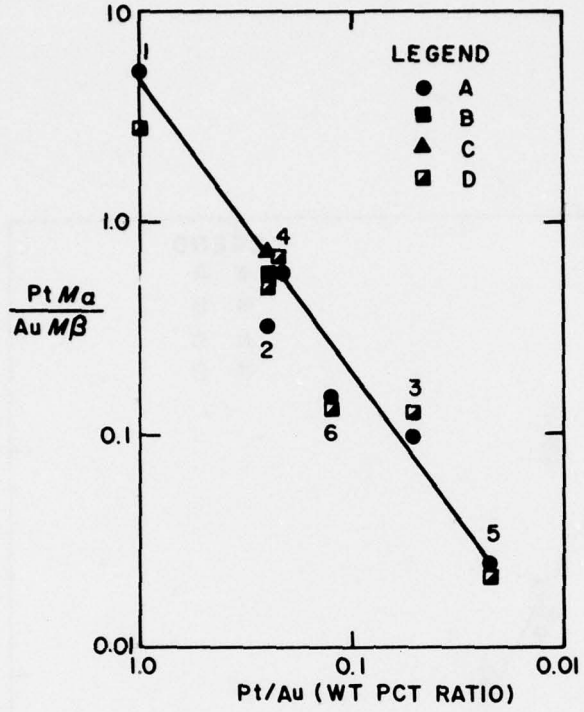

Figure B-2. XRFS calibration curve for Pt (rejected).

The only Pd line which was considered to be sufficiently strong and free of interference for satisfactory use was Pd $L\alpha$. Figures B-3 and B-4 show the variation in the intensity of Pd $L\alpha$ with the two Au lines considered for Pt analysis. Again, Au $L\alpha(2)$ allowed a smooth curve to better fit the data. The data for the composition number 7 standards containing binder agents (Table B-1) are not understood and deserve further attention.

A plot of Pd-to-Pt ratio for a fixed Au concentration of 80 wt pct in the metal phase is shown in Fig. B-5. A slope of 45° (theoretically ideal) is evident for the higher Pd compositions in Fig. B-5.

Calibration curves have been prepared for each of the XRFS detectable elements in the binder phases of the standards. The presentation format illustrated by Fig. B-6 for Si is a plot of the variation of Si $K\alpha$/Au $L\alpha(2)$ ratio vs the ratio of Pt-to-Pd by wt pct. A curve has been drawn on the figures through the data from the standards containing 80 wt pct Au in the metal phase. The extremes of the figure correspond to no Pt (left) and no Pd (right). The effect of changing the fraction of Au in either Au-Pt or Au-Pd

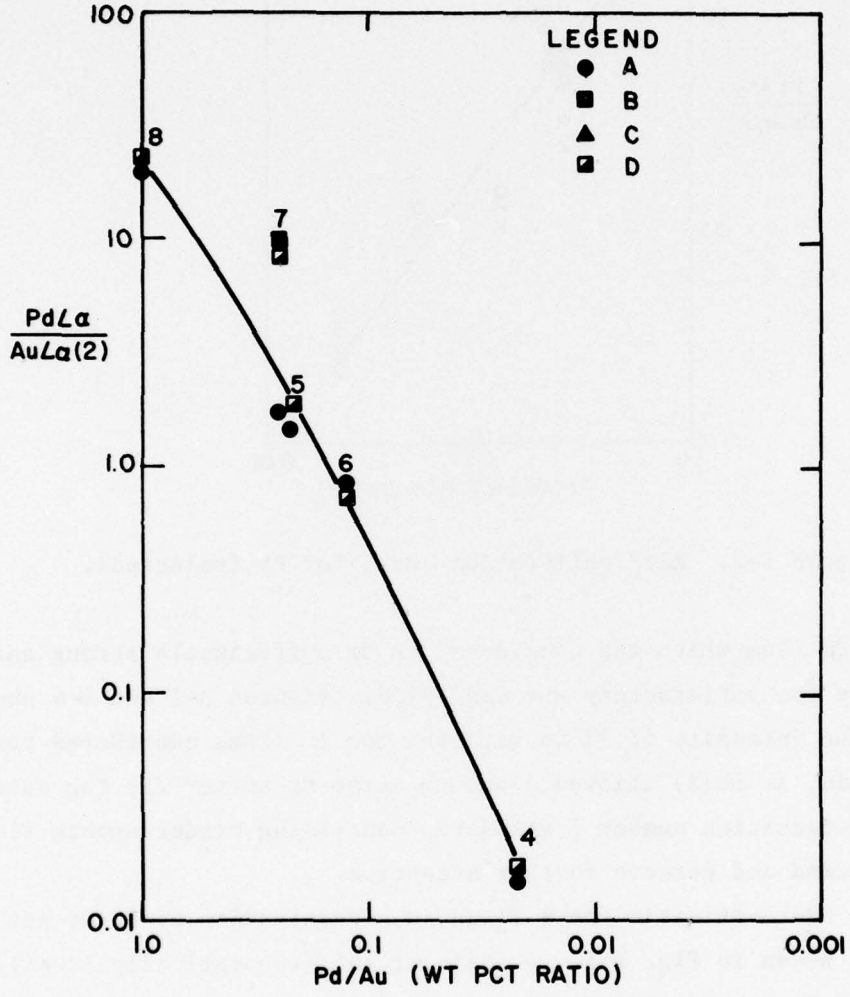

Figure B-3. XRFS calibration curve for Pd (preferred).

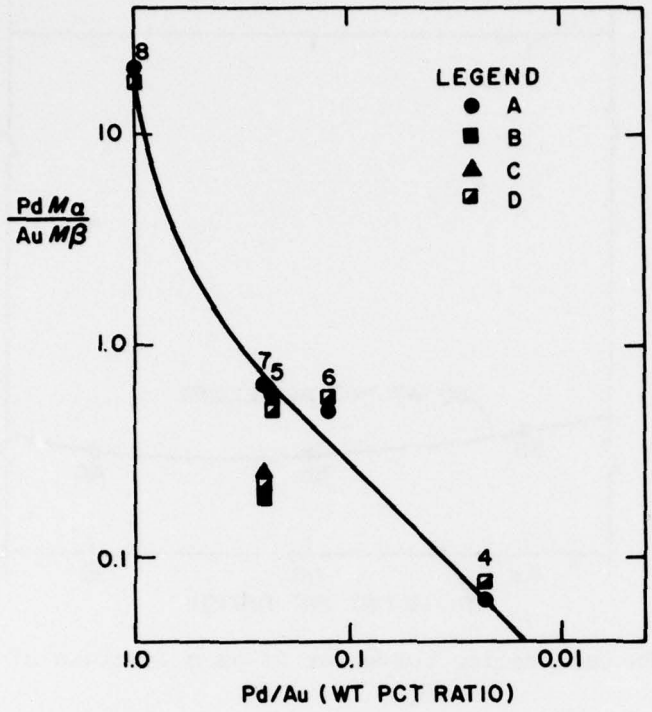

Figure B-4. XRFS calibration curve for Pd (rejected).

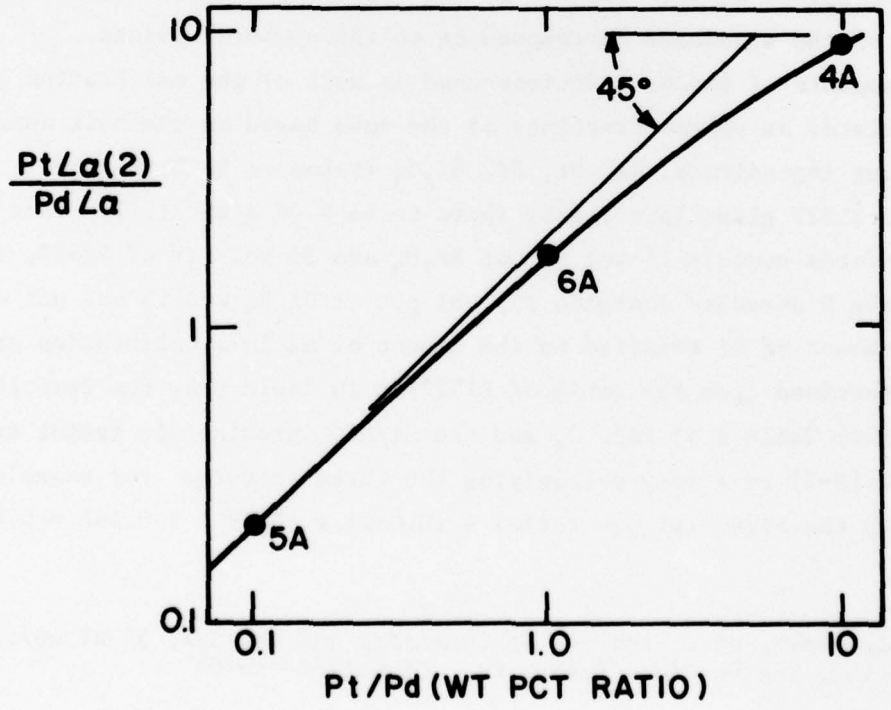

Figure B-5. XRFS calibration curve for Pt/Pd in 80 wt pct Au.

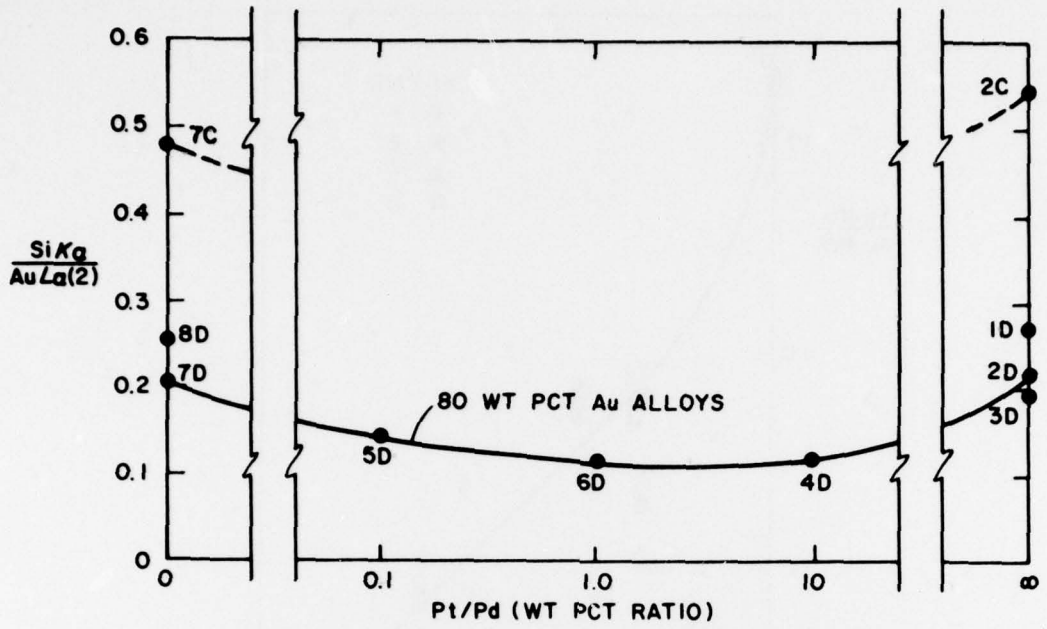

Figure B-6. XRFS calibration curve for Si as a function of Pt/Pd in Au.

binary noble metal alloys can be noted from the variation in Si $K\alpha$/Au $L\alpha(2)$ between the points at the extremes of the figure; *see Table B-1 for the compositions of the standards corresponding to the numbered points.*

The amounts of binder additions used in each of the calibration standards were calculated as volume fractions of the inks based on the bulk densities of the starting ingredients, Au, Pt, Pd, Bi_2O_3 (taken to be 8.90 g/cm^3), and Drakenfeld E1527 glass (previously shown to be 4.06 g/cm^3 [1]). That is, B and C standards contain 15 vol pct of Bi_2O_3 and 30 vol pct of E1527, respectively. The D standard contains 7.5 vol pct of Bi_2O_3 and 15 vol pct of E1527.

The amount of Si relative to the amount of Au in a calibration standard can be determined from the ratio of E1527/Au in Table B-1, the fraction of Si in E1527 from Table 2 of Ref. 2, and the Si/SiO_2 gravimetric factor taken from a handbook [B-3] by simply multiplying the three factors. For example in standard 4D the Si/Au (wt pct ratio) = (0.050) x (0.293) x 0.467 = 0.0068.

B-3. R. C. Weast, ed., *Handbook of Chemistry and Physics*, 51 st edition p. B-183, The Chemical Rubber Co., Cleveland (1970).

In the same format as Fig. B-6, Figs. B-7, B-8, B-9, and B-10 are the calibration curves for the binder elements Pb, Bi, Ti, and Cd. The Cd signal from some of the standards was weak, compromising the precision of parts of Fig. B-10.

D. EXAMPLE ANALYSIS BY USE OF THE METHOD

The procedure to analyze an unknown Au-Pt-Pd ink sample from XRFS recorder chart data, assumes identical sample preparation technique and x-ray exposure to those used with the calibration standards. The suggested analytical procedure is as follows:

1. Draw a smooth line representing the x-ray background on the XRFS recorder chart of the unknown, using straight line segments, where that gives a good fit, and a smooth curve from 10° to 37.5°.* We used straight lines segments, joined end-to-end, from 37.5° to 54.5°, from 54.5° to 70°, from 70° to 100°, and from 100° to 112°.
2. Measure the heights (background-to-peak) of the characteristic x-ray peaks that are indicated to be the best lines for each element of interest in Table B-2. Divide each of the other peak heights by the height of the Au $L\alpha(2)$ peak.
3. Use the Pt $L\alpha(2)$/Au $L\alpha(2)$ ratio with Fig. B-1 to determine a value for the Pt/Au wt ratio.
4. Use the Pd $L\alpha$/Au $L\alpha(2)$ ratio with Fig. B-3 to determine a value for the Pd/Au wt ratio.
5. Add the Pt/Au and Pt/Au wt ratios. If the sum is $\sim$0.25 the method should be quantitative since most of the calibration standards contain $\sim$80 wt pct gold.
6. Divide the Pt/Au wt ratio by the Pd/Au wt ratio to obtain the Pt/Pd wt ratio.
7. The Pt/Pd ratio and the ratio of the height of the selected peak for each binder element to the height of Au $L\alpha(2)$ are analyzed using the calibration curve for the binder element. Take the element Si as an example. The Pt/Pd ratio measured for the unknown determines the x-axis position on the calibration curve, Fig. B-6.

*The angles used throughout are 2θ goniometer angles corresponding to a PET analyzing crystal.

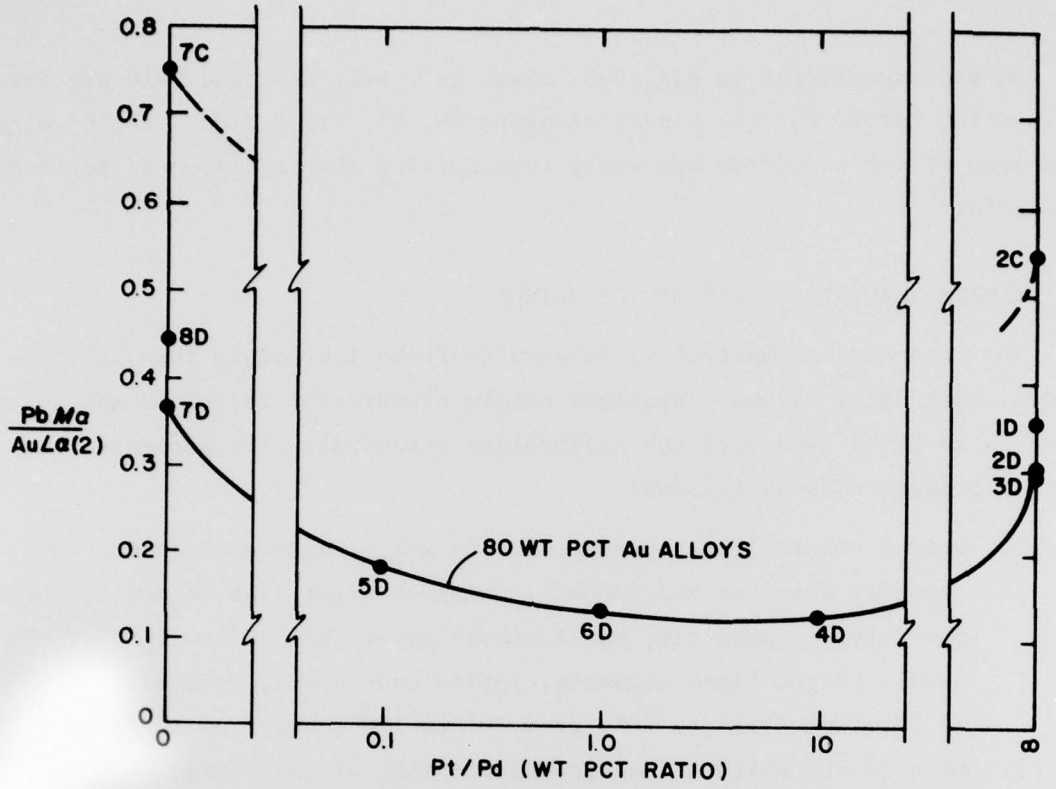

Figure B-7. XRFS calibration curve for Pb as a function of Pt/Pd in Au.

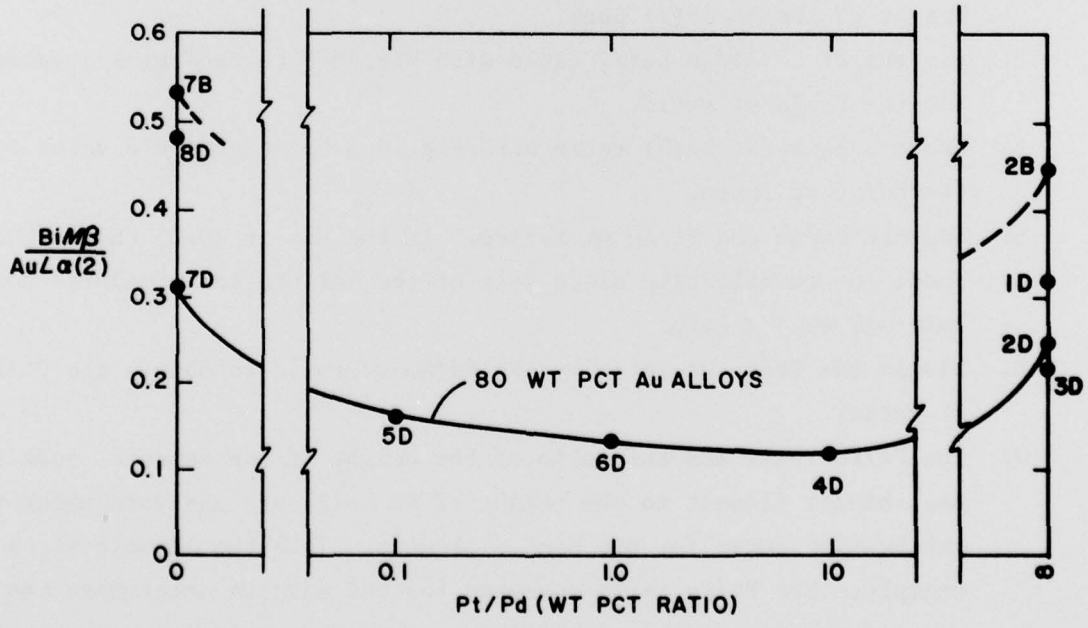

Figure B-8. XRFS calibration curve for Pi as a function of Pt/Pd in Au.

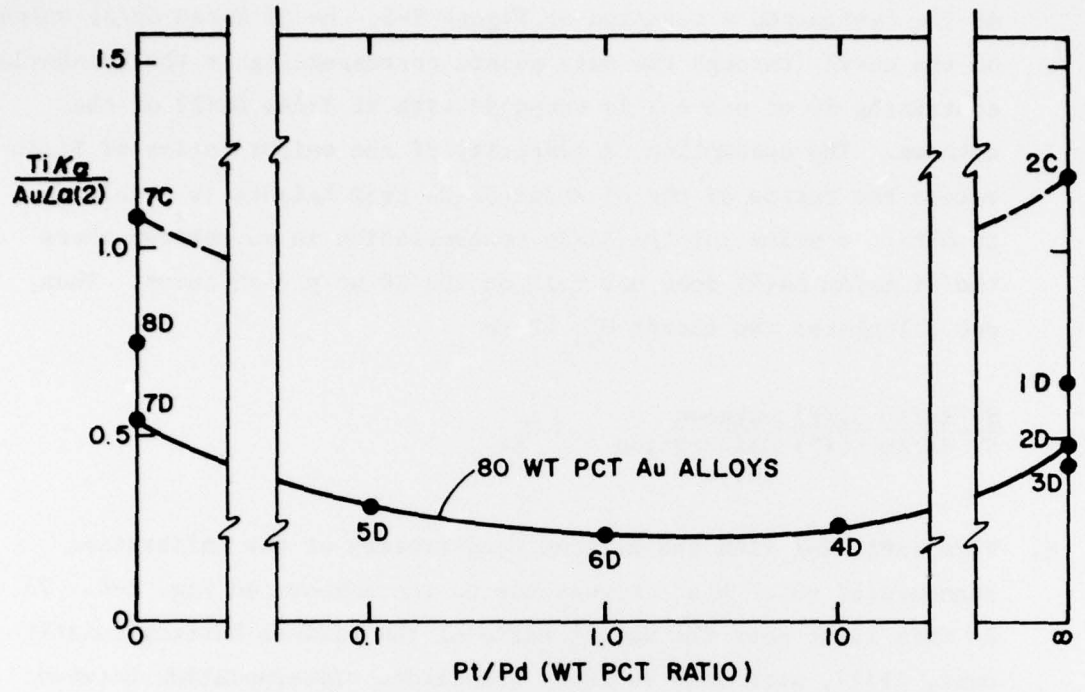

Figure B-9. XRFS calibration curve for Ti as a function of Pt/Pd in Au.

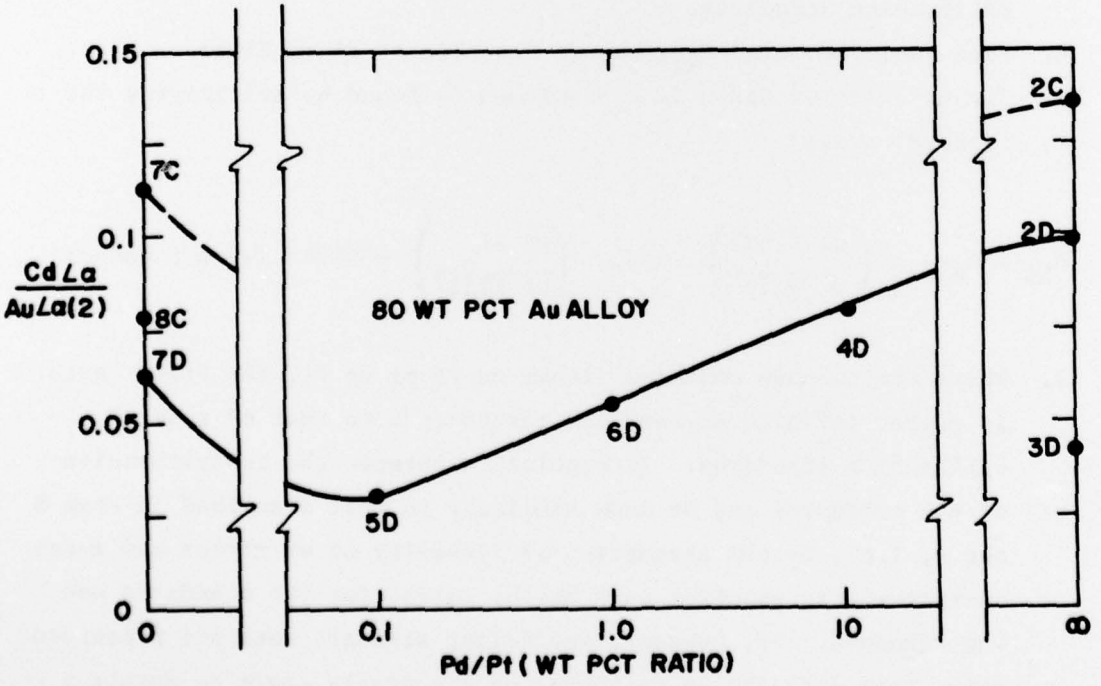

Figure B-10. XRFS calibration curve for Cd as function of Pt/Pd in Au.

At the designated x position on Figure B-6, the Si $K\alpha$/Au $L\alpha(2)$ value on the curve (through the data points corresponding to the standards containing 80 wt pct Au) is compared with Si $K\alpha$/Au $L\alpha(2)$ of the unknown. The assumption of linearity of the weight ratios of Si/Au versus the ratios of the Si $K\alpha$/Au $L\alpha(2)$ peak heights is required to obtain a value for the Si/Au concentration in an unknown where the Si $K\alpha$/Au $L\alpha(2)$ does not fall on the 80 wt pct Au curve. Thus, one calculates the factor M_{Si} where

$$\frac{\text{Si } K\alpha/\text{Au } L\alpha(2) \text{ unknown}}{\text{Si } K\alpha/\text{Au } L\alpha(2) \text{ Calibration Curve}} \equiv M_{Si}$$

8. From Table B-1 find the silicon constituency of the calibration standard(s) which best corresponds to the unknown on Fig. B-6. To do this first note the weight ratio of the silicon bearing constituent, E1527, with gold in these standards. Interpolation between the constituencies of calibration standards should be employed when the Pt/Pd ratio of the unknown lies in between those of the closest calibration standards.
9. From Table B-3 find F_{Si}, the wt fraction of Si in E1527.
10. The wt ratio of Si/Au in the unknown is found by multiplying the factors, i.e.,

$$M_{Si} \times C_{E1527} \left(\frac{\text{wt E1527}}{\text{wt gold}}\right) \times F_{Si} \left(\frac{\text{wt Si}}{\text{wt E1527}}\right) = \text{Si/Au (wt pct ratio)}$$

11. Where the unknown contains either no Pd or no Pt, the Pt/Pd ratio is either infinite or zero and corresponds to that of several calibration standards. Interpolation between the constituencies of the standards may be made similarly to that described in step 8 above, i.e., by the assumption of linearity of wt ratios and x-ray characteristic spectral peak height ratios for the standards and the unknowns. If, however, sufficient standard data are presented here, this data may be replotted on a suitable scale to enable a better approximation than linear interpolation. Whether by linear

TABLE. B-3. F VALUES*-THE FRACTIONS OF ELEMENTS AND OXIDES IN THE BINDER ADDITIVES TO THE CALIBRATION STANDARDS

E1527

PbO	-	0.513	Pb	-	0.476
SiO_2	-	0.283	Si	-	0.137
CdO	-	0.032	Cd	-	0.028
TiO_2	-	0.027	Ti	-	0.016

Bi_2O_3

Bi_2O_3	-	1.000	Bi	-	0.897

or by smooth curve interpolation (or extrapolation) a value of C_{E1527}, may be determined that when multiplied by an F value from Table B-3 will yield a value for the wt radio of a glass constituent and gold. No "M" factor is required in the product.

12. All the other binder elements are determined similarly. The weight ratios of the glass constituents in oxide form may be calculated by substituting the appropriate "F" values for the oxides from Table B-3. Exactly similar steps will allow the determination of Bi or Bi_2O_3.

*Calculated from the atomic absorption spectrometric analysis of E1527 [B-1] and gravimetric factors [B-4].

APPENDIX C

SOLDERED WIRE TENSILE PEEL ADHESION TEST SPECIMEN PREPARATION AND TESTING

The soldered wire, tensile peel specimen test procedure used with these samples was nominally that described earlier [C-1] as method 2. The modified test procedure is described below. Additional details and discussion of the method and data taken to correlate the method with other adhesion test methods will be presented at a later date.*

TEST PROCEDURE

1. Screen, dry, and fire special test patterns with four $(0.1\text{-in.})^2$ test pads symmetrically spaced about the center of a 1 x 1 x 0.025 $(\text{in.})^3$ substrate.
2. Burnish the substrate surface to assure complete wetting by the solder, using a coarse grit, rubber-base eraser in a motor-driven Teledyne Post (Engelwood, NJ) erasing machine.
3. Dip in mildly activated rosin flux (Kester 1544).
4. Immerse in a temperature-controlled solder pot at 210° $\pm$ 2°C for 5 seconds (62Sn-36Pb-2Ag solder).
5. While the solder is still molten, wipe all the excess from the substrate.
6. Remove flux residues by soaking in trichloroethylene.
7. Dip the cleaned substrates in nonactivated rosin solder flux (Alpha 100), predry in air at room temperature, and bake dry at 125°C for 30 minutes. Parts can now be stored indefinitely without loss of solderability.
8. Place two annealed 0.032-in.-diam OFHC copper wires and the substrate into a low thermal mass jig that positions the wires, each against two of the thick-film test pads, and centered over them.

C-1. T. T. Hitch and K. R. Bube, *Basic Adhesion Mechanisms in Thick and Thin Films*, Final Report, Naval Air Systems Command Contract No. N00019-75-C-0145, January 30, 1976.

* T. T. Hitch, *"Reproducible Adhesion Test for Soldered Thick-Film Conductors,"* Final Report, Naval Avionics Facility, Indianapolis, Contract No. N00163-76-C-0287, to be published.

9. Place the jigged assembly into a holder which positions it over the heat source. A Serpentine II (Sylvania Emissive Products, Exeter, NH), fitted with an expander nozzle, is the 2000-W heat source.
10. Place a fixed volume (0.031-in.-diameter x 1/4-in.-long), vee-shape-bent piece of 62Sn-36Pb-2Ag solder wire over the copper wire on each test pad.
11. Flux each pad with mildly activated rosin flux (Kester 1544).*
12. Heat the jigged assembly through a controlled temperature-time cycle using hot air as the heat exchange medium. The *7-second after solder melts cycle* is shown in Fig. C-1.
13. Remove flux residue by soaking in trichloroethylene.
14. Reject, before testing, any soldered-wire test pads which do not appear uniform.
15. Bend up the wires to conform to the test geometry (0.050-in. from center of the wire to edge of pad).
16. Cut the copper wires from between adjacent pads.
17. Wait at least 24 hours to allow stress relaxation in the solder.
18. Test in an Instron at 0.5 in./min crosshead speed.

* A device to meter flux for this operation is being considered. However, manual application of the flux has caused no known problem in this study.

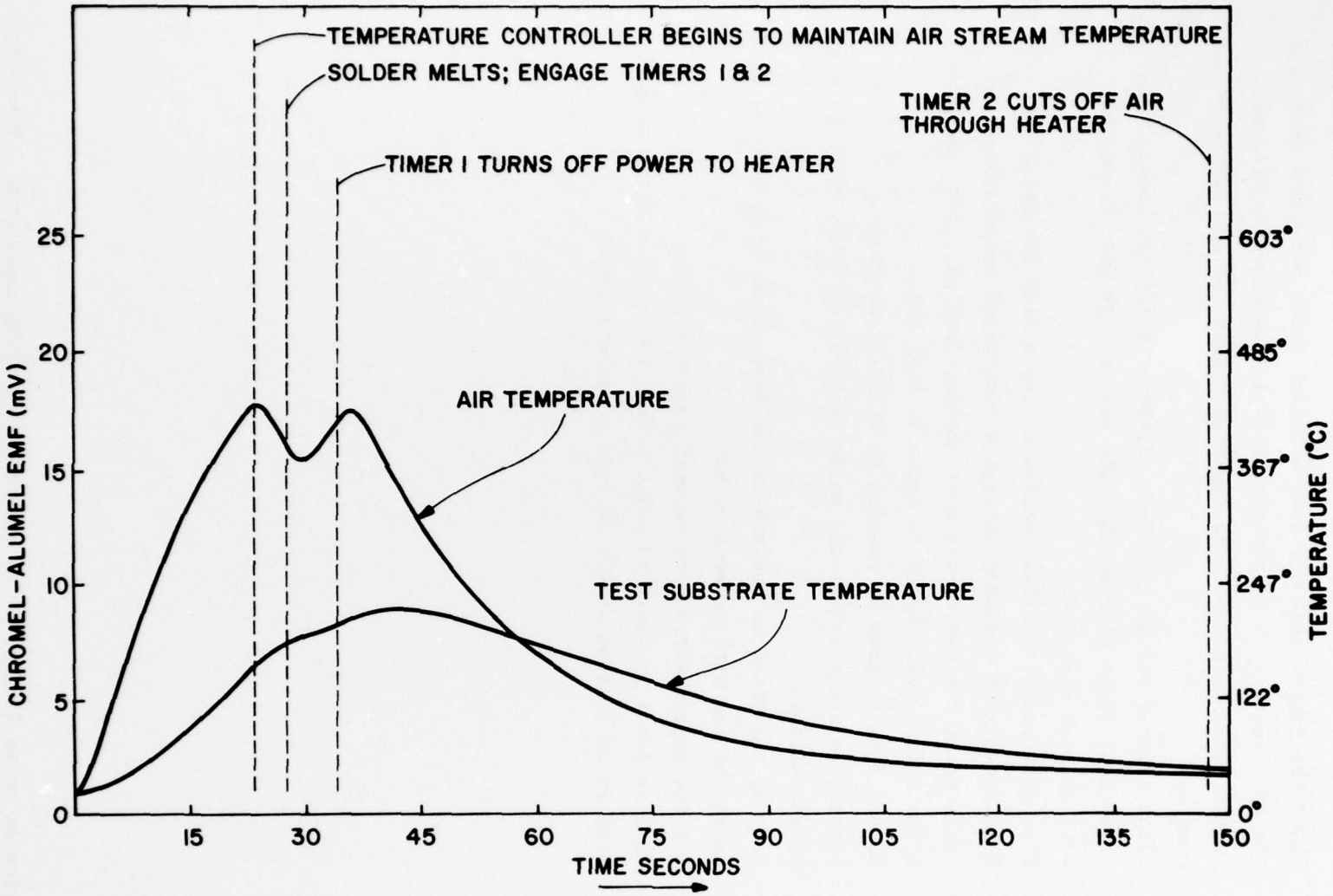

Figure C-1. Measurement of substrate and heat source air temperatures during soldered wire, tensile peel adhesion test specimen solder assembly.

APPENDIX D

MEASUREMENT OF THE SOLDERABILITY OF THICK-FILM CONDUCTORS

The use of a Meniscograph (sold by Hollis Engineering, Nashua, NH) to measure the solderability of thick-film conductors has been described by Pantanelli [D-1] and by Jellison et al [D-2]. Test pattern masks were made available to RCA, courtesy of Bell Laboratories, Allentown, PA, thus our samples employed the same geometry film patterns as those of Pantanelli.

1. Specimen Fabrication

Two wettability test patterns were screened together onto each $(1.00\text{-in.})^2$ x 0.025-in. "A" (96 wt pct alumina) substrate and fired at the desired furnace profile. The specimen was reprinted on the bare side of the substrate so that the patterns on both sides were superimposed. Then the specimens were refired at the chosen furnace profile in fixtures designed to prevent the ink patterns from touching anything. After laser scribing, using a Coherent Radiation Model 610 CO_2 laser at RCA's Solid State Technology Center in Somerville, NJ, the substrates were broken. The specimens, now 1.00-in x 0.394-in. x 0.025-in., had thick-film conductor covering nearly the full width of the ceramic for the first 0.30-in. of the specimen length on the ends to be tested.

A third firing through the same furnace profile, again using fixtures to hold the specimens off the furnace belt, ensured that no film damage from the laser or scratched on the film from handling during breaking would accelerate wetting of the specimens. A pronounced acceleration of solder wetting had been noted by one of the authors to be due to scribe marks in thick-film conductors during earlier unpublished studies of thick-film with the Meniscograph.

D-1. G. P. Pantanelli, "Measurement of the Solderability of Thick-Film Circuits," Proc. Int'l Microelec. Symp. (ISHM) p. 336 (1974).

D-2. J. L. Jellison, D. R. Johnson, and F. H. Hosking, "Statistical Interpretation of Meniscograph Solderability Tests," Proc. Int'l Microelec. Symp. (ISHM) p. 184 (1975).

2. Experimental Technique

The test area of each specimen was immersed in Kester 1544 (mildly activated) soldering flux, the specimen end touched to a blotter, and the flux allowed to dry for ∿10 s.* The specimen was mounted in the sample holder and the Meniscograph test sequence started.

The solder used was 62Sn-36Pb-2Ag, the solder pot was adjusted to 230°C. An immersion depth into the Meniscograph solder pot of ∿4 mm (immersion selector position 4) was used on most of the specimens. On a few specimens (Ag-Pt-Au ink No. 22, in particular) an immersion depth of 4 mm so great that in the time of test (10 s), solder wetted the entired remaining pad area. When this occured, a new specimen lot was run at a 2-mm immersion depth (immersion selector position 2). The data based on 2-mm immersion depths have been normalized on the Meniscograph data curves of subsection III.B.5 in the main body of this report so that all the data presented as solid lines are representative of a constant 4-mm immersion depth. The 2-mm immersion depth wetting curves which are shown as dashed lines.

*In earlier studies fully dried flux was found to be too efficient an insulator, and prevented the solder bath from electrically contacting the specimen fast enough for proper Meniscograph immersion depth control.

APPENDIX E

THE CHEMICAL AND PHYSICAL ANALYSES OF ALUMINA SUBSTRATES

The analyses presented here were performed by RCA on two lots of ceramics which were purchased by Purdue University for use in the three coordinated studies and distributed to the research teams at NRL and to RCA. One lot each of 96 wt pct alumina, Code a, and of 99.5 wt pct alumina, Code B, were purchased and analyzed. These data for substrate analyses may be compared with the analyses of other lots of the same manufacturer's substrate types presented earlier in Appendix E of Ref. E-1.

All the data presented in this final report which describe thick films that were printed and fired at RCA Laboratories were taken using A and B substrates either from the lots described here or in the earlier report [E-1]. All the model ink studies and the work on B substrates described in subsection III.B.2. used in substrate lots described in Ref. E-1. In the commercial ink studies described in subsections III.B., all of the A substrates, as well as the B substrates used with the six inks selected for detailed study, were from the lots described in this appendix.

Auger spectrometric analyses, performed on the earliest lots of ceramics by RCA, will be performed by one of the other research groups in accordance with an agreement between the principals of the RCA, NRL and Purdue University coordinated investigation of "Basic Adhesion Mechanisms in Thick and Thin Films."

Bulk chemical analyses of the substrates were performed using three techniques. Solids mass spectrometry and emission spectrophotometry were used to scan semiquantitatively for impurities. Atomic absorption spectrometry was used to measure quantitatively the amounts of the principal constituents of the substrates, i.e., Al, Si, and Mg. The results of those analyses are shown in Table E-1. All the analyses performed detect only the elements present. Where Table E-1 reports oxides, that has been accomplished by calculating the weight concentrations on the basis that for each

E-1. T.T. Hitch and K.R. Bube, *Basic Adhesion Mechanisms in Thick and Thin Films*, Final Report, 31 January 1975, NASC Contract No. N00019-74-C-0270.

TABLE E-1. BULK CHEMICAL ANALYSES OF SUBSTRATE LOTS PURCHASED IN 1977 FOR CONTRACT USE

Constituent	Substrate	
	A	B
Al_2O_3	93.7	98.9
MgO	1.31	0.47
SiO_2	3.6	0.4
BaO	0.008	0.04
CaO	0.1	0.04
Cr_2O_3	0.003	0.001
Cl	0.003	0.003
F	0.003	0.002
Fe_3O_4	0.2	0.3
Ga_2O_3	0.03	0.08
K_2O	0.008	0.001
Mn_2O_3	0.001	0.003
Na_2O	0.001	-
TiO_2	0.02	0.01
ZrO_2	0.003	0.007

element, the oxide phase in equilibrium at 1300°K in air is the one present. Where a single significant figure is present in Table E-1 for materials reported as oxides, the number is the arithmetic mean of the solids mass spectrometry (M.S.) and emission spectrometric (E.S.) data. The data for elements which are not reported as oxides are from M.S. data; they are not detected by E.S. Impurities present in amounts less than approximately 10 ppm by wt were ignored.

Neither of the substrates contains as much alumina as the vendor's compositions indicate, but this is unchanged from our earlier analyses of similar materials [E-1]. The magnesium and iron levels are higher and silicon is lower in both materials than they were in the similar materials analyzed for the 1974 contract [E-1].

Table E-2 shows the local surface roughness of each substrate. The data for each measurement were taken using a 0.15-in. traverse distance, on the Talysurf described in Ref. E-1. Each centerline average (CLA) shown is the arithmetic mean of six CLA readings. These data agree satisfactorily with the advertised nominal surface roughnesses of substrates A and B, which are 25 and 8 μin.

In summary, the four substrates meet the manufacturers' claims in general, except for the purity. The lower-than-advertised alumina content in these materials appears to be an intentional deviation from what is advertised.

TABLE E-2. SUBSTRATE SURFACE ROUGHNESS MEASUREMENTS

Substrate	A		B	
Side	Front	Back	Front	Back
Average Roughness (μin.)	19.7	23.1	8.6	17.8
V (pct)	5.9	3.7	3.5	5.8